1-1-2016

Detection of Glucose Based on Gold & Silver Nanoparticles using Z-scan Technique

Fatema Abdulwahab
RCSI-Medical University of Bahrain, fabdulwahab@rcsi.ie

Detection of Glucose Based on Gold & Silver Nanoparticles using Z-scan Technique

By

Fatema Abdulwahab, BSc

Department of Medical Sciences

Royal College of Surgeons in Ireland – Medical University of Bahrain

A thesis submitted to the School of Postgraduate Studies, Faculty of Medicine and Health Sciences, Royal College of Surgeons in Ireland, in fulfillment of the degree of Master of Science

Supervised by:

- Prof. Fryad Zeki Henari (RCSI- Bahrain)
- Dr. Kenny Winser (RCSI- Dublin)

June, 2016

I declare that this thesis, which I submit to RCSI for examination in consideration of the award of a higher degree <Master of Science> is my own personal effort. Where any of the content presented is the result of input or data from a related collaborative research program this is duly acknowledged in the text such that it is possible to ascertain how much of the work is my own. I have not already obtained a degree in RCSI or elsewhere on the basis of this work. Furthermore, I took reasonable care to ensure that the work is original, and, to the best of my knowledge, does not breach copyright law, and has not been taken from other sources except where such work has been cited and acknowledged within the text.

Signed

Fatema Abdulwahab

_____

RCSI Student Number

14126460

_____

Date

01/06/2016

_____

Table of Contents

Abbreviations

σ	Non-locality
θ	On-axis phase shift
α_0	Linear absorption coefficient of the medium
α	Linear absorption coefficient
β	Nonlinear Absorption Coefficient
λ	Wavelength
Δφ	Nonlinear induced phase shift
ΔE	Energy difference
ΔT_{p-v}	Transmittance change between peak and valley
Ag	Silver
$AgNO_3$	Silver nitrate
Au	Gold
Au-Ag	Gold-Silver
c	Speed of light
C	Carbon
C_P	Specific heat per volume at constant pressure
Cl	Chlorine
CW	Continuous Wave
$\frac{dn}{dT}$	Thermo-optical
D	Diameter
E	Electric field
f	Focal length
Fig.	Figure
$HAuCl_4$	Gold (III) chloride trihydrate
hv	Photon energy
I_0	On-axis irradiance at focus
I	Irradiance
k	Thermal conductivity

k	Wave vector
L_{eff}	Effective thickness of sample
Mid-IR	Mid infrared
min	Minutes
n	order
n	The total refractive index
n_2	Nonlinear Refractive Index
N	Nitrogen
Na	Sodium
NIR	Near infrared
NLO	Nonlinear Optics
nm	Nanometers
NPs	Nanoparticles
O	Oxygen
P	Power
Pa	Pascal
q	Charge
r_0	Radius of curvature
rpm	Revolutions per minute
S	Aperture linear transmittance
SEM	Scanning Electron Microscope
SPR	Surface Plasmon Resonance
t_c	Thermal diffusion time
T	Transmittance
T_N	Time dependent far-field on-axis transmittance
TEM	Transmission Electron Microscope
UV	Ultraviolet
w_0	Gaussian beam spot radius at focus
ω	Frequency
χ^n	Nonlinear susceptibility
XRD	X-ray Diffraction

z Sample position

List of Figures

List of Tables

Abstract

Diabetes is a common chronic disease, characterized by defects in insulin action, secretion or both causing hyperglycemia. Diabetes can have serious long-term complications as it important to control blood glucose levels. Chemical and optical methods are used mainly in measuring glucose levels. Chemical methods require drawing blood several times a day which is uncomfortable for the patient. Optical sensor measurements are affected by physical and chemical parameters and environmental changes.

In this study, we propose a method for detecting and quantifying blood glucose levels based on the nonlinear optical properties measurements using the z-scan technique. Gold, silver and gold/silver (core/shell) nanoparticles were synthesized using a wet chemistry where trisodium citrate was used as a reducing agent. A green synthesis method used curcumin and glucose as reducing agents. These nanoparticles are characterized by their plasmon absorbance band, and their shapes and sizes are confirmed by TEM. Glucose conjugated nanoparticles are either synthesized or mixed with glucose. The compositions of these conjugates were confirmed by TEM. Mie theory was used to determine the size of the nanoparticles. Nanoparticles conjugated with glucose were subjected to nonlinearities measurements using the z-scan technique. The z-scan experiments were preformed using 488 nm and 514 nm CW argon-ion laser with adjusting power of 15 – 30 mW to measure the nonlinear refractive index (n_2). Z-scan measurements indicated that studied samples exhibited nonlinear optical properties. The experimental results show that the nonlinear refractive index was dependent on the concentration of glucose conjugated with metal particles. Thus, the nonlinear refractive index value of the given glucose sample may be used as a quantifying indicator.

Keywords: nanoparticles, colloidal, z-scan, nonlinear properties, absorption spectra, glucose detection.

Acknowledgements

The ultimate support, encouragement and care that I received were my power to work hard to the end. I believe that any degree is the beginning of a new journey.

Special thanks to my parents, husband, sister, brother, uncles, aunts, family and friends for their support, encouragement and help.

Deepest appreciation and thanks to my supervisor Prof. Fryad Zeki Henari for his help, support, encouragement and advice.

I am also thankful to Dr. Kenny Winser for his help and advice.

Special thanks to Mr. Timo Meerloo from University of California (UCSD) for imaging and analyzing nanoparticles using a TEM microscope.

Special thanks to Dr. Ebrahim Rajab for providing diabetic blood samples.

My thanks also go to Dr. Khalil Ebrahim for his advice and support.

I am also thankful for Mrs. Hanan Abbas and Dr. Ahmed Al-Saei from the University of Bahrain (UOB) for imaging and analyzing nanoparticles using SEM and XRD.

Finally, special thanks to all who helped and advised during the study, Dr. Seamus Cassidy, Fatma Al-Hannan and Mr. Ian Reid.

"This thesis is dedicated to my parents, Ahmed, Amira and Adel for their endless love, support and encouragement"

Chapter 1: Introduction

Diabetes is a disease that currently affects 380 million people worldwide (1). It is one of the commonest chronic diseases in Kingdom of Bahrain affecting 15% of the population (2). According to the World Diabetes Federation, Bahrain is ranked eighth in terms of diabetes spread, with new cases continually developing (3). Diabetes is considered in Bahrain as a main killer with 15% of all deaths caused by diabetes (4). Obesity, lack of activity, lifestyle and food habits are the major causes of diabetes in Bahrain (5). Bahrain ranks 4th in obesity among the Gulf countries (6). This makes the population susceptible to diabetes, although the causes of the disease are not known for certain. Diabetes is a disease caused by defects in insulin secretion, which leads to hyperglycemia. There are two major types of diabetes, type I and type II. In type I diabetes, the patient's body does not produce insulin. In type II diabetes, the patient's body does not use insulin properly (7). Type II diabetes is the more common type in the Bahrain population (8). Insulin is a hormone produced by the pancreas that allows the metabolism of carbohydrates, fats and proteins. Insulin regulates blood sugar level and inhibits it from getting too high (hyperglycemia) or too low (hypoglycemia) (9). Without insulin blood glucose level will increase and are excreted through the kidney causing excessive urination. Furthermore, for energy metabolism body will use stored fat which leads to the production of ketones, which affects patients' health (10). Factors such as genetics, obesity, food habits and lack of exercise are believed to play a major role in diabetes. There is no permanent cure for diabetes except medication and insulin injections. However, stem cell research gives the promise of replacing inactive pancreatic beta cells with developed beta cells to produce insulin (11). For now, there is no cure for diabetes so continuous treatment is the only alternative to preventing the resultant serious complications for the patient. Treatment includes continuous blood glucose monitoring combined with insulin tablets or injections. A commitment to a strict diet control of sugar intake, and regular exercise is also required (12). Several methods to

monitor glucose levels have been reported, which include, optical, electrochemical and enzymatic methods. At the moment, many glucose sensor devices are available for monitoring glucose levels. These devices are used for clinical diagnosis and treatment of diabetes. In recent years, the determination of glucose level with the use of nanoparticles has attracted interest because of their unique optical properties. These unique properties motivated many researchers to study optical nonlinearities of the combined nanoparticles and glucose with the aim of monitoring the glucose level.

In this study, we proposed a method for synthesizing gold nanoparticles using glucose, gelatin and microwaves. Nanoparticles were used for the detection and quantifying of glucose using UV-Vis spectroscopy and z-scan technique. The nonlinear properties of gold, silver and gold-silver nanoparticles reacted with glucose were investigated using z-scan technique. Z-scan technique is an effective tool, easy to use, simple, highly sensitive and inexpensive (13–15). Real time and accurate readings of glucose may be obtained using this method.

1.1 Aims

The major goal of this work is to detect and quantify glucose combined with gold (Au), silver (Ag), combined gold & silver (Au-Ag) nanoparticles using the z-scan technique in prepared solutions and in diabetic whole blood or plasma.

a. The synthesis of gold (Au), silver (Ag) and gold-silver (Au-Ag) nanoparticles (NPs) by the wet chemistry method using trisodium citrate as a reducing agent.

b. The synthesis of gold (Au), silver (Ag) and gold-silver (Au-Ag) nanoparticles (NPs) by the green synthesis method using either glucose, curcumin, gripe water, coffee, tea or hibiscus as a reducing agent.

c. Study the changes of absorbance and peak position of nanoparticles surface plasmon resonance (SPR) band with different concentrations of glucose.

d. Study the changes in the nonlinear refractive index of nanoparticles using different concentrations of glucose.

e. Investigate the nonlinear refractive index of whole diabetic blood and plasma.

Chapter 2: Diabetes

Diabetes mellitus is a chronic disease the prevalence of which is increasing all over the world. It is a result of defects in insulin action, or the secretion of insulin or both of these actions. This causes hyperglycaemia (high blood sugar). This can cause the failure or dysfunction of eyes, kidneys, heart and blood vessels (16).

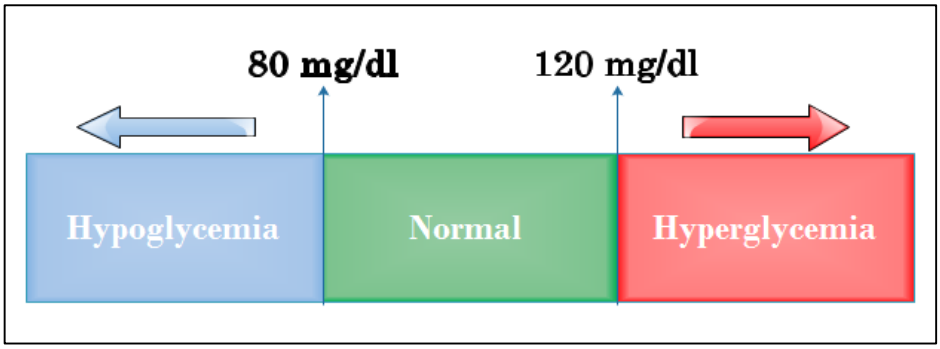

Figure 2.1: Blood glucose levels.

Diabetes causes excess sugar to appear in the urine. Diabetes is named Diabetes Mellitus. It is derived from Greek and Latin words; diabetes is a Greek word meaning siphon or pass through, while mellitus is a Latin word meaning honeyed or sweet (17).

Frequent urination was the first observed as a symptom of diabetes by an Egyptian physician in 1552 B.C. The discovery of insulin is related to studies of the pancreas. In 1889, Oskar Minkowski and Joseph von Mering proved that the removal of a dog's pancreas caused diabetes (18). In 1910, Sir Edward discovered the presence and the production of a substance in non-diabetics and named it insulin. Insulin is derived from a Latin word insula, meaning island (19).

2.1 Physiology and Pathophysiology

There are many hormones that regulate glucose level in blood such as insulin, glucagon, amylin, glucagon-like peptide-1 (GLP-1), glucose-dependent

insulinotropic peptide (GIP), epinephrine, cortisol and growth hormone. Insulin and amylin are produced by the Beta cells of the pancreas. Alpha cells in the pancreas produce glucagon, while L-cells in the intestine produce glucagon-like peptide-1 (GLP-1) and glucose-dependent insulinotropic peptide (GIP). The main role of these hormones is to keep the glucose level in blood within a specific narrow range (70 - 99 mg/dL). Insulin is the only hormone that lowers blood glucose level (20). Glucose is the main source of fuel in the body. Different tissues have different membrane permeability to glucose. The diffusion of glucose to the cells is controlled by glucose transporters. When carbohydrates are digested, glucose is produced. Then glucose is transferred from blood to cells and used as energy. Insulin is the main hormone for glucose regulation. It is synthesized in the beta cells located in islets of Langerhans in the pancreas. Blood glucose is decreased when glucose is transferred from blood into the muscle, liver or adipose tissues. Insulin is required by the muscle, liver and adipose tissues to activate insulin receptors, which facilitate the glucose transfer. In the cell, glucose may be oxidized for energy (glycolysis) or stored in muscle and liver (glycogenesis) (21,22). Small amounts of insulin are always secreted by the pancreas into the blood. When blood glucose levels rise, higher amounts of insulin is required. A patient who is diagnosed as a diabetic, may lack insulin because of low production of insulin or may not have enough insulin receptors to reduce the level of blood glucose.

There are three types of diabetes namely type I, type II and gestational diabetes.

Type I which is also known as insulin dependent diabetes. 10% of people with diabetes suffer from diabetes type I. In this type beta cells are destroyed by the immune system. Either little or no insulin is produced. Type I generally develop in children or young adults (below 30), but it can develop at any age. The signs and the symptoms of type I is usually acute and rapid. They are urination, hunger, thirst, weakness, drowsiness, vomiting, weight loss and blurred vision. Type I is usually treated using insulin, exercise and dietary changes.

Type II is the most common type of diabetes, also known as non-insulin dependent. In this case, insulin is produced but not used effectively (insulin resistance). In fact, enough insulin is produced but there are not enough insulin receptors. Symptoms usually develop gradually, like urination, hunger, thirst, weakness, drowsiness, numbness in legs, feet or fingers, skin infection, slow healing of cuts and blurred vision. Type II is usually treated using non-insulin medications, dietary changes and weight loss.

About 4% of women develop gestational diabetes during pregnancy. Its pathophysiologic process is similar to type II. The placenta that connects baby and mother's blood supply, produces different types of hormones. Some of these hormones are insulin blocking hormones, which affects the function of insulin and raise blood glucose levels. Usually, gestational diabetes will disappear after baby is born, but it will put the mother at higher risk of developing type II diabetes (12,22–25).

Diabetes may cause serious long-term complications. It may cause eye problems such as night sight difficulties and even blindness. Skin and specially feet may develop infections and sores that cause pain, itching and amputation. Diabetes raises a patient's risk of heart attack and stroke because of the difficulty to control blood pressure and cholesterol. Furthermore, it can cause nerve damage, which cause pain, tingling, loss of feeling and erectile dysfunction. High blood sugar increases kidneys filtration rate and with time, this can cause kidney damage. Patients with kidney damage may require dialysis or kidney transplant. Patients may develop digestion and bowel movement problems. In order to prevent diabetes long-term complication's patient should control diabetes. Healthy diet, exercise and medications are most important for diabetes control. To avoid long-term complication's patients should keep their blood glucose, blood pressure and cholesterol levels in a normal range. Heart disease and strokes may be prevented by taking medications prescribed by a doctor. For healthy feet, regular feet check-up must be done every day, and proper socks and shoes must be worn (26).

2.2 Glucose Monitoring

Many methods are used to test blood glucose. They include optical, electrochemical, and enzymatic methods. Monitoring blood glucose is important to control glucose levels and avoid diabetic complications. Dextrostix [Fig. 2.2] were the first blood glucose test strips invented by Ernie Adams from Miles laboratories in 1963, where a drop of blood was added to the strip and then washed out. A blue color developed whose intensity was proportional to the glucose concentration. By comparing the color to a color chart, the glucose level was estimated (27).

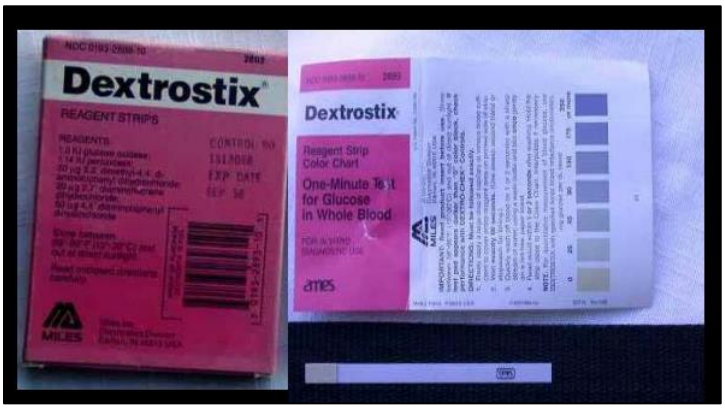

Figure 2.2: Dextrostix strips (79).

Point sample refers to whether the sample was taken from blood or urine for reading glucose level. This can be read by a finger-prick glucometer or a urine dipstick (28). For real-time readings and optimal glucose control, continuous glucose monitoring may be used. Sensor's collect readings every 5 minutes. A sensor is implanted under the skin and collects readings from tissue fluids. Using radio waves the sensor transfers the readings to the meter. Usually, sensors are replaced every few days (29). On other hands, some monitors do not require sensor implementation. Both invasive and non-invasive methods are used for glucose detection; invasive methods require puncturing the skin and drawing the blood, while non-invasive methods do not require skin penetration or blood

extraction. Microscopic holes created by weak lasers or ultrasounds are considered as non-invasive (30).

In general, chemical sensors are based on producing of signals from chemical information. The chemical information may be as a result of chemical reaction or a physical property. Most chemical sensors consist of two main components; a chemical recognition system (receptor) and physicochemical transducer. Simply the receptor interacts with molecules leading to changes in physical properties and the production of electrical signal. Basically, the strip consists of two main chemical's glucose oxidase and ferricyanide. The blood sample reacts with glucose oxidase, and gluconic acid is produced. Then gluconic acid reacts with ferricyanide and ferrocyanide is produced. Ferrocyanide affects the current within the electrode giving a glucose measurement (31). This type of sensor is considered accurate, but it requires skin puncturing and blood drawing, which causes pain.

Figure 2.3: Glucose monitor (80).

Optical, mechanical, magnetic and thermal sensors are considered as physical sensors (32). Optical sensors detect chemical or physical parameters by measuring changes in the measurement of a specific optical property. The optical property measured may be absorbance, reflectance, luminance or scattering. Recently, the nonlinear refractive index and the nonlinear absorption coefficient were employed for monitoring glucose levels (33). There are many types of glucose optical sensors.

NIR and Mid-IR spectroscopy techniques based on focusing the body with a beam of light in the range of 750-2500 nm for NIR and in the range of 2500-

10000 nm for Mid-IR. When the light is focused on the body, it is scattered or absorbed due to interaction with tissue components. According to Beer's Law, reflected or transmitted light is described by $I=I_0e^{-\mu_{Tot}d}$. Where I is the reflected/transmitted intensity, I_0 is the incident light intensity, μ_{Tot} is the sum of attenuation coefficient and d is the optical path length in tissue. NIR spectroscopy depth range is 1-100 mm, while Mid-IR is a few micrometers. However, these techniques have many limitations, for example, body temperature and the effect of diabetes on the skin may affect glucose measurements. There is also, poor penetration in Mid-IR spectroscopy.

Raman Spectroscopy uses laser light to produce oscillations in molecules. These oscillations affect the emission of scattered light, which is dependent on the concentration of solute in the solution. The spectral interval of 200-1800 cm^{-1} is considered as the interval of Raman's spectroscopy. In this band glucose is clearly differentiated from other compounds. The stability of the laser wavelength and intensity are the main limitations of this technique.

Fluorescence Technology is also used to monitor glucose levels, and it is based on using light with specific wavelength to excite human tissues to generate fluorescence. Fluorescent intensity is dependent on the concentration of glucose. The limitation of this technique is that skin pigmentation or redness may affect glucose measurements.

In Ultrasound Technology, pico to nanoseconds laser pulses with specific wavelength are used to excite a fluid. As a result of light absorption heating occurs within the medium, and a detectable ultrasound pressure wave is generated. This technique has many limitations, such as expensive instrumentation, sensitivity to environment and sensitivity to chemical and physical interferences.

In the Fluid Harvesting technique, microscopic holes are created in the skin using laser light or ultrasounds. Then a glucose sensor is placed on the skin where interstitial fluids containing glucose migrate through the micropores and glucose is directly measured. The laser based technique is called biophotonic

and ultrasound based technique is called sonophoresis. The main limitation of this technique is the difference between glucose in the interstitial fluid and blood.

Thermal spectroscopy is also used for the detection of glucose. This technique is based on the effect of glucose present on the naturally emitted IR radiation from the body. Thermal gradient spectroscopy is used to detect the absorptive effect of glucose on body's IR.

In Ocular spectroscopy a special lens with a hydrogel of boronic acid derivatives is used. Hydrogel thickness is about 7 μm. Glucose concentration in tears is affected by the reversible covalent bonds created by the boronic acid derivative with glucose. Also, as a result of this binding phenomenon changes in reflected light wavelength can be detected if the lens is illuminated with a light source. Some patients may not be comfortable with this technique and there might be some difference between glucose in blood and in tears (30).

Chapter 3: Nanoparticles

The physicist Richard Feynman is considered as the father of nanotechnology. In 1959, Feyman's talk about manipulating and controlling individual atoms was the key to nanotechnology. The term nanotechnology was later given by Professor Norio Taniguchi. The study and application of particles in the nanoscale in all the fields is called nanotechnology or nanoscience (34). Particles of matter sized between 1 – 100 nm are considered as nanoparticles or nanomaterial. In such a small scale surface area to volume ratio become significant. This affects the physical and chemical behaviour of nanoparticles resulting in properties that differ from the bulk samples of the same material.

Nanoparticles are found in nature or can be made by humans. In nature nanoparticles include organic (proteins, polysaccharides and viruses) and inorganic compounds (iron oxyhydroxides, aluminosilicates and metals), which are produced as a result of weathering, volcano eruptions, wildfires and microbial processes natural nanoparticles are produced. Human made nanoparticles include quantum dots, carbon nanotubes, nanorods, nanocrystals, nanowires, and nanoribbons (35,36).

3.1 History

Nanoparticles existed in nature a long time ago. Nanoparticles were used by artisans as color pigments in luster and glass technology. In the 9th century nanoparticles were used by artisans in Mesopotamia to generate a glittering effect on the surface of pots. In Italy during the Renaissance Period (1450-1600AD), the people in Umbria, used nanotechnology to produce iridescent or metallic glazes. By using copper and silver metal particles, they achieved an iridescent look in their glazes due to the light bouncing off at different wavelengths. The Italians were not the only ones interested in nanotechnology. More than a thousand years ago the Chinese were creating a red color in their ceramic porcelains using gold nanoparticles as an 'inorganic dye'.

Figure 3.1: Deruta ceramicists produced by Italians (37).

One of the unusual examples of gold nanoparticles is the Lycurgus Cup which was made by the Romans in the 4th century. The Lycurgus Cup appears green in reflected light or daylight but red when light is illuminated from inside and transmitted through the glass. This unique optical property is the result of the presence of tiny amounts of colloidal gold and silver in the glass (36,38).

Figure 3.2: Lycurgus Cup in the British Museum (81).

Medieval stained glass art works are one among the most documented examples of nanotechnology known in history. Although the artists were unaware of it, they were the first nanotechnologists. They generated the ruby-red color in the windows by trapping gold nanoparticles in the 'glass matrix'. They also generated deep yellow color by trapping silver nanoparticles. Recently it has been found

that it is the size of the metal (whether it be gold or silver) nanoparticles that define the variations in colour.

Figure 3.3: Medieval Stained Glass (37).

Between AD300 and AD1700 the Damascus steel sword was made in the Middle East. These swords are known for their impressive strength, shatter resistance and exceptionally sharp cutting edge. The steel blades contain oriented nanoscale wire-and-tube-like structures, which most likely enhanced the material's properties (39).

3.2 Synthesis

Nanoparticles are classified according to their dimensions, be it in one, two or three dimensions. Thin films are considered as one dimensional nanoparticles with a size of 1 – 100 nm. One-dimensional thin films have been used for decades in many applications such as information storage, sensors, optical devices and recently in solar cells.

Two dimension nanoparticles such as carbon nanotubes (CNTs) have a diameter of 1 nm and length of 100 nm. Carbon nanotubes are made of single or multi layers of graphite that are rolled up into a cylinder. These nanotubes are excellent conductors, very strong and chemically stable.

Three dimension nanoparticles such as fullerenes (carbon 60), dendrimers and quantum dots (QDs) have many applications.

Fullerenes are made of 28 to more than a 100 carbon atoms (C_{60}) which are shaped into a spherical cage. Fullerenes can reshape again after being subjected to extreme pressure. They are being used in many applications such as solar cell's production.

Dendrimers are controlled-structure polymers with nanometric dimensions of 1 – 100 nm. Multiple functional groups are attached to their surface, which make the dendrimers suitable for drug delivery. Dendrimers are used in many pharmaceutical applications such as production of anticancer agents, antimicrobial drugs and screening agents.

Quantum dots consist of a tiny droplet of free electrons, be it single or several thousand electrons. Usually, quantum dots size range from 2 - 10 nm in diameter. Quantum dots are synthesized from many semiconductor materials such as cadmium selenide. Quantum dots are being used in fast DNA testing, drug delivery, vivo imaging, tissue engineering and information storage (40).

There are two main methods to synthesize nanoparticles, Bottom-Up and Top-Down [Fig.3.4]. In bottom-up method, nanoparticles are built from atoms or molecules. Top-down method involves breaking larger particles into nanoparticles. Nanoparticles are synthesized using a variety of materials. Synthetic method and materials are dependent on the size required, stability and surface characteristics such as charge (41).

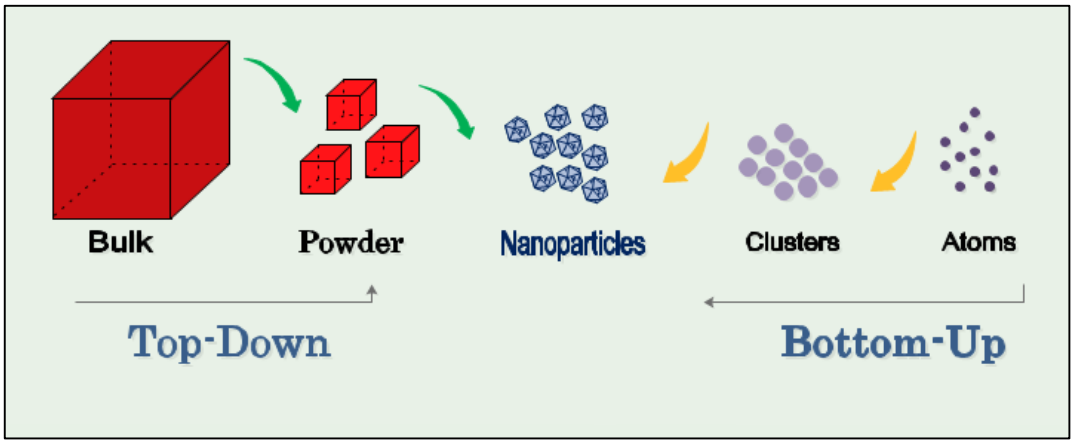

Figure 3.4: Schematic representation of Top-Down and Bottom-Up synthesis methods of nanoparticles.

There are many methods for nanoparticle synthesis, which include gas condensation, vacuum deposition & vaporization, chemical precipitation, sol-gel technique and electrodeposition.

The first method used for the production of nanocrystalline metals and alloys, was gas condensation. In this method, thermal evaporation sources are used to vaporize inorganic or metallic materials. A high residual gas pressure (greater than 3 mPa) causes a collision between evaporated atoms and residual gas molecules, leading to the formation of ultrafine particles (100 nm).

In vacuum deposition & vaporization, elements or compounds are vaporized in a process similar to gas condensation with a pressure less than 0.1 Pa, but after vaporization, they are deposited in a container with a pressure of 10 – 0.1 MPa. Ultrafine clusters (1 – 100 nm) can form by vapor phase nucleation in a dense vapor cloud by multibody collisions, where collisions and cooling for nucleation occur when atoms pass through the gas.

Another method for nanoparticle synthesis is the chemical vapor deposition. A solid is deposited during the change from a gas or a vapor. Energy is provided for reaction activation using several methods. One such is thermal energy where a high temperature above 900 ℃ is used. Another is formation of plasma at a temperature of 300 – 700 ℃. Ultraviolet radiation may also be used.

In chemical vapor condensation, at a reduced pressure a vapor of metal organic precursor's pyrolysis occurs. Mechanical attrition involves structural decomposition of coarser grained structures.

In a chemical precipitation method a precipitation technique is used to control the size. A reaction between constituent material in suitable solvent leads to the synthesis of nanoparticles. Before the precipitation reaction, a dopent is added to the parent solution. To maintain separation between formed particles a surfactant is added. The nanoparticles formed are centrifuged, washed, dried and subjected to UV.

The sol-gel technique involves the formation of a stable colloidal suspension (sol) and continuous network surrounding a liquid phase which is the gel. It includes four stages; hydrolysis, condensation, growth and agglomeration of particles. In hydrolysis, tetraethyl orthosilicate $Si(OC_2H_5)_4$ and water are mixed in ethanol. Silanols (Si-OH) are produced as intermediates. Hydrolysis of tetraethyl orthosilicate $Si(OC_2H_5)_4$ will result silicic acid $Si(OH)_4$. A catalyst such as HCl and NH_3 is used to accelerate hydrolysis and control the pH. In condensation, formation of siloxane bond is resulted due to water or alcohol production. Monomer, dimer, cyclic tetramer and high-order rings are products of condensation reaction. In the growth and agglomeration step, more siloxane bonds are formed, molecules will aggregate forming a network, which turns into a gel after drying.

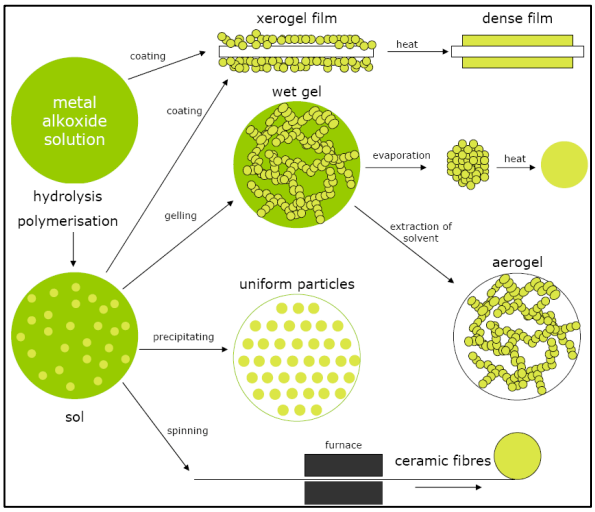

Figure 3.5: Sol-Gel technique (82).

Strong and uniform nanostructured materials are synthesized by electrodeposition. Films are produced using the electrodeposition method, while coatings are applied by the chemical vapor deposition or condensation (42,43).

The chemical reduction method is the most common method for the synthesis of nanoparticles. It is considered as a chemical method. In this method an organic or inorganic reducing agents such as citrate, ascorbate, sodium borohydride ($NaBH_4$), elemental hydrogen and Tollens reagent are used. Citrate is the most common reducing agent used, which leads to the production of size controlled monodispersed spherical nanoparticles. As a consequence of weakly bound citrate coating, the nanoparticles have a negative surface charge that is easily characterized by their plasmon resonance absorption band. Generally the reducing agent is used to reduce metal ions to an uncharged metal atom. These atoms nucleate and form clusters followed by the formation of nanoparticles. Core/Shell nanoparticles can be synthesized by synthesizing small colloidal nuclei, followed by its enlargement using a different metal. Various shells such as conductive, nonmetallic graphite or semiconductors can be used to cap metallic nanoparticles. There are many types of chemical reduction methods such as microemulsion techniques, UV-initiated photoreduction, photoinduced reduction, microwave assisted, Tollens method and irradiation method (44,45).

Synthesized nanoparticles are characterized by their size, morphology and surface charge. Microscopic techniques such as scanning electron microscopy (SEM), transmission electron microscopy (TEM) and atomic force microscopy (AFM) are used for nanoparticle analysis. Using these technique’s their average diameter, size distribution and stability can be studied (40).

3.3 Nanoparticles Applications

3.3.1 Applications in Diabetes

Nanotechnology is used for diabetes management and treatment. Glucose nanosensors such as the Layer By Layer technique (LBL), carbon nanotubes and quantum dots are used for glucose monitoring. Generally, glucose nanosensors are implanted in the skin, and they are glucose responsive and fluorescent based.

The layer by layer technique uses a very thin film each with a thickness of 10 nm built up from positively and negatively charged polymers. It's implanted in the dermis or subcutaneous tissue with the semi-permeable capsules containing and protecting sensors materials. These capsules allow the entry of glucose from interstitial fluid. Near infrared radiation is used to excite glucose sensors and the fluorescence emission detected from outside the body (46,47).

Carbon nanotubes are electrically conductive, made of graphite sheets rolled into cylinders. They can be single or multi walled nanotube. The concentration of insulin is directly related to the current in the electrode of the nanotube. Insulin concentration is monitored in real time. In the presence of glucose, insulin molecules are oxidized and the transfer of the produced electrons is detected by the sensor. As more insulin is produced, the current in the sensor increases (48).

Quantum dots size ranges from 2 – 10 nm. They are made of a semi-conductor crystal such as cadmium selenide and covered with a shell such as zinc sulphide. In several biosensors applications, quantum dots have been used as a fluorescent probe because of their high intensity fluorescence over a wide range of wavelengths (usually 20 – 40 nm) (49). The emission wavelength is dependent on the particle size (50).

Nanotechnology is used also in insulin delivery. Insulin can be delivered orally using insulin prodrugs (insulin-polymer conjugation), micelles, liposomes, solid lipid nanoparticles and nanoparticles of biodegradable polymers.

Liposomes consist of enzyme inhibitor (glycocholate), which protects insulin against enzymatic degradation by pepsin, trypsin and achymotrypsin. Recently, permeation enhancer has been developed for oral delivery of insulin, which allows insulin to cross the epithelial layer after oral administration.

Microspheres are the most promising systems for oral insulin delivery. They consist of enzyme inhibitors to protect insulin inside its matrix from enzymatic degradation and permeation enhancer that allows insulin to cross epithelial layers.

Nanopumps are used to pump insulin into the patient's body at a constant rate, balancing the glucose level.

An artificial pancreas is developed using nanotechnology. This idea was introduced in 1974. A sensor is implanted in the patient's body. This reads the glucose level and pumps insulin in response to the reading from a small reservoir into the blood. An alternative method is to use a tiny silicon box made of animal pancreatic beta cells with 20 nm diameter nanopores. These pores allow the passage of glucose and insulin only (51).

3.3.2 Other Applications

Nanoparticles are being used in many field's including energy, electronics, manufacturing and medicine (52).

In medicine, nanoparticles are used to improve quality in imaging, cancer treatment, tumor destruction, drug delivery, implants, antimicrobials and protein detection (53).

Silver nanoparticles have unique antibacterial, conductive and optical properties. In the diagnostic field, silver nanoparticles are used as biological tags in biosensors. Because of their antibacterial properties, silver nanoparticles are used in paints, plastics, cosmetics and wound dressings. Also, silver

nanoparticles are used in conductive inks and integrated into composites to improve thermal and electrical conductivity. In the optical field silver is used to enhance light and improve optical spectroscopies (54).

Gold nanoparticles are used in the diagnostic field to detect heart disease, cancer, infection and uric acid sensing (55). Also, it is used to coat therapeutic delivery agents. Gold nanoparticles are used as sensors, probes and conductors. In some chemical reactions, gold nanoparticles are being used as catalysts. Gold nanoparticles are used in cancer treatments because nanoshells and nanorods absorb near IR and heat up rapidly killing the tumor cells (56).

Chapter 4: Experimental Methods

4.1 Synthesis

Different methods were followed in order to find the cheapest and the easiest method for synthesizing gold, silver and gold-silver nanoparticles, and to find the most suitable and accurate method for detecting and quantifying glucose levels. Generally, nanoparticles are synthesized using a reduction method. A reducing agent is used to reduce silver and gold. In wet chemistry methods, trisodium citrate is used as a reducing agent, while in green synthesis method's curcumin, hibiscus, gripe water, coffee, tea and glucose are used as reducing agents. General chemical reactions for gold and silver are given below.

$$Ag^{+} + \text{reducing agent} \rightarrow Ag^{0}$$

$$Au^{+3} + 3e^{-} \rightarrow Au$$

Gold-silver/core-shell (Au-Ag) nanoparticles are made of gold core surrounded by silver shell. General chemical reaction for gold-silver/core-shell (Au-Ag) nanoparticles is given below (57)

$$3Ag + AuCl_4^{-} \rightarrow Au + 3Ag^{-} + 4Cl^{-}$$

The glucose concentrations used were less than 30 mM in order to prevent saturation as glucose is capped at the surface of nanoparticles and a limited amount of surface area is available. At a higher glucose concentration excess glucose will not be able to interact with nanoparticles surface (58). In some synthetic methods, the size of the nanoparticles increases linearly with glucose concentration, as explained in (59). In other methods as the concentration of glucose increases, nanoparticles with smaller sizes are synthesized, as explained in (58). The size and the shape of the nanoparticles are dependent on the nature and the concentration of the capping agents and other factors like the solvent used and the pH value. Nanoparticle's size affects the surface plasmon resonance band, whereas the size of the nanoparticles increases, the SPR band absorbance increases and peak position shifts towards longer wavelengths (red

shift) (60). Furthermore, according to Unser, et al. (58), as the size of the nanoparticles decreases, the SPR band absorbance decreases and peak position shifts to shorter wavelengths (blue shift). Capping agents stabilize and restrict the growth of the nanoparticles. Thus as the concentration of the capping agent increases, nanoparticles with smaller sizes obtained. (61). In some cases glucose acts as a capping agent, in such cases negative relation between the absorbance/peak position shift (blue shift) of the surface plasmon resonance band and the glucose concentration is observed.

4.1.1 Preparation of Silver Nanoparticles

Green Synthesis

Synthesis of silver nanoparticles (AgNPs) using glucose and starch:

Silver nanoparticles were synthesized by mixing 200 µL of 0.1 M $AgNO_3$ with 500 µL of 0.1 M glucose in a flask. Then 10 mL of 0.2 % starch was added. The solution was heated to boiling temperature and left boiling for 10 minutes. Color changed to yellow, and it was allowed to cool to room temperature.

$$2AgNO_3 + C_6H_{12}O_6 + H_2O \rightarrow 2Ag + 2HNO_3 + C_6H_{12}O_7$$

In this reaction, silver is reduced by glucose forming silver metals. Formed silver nanoparticles are coated by starch to prevent aggregation (62).

Synthesis of silver nanoparticles (AgNPs) using coffee and tea:

Both coffee and tea consist of caffeine and polyphenols. Caffeine and polyphenols act as reducing and capping agents. Silver is reduced by coffee or tea and nanoparticles are formed. Then both the coffee and tea act as a capping and stabilizing agent to prevent aggregation (63).

Silver nanoparticles were synthesized using coffee, by dissolving 0.4 g of coffee (Nescafe Red Mug) in 50 mL of water and adding 10 mL of coffee extract to 2 mL of 0.1 M $AgNO_3$. The mixture was shaken and left in room temperature to settle.

The same procedure was used for the synthesis of silver nanoparticles using tea, by boiling 1 g of tea (Ahmed Tea English Breakfast) in 50 mL of water and filtering it using 25 µL Teflon filter. Add 10 mL of tea extract to 2 mL of 0.1 M $AgNO_3$. The mixture was shaken and left in room temperature to settle.

Synthesis of silver nanoparticles (AgNPs) using hibiscus:

Three different methods were used to synthesize silver nanoparticles using hibiscus. The reduction of silver nitrate and silver nanoparticles formation is carried out at a pH 6.8.

Hibiscus leaves (1 g) washed and boiled in 10 mL of distilled water for 5 minutes. The extract is centrifuged at 1000 rpm for 5 minutes. Using Whatman No.1 filter paper the solution was filtered. The resulting extract (0.6 mL) of hibiscus extract was mixed with 30 mL of 5 mM $AgNO_3$. The mixture stirred for 2 minutes at 30 ℃. A reddish solution obtained after 40 minutes [Fig. 4.1] (64).

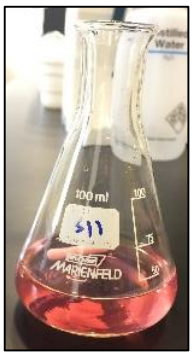

Figure 4.1: Silver nanoparticles synthesized using hibiscus.

Another method was used to synthesize silver nanoparticles using hibiscus. A sample was prepared by stirring 20 g of hibiscus in 200 mL of water

for 30 minutes and filtering the extract. Then 2 mL of hibiscus extract was vigorously stirred with 2.5 mL of 0.8 mM $AgNO_3$ for 1 minute. NaOH was used to adjust the pH to 6.8. The color of the solution turned into golden yellow (65).

In third method the hibiscus extract was prepared by boiling 1 g of hibiscus in 10 mL of water, then filtering and centrifuging at 6000 rpm for 20 minutes. A hibiscus extract (2 mL) was mixed with 18 mL of 1 mM $AgNO_3$ and stirred overnight. Color changed from brown to red [Fig. 4.2] (66).

Figure 4.2: Silver nanoparticles synthesized using hibiscus.

Synthesis of silver nanoparticles (AgNPs) using curcumin:

In this method, 0.019 g of curcumin was dissolved in 1 mL of ethanol and distilled water added to a volume of 15 mL. Then 10 mL of 1 mM $AgNO_3$ were mixed with 2 mL of curcumin and placed in an oven at a temperature of 90 ℃ for 120 minutes. In this reaction, the keto-enol group of curcumin reduced silver into silver nanoparticles and act as capping agent (67).

Synthesis of silver nanoparticles (AgNPs) using glucose and gelatin:

Silver nanoparticles were synthesized using glucose and gelatin. To prepare a 1 M $AgNO_3$, 1.7 g of $AgNO_3$ were dissolved in 10 mL of distilled water. 1.5 mL of 1% wt. gelatin, 10 mL of 1 M $AgNO_3$ and 0.5 mL of 1 M NaOH were added in a

flask. The mixture was heated to 50 ℃ using a preheated hot plate. Heating was continued to boiling for about 1.10 – 1.55 minutes. A dark brown color was observed. Following that 10 mL of glucose (0.001, 0.01, 0.1, 1, 5, 10 and 20 mM) was added to the solution and heating continued until it boils for about 1.10 – 1.50 minutes. Then the solution was allowed to cool to room temperature. Finally the mixture was centrifuged at 6,000 rpm for 5 minutes.

$$Ag^{+} + gel \rightarrow [Ag(gel)]^{+}$$

$$2\left[(Ag(gel)^{+}\right] + 2OH^{-} + C_5H_{11}O_5\text{-}CHO \rightarrow 2Ag + 2gel + H_2O + C_5H_{11}O_5$$

In this reaction, a gelatinous complex is formed after mixing silver with gelatin. The silver ions in the gelatinous complex are reduced by glucose and react with OH^{-} to form silver nanoparticles. At the same time, glucose is oxidized forming gluconic acid (68).

Figure 4.3: Silver nanoparticles synthesized using different concentrations of glucose and gelatin.

<u>Synthesis of silver nanoparticles (AgNPs) using gripe water:</u>

Silver nanoparticles was prepared by mixing 6 mL of 0.6 mM $AgNO_3$ with 10 mL of gripe water. Gripe water acts as a reducing and a stabilizing agent. The solution stirred for 22 hours, and the color changed to a yellowish color [Fig. 4.4] (69). This method was successful for synthesizing nanoparticles, but not successful in the detection of glucose due to instability of the produced silver nanoparticles and may be due to the existence of different compounds in gripe water.

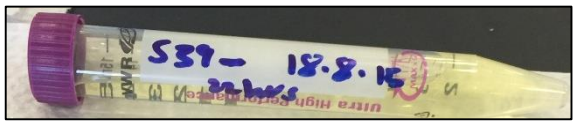

Figure 4.4: Silver nanoparticles synthesized using gripe water.

Wet chemistry

Synthesis of silver nanoparticles (AgNPs) using trisodium citrate:

In this method, 0.0849 g of $AgNO_3$ was dissolved in 500 mL of water, and the solution heated to boiling. 5 mL of 1 % trisodium citrate was added dropwise while the solution was mixing vigorously. The mixture was left on a hot plate for two hours. A greenish solution was observed (70) as shown in Fig. 4.5. Then the prepared silver nanoparticles were mixed with different concentrations of glucose (2, 6, 10, 15, 20 and 30 mM).

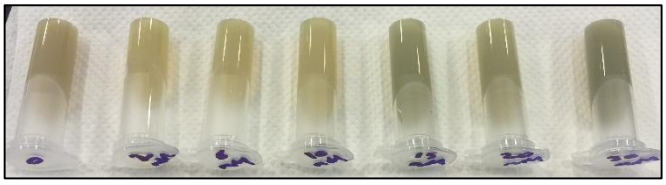

Figure 4.5: Silver nanoparticles synthesized using trisodium citrate and mixed with different concentrations of glucose.

In this reaction, silver nitrate is reduced by trisodium citrate to form silver nanoparticles (71).

$$4Ag^{+} + C_6H_5O_7Na_3 + 2H_2O \rightarrow 4Ag^{0} + C_6H_5O_7H_3 + 3Na^{+} + H^{+} + O_2\uparrow$$

Synthesis of silver nanoparticles (AgNPs) using $AgNO_3$, glucose and NaOH:

2 mM $AgNO_3$ was prepared by dissolving 1.7 mg of $AgNO_3$ in 5 mL of distilled water. In this method, 500 µL of different glucose concentrations (1, 2, 4, 7, 9, 10, 20 and mM) were mixed with 10 µL of 1 M NaOH while vortexing. After 10 seconds, 500 µL of 2 mM $AgNO_3$ was added. Color changes within 1 minute, and

vortexing continued to ensure reaction completion (58). The yellowish color observed and as glucose concentration increases, a darker yellow color is observed as shown in Fig. 4.6.

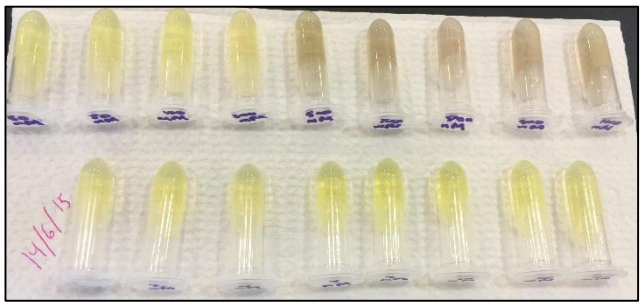

Figure 4.6: Silver nanoparticles synthesized using $AgNO_3$, different concentrations of glucose and NaOH.

4.1.2 Preparation of Gold Nanoparticles

Green Synthesis

Synthesis of gold nanoparticles (AuNPs) using curcumin:

In this method, 3.68 mg of curcumin were dissolved in 2 mL of 10 mM NaOH and volume raised to 10 mL using distilled water.1 mM of $HAuCl_4$ was prepared by dissolving 2.4 mg of $HAuCl_4$ in 6 mL of distilled water. 6 mL of 1 mM $HAuCl_4$ was added to 8 mL of water. Then 6 mL of curcumin was added to the mixture dropwise. The mixture was allowed to stir for 2 hours and color changed from yellow to red [Fig. 4.8]. As Shown in Fig. 4.7 in this reaction gold chloride is reduced by curcumin carbonyl group. Curcumin functional groups such as hydroxyl and carbonyl stabilize gold nanoparticles. Gold nanoparticles synthesized using curcumin are stable for three months (72).

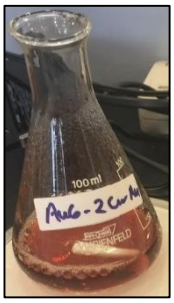

Figure 4.8: Gold nanoparticles synthesized using curcumin.

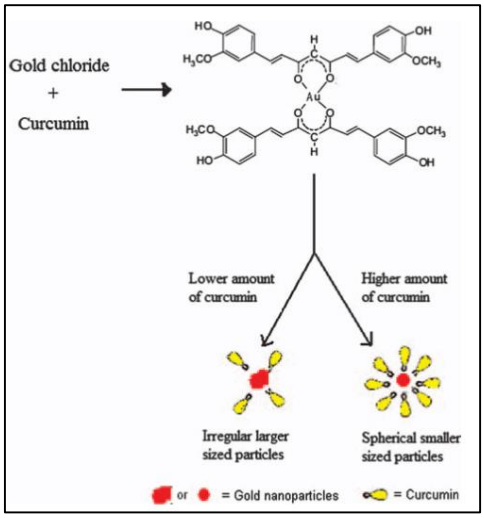

Figure 4.7: Formation mechanism of gold nanoparticles synthesized using curcumin (70).

According to Sindhu, et al. (73) this reaction [Fig 4.9] consists of six steps:

1) Deprotonation: curcumin form Cur^{-3}due to hydrogen dissociation from its hydroxyl and α-hydrogen's groups.

2) Reduction: Au^{+3} is recued to Au^{0} by curcumin O^{-} electrons.

3) Nucleation: Au^{0} atoms nucleates and form clusters.

4) Growth: bigger clusters are formed as more Au^{0} atoms added to the surface.

5) Cleavage: clusters size leads to instability and it cleaves into smaller fragments.

6) Maturation: spherical and solid curcumin conjugated gold nanoparticles are formed (73).

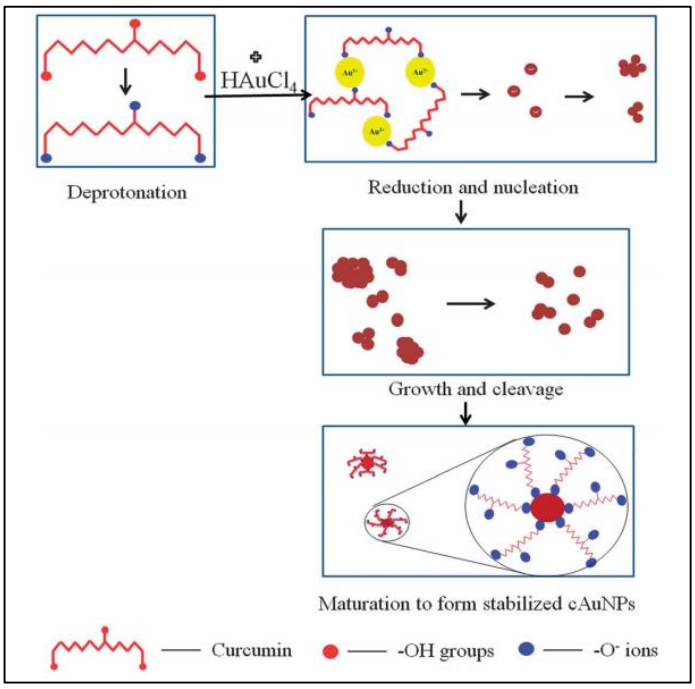

Figure 4.9: Synthesis mechanism of Curcumin conjugated gold nanoparticles (68).

Synthesis of gold nanoparticles (AuNPs) using starch and glucose:

For the preparation of 0.5 mM $HAuCl_4$, 1 mg of $HAuCl_4$ were dissolved in 5 mL of distilled water. To synthesize gold nanoparticles, 5 mL of 0.5 mM $HAuCl_4$, 5 mL of glucose of different concentrations (1, 5, 10, 15 and 20 mM), 5 mL of 0.6 % starch and 20 mL of phosphate (KH_2PO_4 pH 7) buffer were mixed. The mixture was heated in an oven for 1 – 2 hours at 80 ℃. In this reaction gold was reduced from Au^{+3} to Au^0 by glucose, starch and phosphate buffer (74).

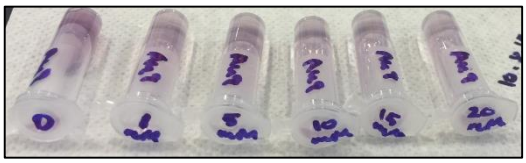

Figure 4.10: Gold nanoparticles synthesized using starch and glucose mixed with different concentrations of glucose.

Synthesis of gold nanoparticles (AuNPs) using glucose and gelatin:

This method is the best, easiest and most accurate. The procedure is a modification of method [silver nanoparticles (AgNPs) synthesized using glucose and gelatin]. 10 mM $HAuCl_4$ was prepared by dissolving 19.7 mg of $HAuCl_4$ in 5 mL of distilled water. In a test tube, 68.4 µL of 1% wt. gelatin, 22.8 µL of 1 M NaOH, 454.6 µL of glucose (1, 2, 3, 5, 6, 7, 9, 11, 12 and 14 mM) and 454.6 µL of 10 mM $HAuCl_4$ were added respectively. Then the test tube placed in the center of the microwave [Samsung – Model: ME6124ST]. The mixture was heated for 30 seconds at low power (power 2) and allowed to cool to room temperature for further analysis. A color change is observed, from colorless to red indicating the formation of gold nanoparticles. As shown in Fig. 4.11 red color varies depending on the glucose concentration. As the glucose concentration increases, a darker red color is obtained. In this reaction, glucose reduces gold chloride to gold atoms, while gelatin stabilizes them.

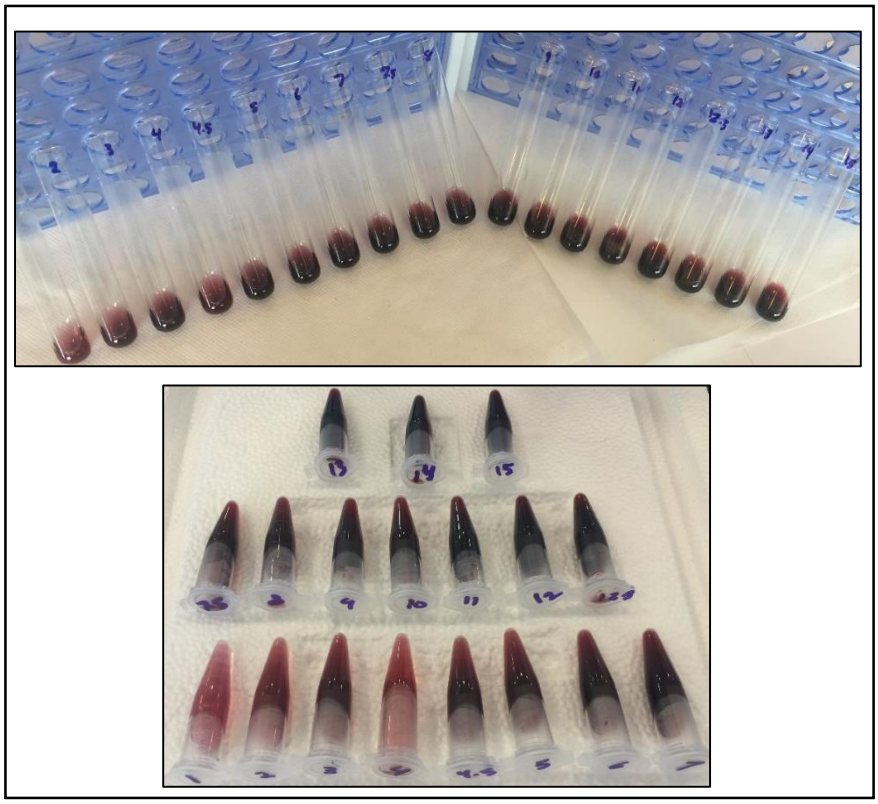

Figure 4.11: Gold nanoparticles Synthesized using different concentration of glucose and gelatin.

Wet chemistry

Synthesis of gold nanoparticles (AuNPs) using trisodium citrate:

For the preparation of 1 mM $HAuCl_4$, 7.9 mg of $HAuCl_4$ were dissolved in 20 mL of distilled water. 20 mL of 1 mM $HAuCl_4$ was stirred and heated to boiling. Then 2 mL of 1 % trisodium citrate was added. The solution was left boiling until the color changes to deep red [Fig. 4.12]. Gold is reduced from Au^{+3} to Au^0 by trisodium citrate (75). Chemical equation is given below (76)

$$Au^{+3} + 3e^- \rightarrow Au$$

$$2HAuCl_4 + 4Na_3C_6H_5O_7 \rightarrow H_2 + 2Au^0 + 4CO_2 + 4NaC_5H_5O_5 + 8NaCl$$

Figure 4.12: Gold nanoparticles synthesized using trisodium citrate.

Synthesis of gold nanoparticles (AuNPs) using glucose, NaOH and $HAuCl_4$:

0.2 mM of $HAuCl_4$ was prepared by dissolving 0.4 mg of $HAuCl_4$ in 5 mL of distilled water. In this method, 500 µL of glucose (1, 2, 3.5, 4.5 and 5.5) placed in a small tube, then 10 µL of 1 M NaOH was added to it while vortexing. After 10 seconds 500 µL of 0.2 mM $HAuCl_4$ was added. A color change was observed within 1 minute and vortexing continued for another 10 seconds to ensure a completed reaction. Sample with lower glucose concentration the color changed into purple, while higher glucose concentration samples color changed to red [Fig. 4.13]. In this reaction, glucose is used to reduce gold ions into gold nanoparticles and as a capping agent to prevent aggregation (58).

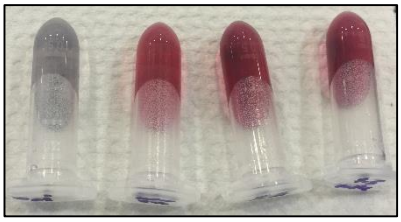

Figure 4.13: Gold nanoparticles synthesized using different concentrations of glucose, NaOH and $HAuCl_4$. Left is lower glucose concentration and right is higher glucose concentration.

4.1.3 Preparation of Gold-Silver (Au-Ag/core-shell) Nanoparticles

Green Synthesis

Synthesis of gold-silver nanoparticles (Au-Ag/core-shell NPs) using gripe water:

Gripe water causes successive reduction of $HAuCl_4$and $AgNO_3$, resulting the formation of gold-silver nanoparticles. Nanoparticles are stabilized by sodium benzoate, sodium methyl paraben, sodium propylparaben and bronopol that is present in gripe water, while Au and Ag nanoparticles are reduced by sodium bicarbonate and sucrose (77). For gold-silver nanoparticles synthesis 2 mL of 0.3 mM $HAuCl_4$ stirred in a flask. In another flask 2 mL of 0.3 mM $AgNO_3$ mixed with 10 mL gripe water. Under continuous stirring the mixture was added to $HAuCl_4$ and stirred for 1 hour [Fig 4.14]. Same method was repeated but the mixture was stirred for 22 hours [Fig. 4.15]. This method was successful for synthesizing nanoparticles, but not successful in the detection of glucose due to instability of the produced gold-silver nanoparticles and may be due to the existence of different compounds in gripe water.

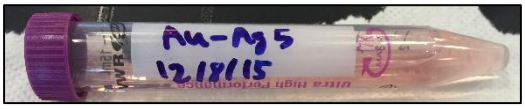

Figure 4.14: Gold-silver nanoparticles synthesized using gripe water, stirred for 1 hour.

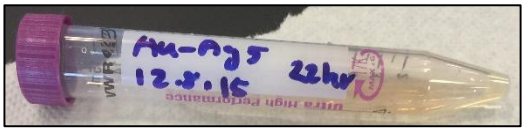

Figure 4.15: Gold-silver nanoparticles synthesized using gripe water, stirred for 22 hours.

Synthesis of gold-silver nanoparticles (Au-Ag/core-shell NPs) using $AgNO_3$, $HAuCl_4$ and glucose:

In this method, 500 µL of glucose (different concentrations 1 - 30 mM) were placed in small tube and 10 µL of 1 M NaOH was added while vortexing. After 10 seconds 200 µL of 0.2 mM $AgNO_3$ and 200 µL of 0.2 mM $HAuCl_4$ were added to the mixture. After 5 – 60 seconds the color changes to pinkish (58) as shown in Fig. 4.16. Different glucose concentrations were used.

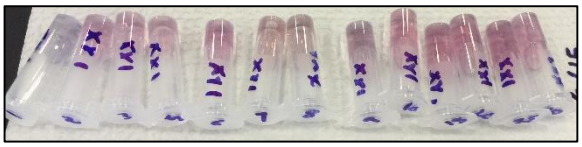

Figure 4.16: Gold-silver nanoparticles using $AgNO_3$, $HAuCl_4$ and different concentration of glucose.

Wet chemistry

Synthesis of gold-silver nanoparticles (Au-Ag/core-shell NPs) using $HAuCl_4$, $AgNO_3$, NaOH and L-ascorbic acid:

This method consists of two steps. First 0.5 mM of $HAuCl_4$ was prepared by dissolving 0.02 g of $HAuCl_4$ in 100 mL of distilled water. Gold nanoparticles were synthesized by boiling 95 mL of 0.5 mM $HAuCl_4$ at 60 ℃, followed by adding 5 mL of 0.5 % trisodium citrate and boiling continues for another 15 minutes. 100 mM $AgNO_3$ was prepared by dissolving 0.085 g $AgNO_3$ in 5 mL of water. Next

step was the mixing of 10 mL of gold nanoparticles, 60 µL of 100 mM L-ascorbic acid, 15 µL of 100 mM $AgNO_3$and 75 µL of 100 mM NaOH to increase the pH. The mixture allowed to stir for 30 minutes. The L-ascorbic acid, $AgNO_3$ and NaOH were added 3 times every 30 minutes. Finally, the solution was centrifuged at 1800 rpm, a temperature of 22 ℃ for 20 minutes and filtered (78). Gold-silver nanoparticles were mixed with different concentration of glucose 1, 2, 3, 4 and 5 mM.

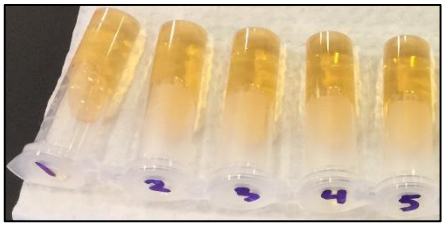

Figure 4.17: Gold-silver nanoparticles synthesized using $HAuCl_4$, $AgNO_3$, NaOH and L-ascorbic acid.

4.2 Characterization

Following the synthesis of nanoparticles, the characterization was performed by recording absorption spectra, which gives information about the surface plasmon resonance band (SPR), sizes and shapes of the nanoparticles. UV-Vis spectrometer Shimadzu UV-1800 was used to record absorption spectra of the samples. Due to nanoparticles unique optical properties, UV-Vis spectroscopy may be used to identify the types of the synthesized nanoparticles. Where nanoparticles synthesized from particular metals, interact strongly with specific wavelengths of light, resulting a surface plasmon resonance band centered at specific wavelength (79). Silver nanoparticles surface plasmon resonance peak ranges from 400 to 530 nm (80), while for gold nanoparticles surface plasmon resonance peak ranges from 515 to 570 nm depending on the size of the nanoparticles (81). Surface plasmon resonance band is also dependent on the shape of the nanoparticles. Spherical nanoparticles exhibit a surface plasmon resonance band of only one peak, while the surface plasmon resonance band of non-spherical shapes such as rod nanoparticles exhibits two peaks. For non-spherical nanoparticles the resonance wavelength depends on the orientation of the particle relative to the orientation of the electric field. Therefore, a collection of nanoparticles can show longitudinal and transvers plasmon resonances (82). Transmission electron microscopy (TEM) was used to confirm the formation of nanoparticles and their shapes. ImageJ 1.5g software was used to determine the size distribution of nanoparticles from the TEM images. Mie plot software also used to estimate the diameter of the nanoparticles by comparing the theoretical and the experimental absorption spectra.

4.2.1 Silver Nanoparticles

Silver nanoparticles (AgNPs) synthesized using curcumin:

[Fig. 4.18] shows the absorption spectrum of the silver nanoparticles that were synthesized using curcumin as a reducing agent [section 4.1.1]. The formation of nanoparticles was confirmed by the presence of a surface plasmon resonance band centered at 433 nm (black line). The absorption spectrum of the sample was taken after one day shows a different absorption peak and a spectrum broadening (red line). This indicates the existence of silver nanoparticles with different size distribution or nanoparticles aggregation, which may be due to curcumin's low stability (67).

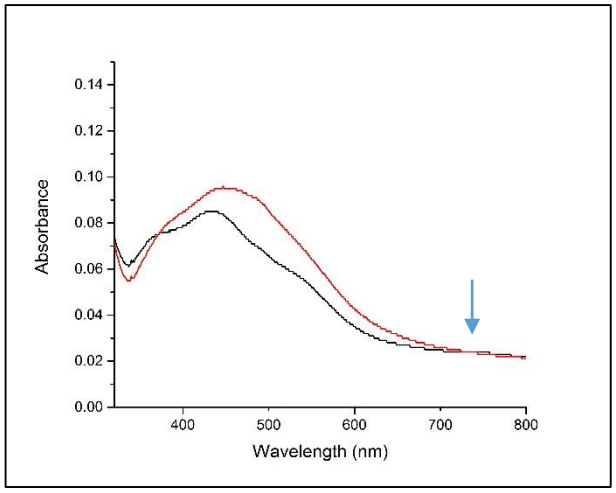

Figure 4.18: UV-Vis absorption spectra of silver nanoparticles prepared using curcumin. λ_{max}=433 nm. The arrow indicates the reference point for the determination of the height of the absorbance.

[Fig. 4.19] is the TEM images of silver nanoparticles. The size distribution of nanoparticles was analyzed using ImageJ 1.5g, software. This is performed by converting pixels on the TEM images into nanometers by applying the scale of the image. Each nanoparticle was marked manually. Polydisperse silver nanoparticles were observed, and the diameter was found to range between 3.5 – 44 nm, with a high yield of size 16.8 nm.

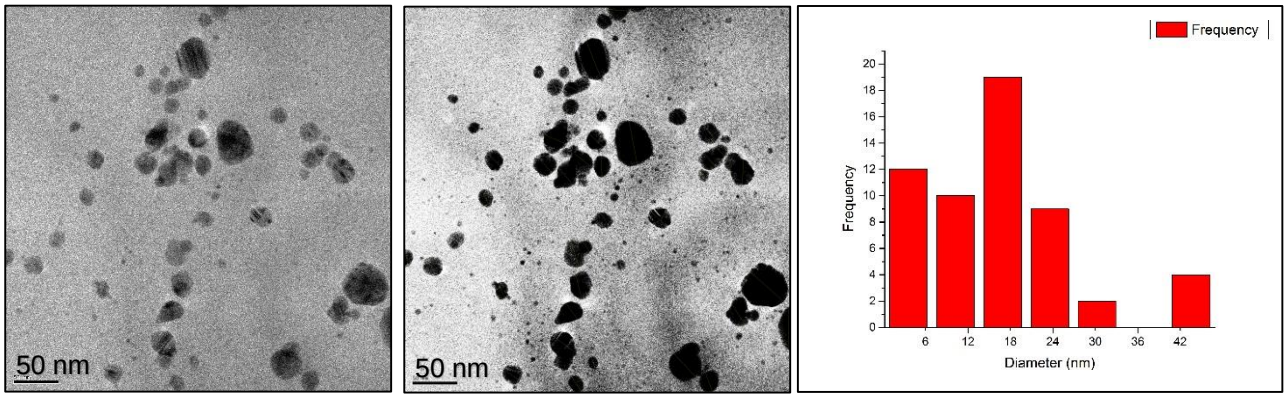

Figure 4.19: TEM image and corresponding size distribution histogram of silver nanoparticles synthesized using curcumin.

Silver nanoparticles (AgNPs) synthesized using trisodium citrate:

[Fig. 4.21] shows the absorption spectrum of the silver nanoparticles that were synthesized using trisodium citrate as a reducing agent and mixed with different concentrations of glucose (2, 6, 10, 20 and 30 mM) [section 4.1.1]. The formation of nanoparticles was confirmed by the presence of a surface plasmon resonance band centered at 420 nm (black line). The absorption spectrum of the sample was taken each day for five days and no peak broadening was observed, which indicates silver nanoparticles stability [Fig. 4.20]. [Fig. 4.22] demonstrates a linear inverse proportional relation between the absorbance of silver nanoparticles surface plasmon resonance (SPR) band with glucose concentration. A small shift in surface plasmon resonance band peak position towards shorter wavelengths (blue shift) is observed as the concentration of glucose increases [Fig. 4.23]. This may be due to different sizes of nanoparticles as shown in TEM images [Fig. 4.24]. Negative correlation between the absorbance/peak position shift of silver nanoparticles surface plasmon resonance (SPR) band and the glucose concentration indicates that the size of the nanoparticles decreases as the concentration of glucose increases [refer to section 4.1]. Hence, both absorbance and peak position of silver nanoparticles surface plasmon resonance (SPR) band can be used for the determination of glucose concentrations.

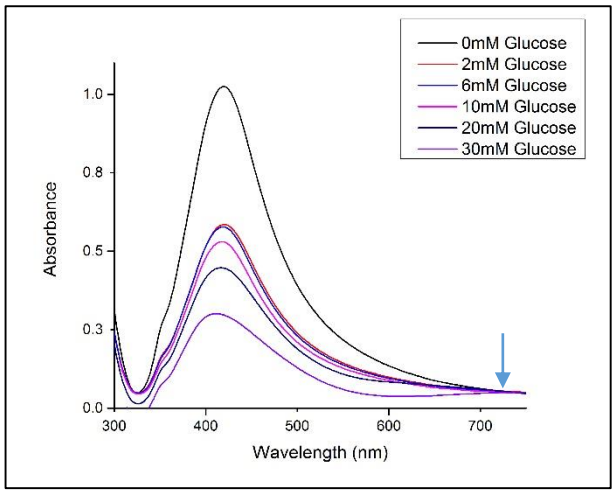

Figure 4.21: UV-Vis absorption spectra of silver nanoparticles synthesized using trisodium citrate mixed with different glucose concentrations at λ_{max}=420 nm. The arrow indicates the reference point for the determination of the height of the absorbance.

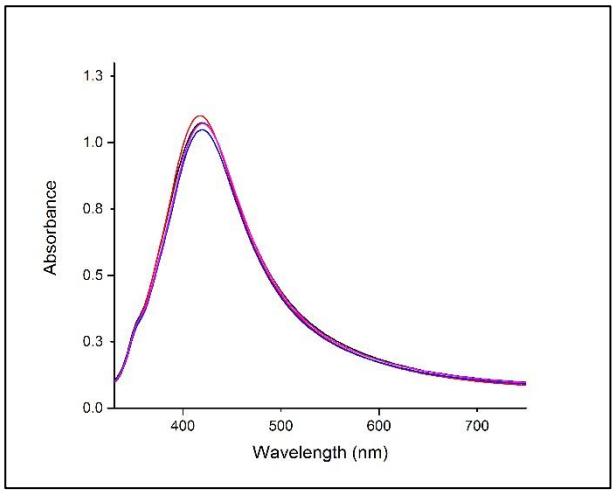

Figure 4.20: UV-Vis absorption spectrums of silver nanoparticles synthesized using trisodium citrate for five days.

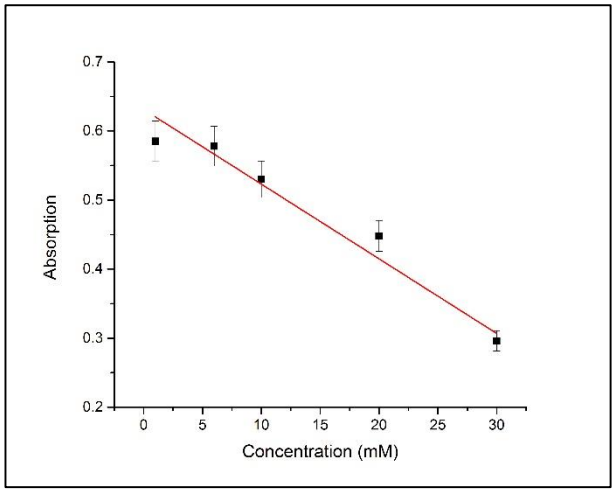

Figure 4.22: UV-Vis absorption spectra of silver nanoparticles synthesized using trisodium citrate changes in absorbance at different glucose concentrations.

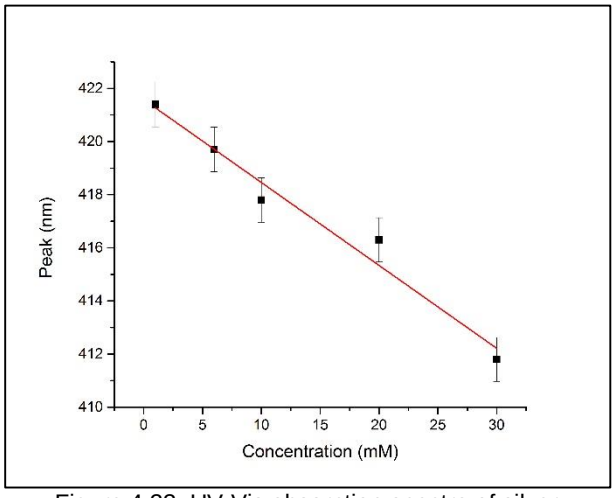

Figure 4.23: UV-Vis absorption spectra of silver nanoparticles synthesized using trisodium citrate changes in peak wavelength at different glucose concentrations.

[Fig. 4.24] is the TEM images of silver nanoparticles. The size distribution of nanoparticles was analyzed using ImageJ 1.5g, software. This is performed by converting pixels on the TEM images into nanometers by applying the scale of the image. Each nanoparticle was marked manually. Polydisperse silver nanoparticles were observed, and the diameter was found to range between 3.5 – 50 nm, with a high yield of size 3.6 nm.

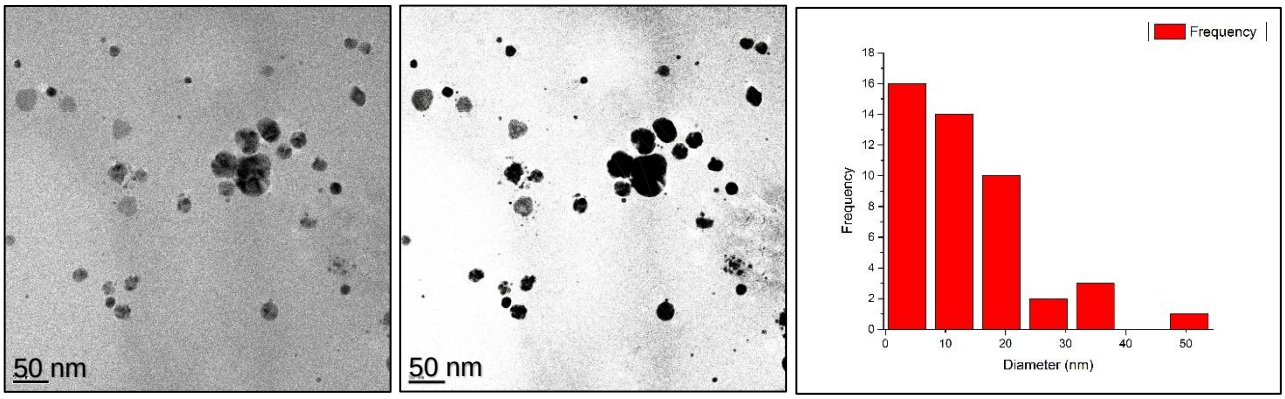

Figure 4.24: TEM image and corresponding size distribution histogram of silver nanoparticles synthesized using trisodium citrate.

Silver nanoparticles (AgNPs) synthesized using glucose and gelatin:

[Fig. 4.25] shows the absorption spectrum of the silver nanoparticles that were synthesized using glucose (1, 5, 10 and 20 mM) as a reducing agent [section 4.1.1]. The formation of nanoparticles was confirmed by the presence of a surface plasmon resonance band centered at 400 nm. The absorption spectrum of a sample was taken each day for five days and a small peak broadening observed, which indicates the existence of silver nanoparticles with different size distribution or nanoparticles aggregation (blue line) [Fig. 4.26]. As shown in [Fig. 4.27] the peak position of silver nanoparticles surface plasmon resonance (SPR) band shifts towards shorter wavelengths (blue shift) as the concentration of glucose increases. This indicates that the size of the nanoparticles decreases as the concentration of glucose increases [refer to section 4.1]. Therefore, the peak position (shift) of silver nanoparticles surface plasmon resonance (SPR) band can be used for the determination of glucose concentrations.

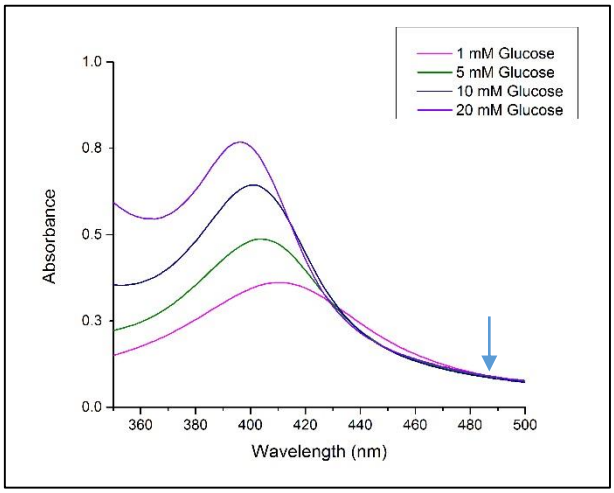

Figure 4.25: UV-Vis absorption spectra of silver nanoparticles synthesized with different glucose concentrations and gelatin. The arrow indicates the reference point for the determination of the height of the absorbance.

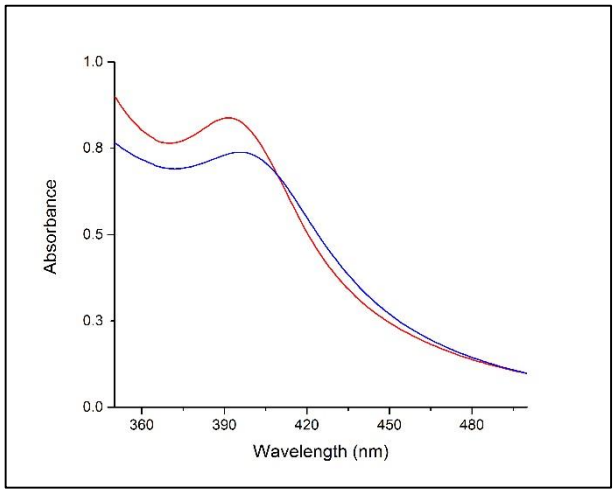

Figure 4.26: UV-Vis absorption spectrums of silver nanoparticles synthesized using 5mM glucose and gelatin after five days.

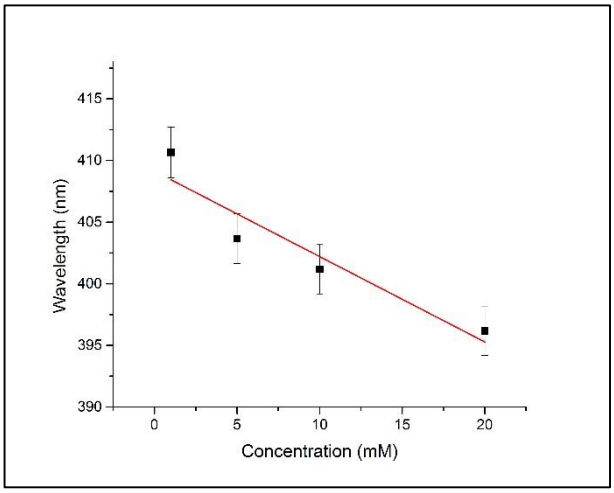

Figure 4.27: UV-Vis absorption spectra of silver nanoparticles synthesized using different glucose concentrations and gelatin changes in absorbance.

[Fig. 4.28] is the TEM images of silver nanoparticles. The size distribution of silver nanoparticles was analyzed using ImageJ 1.5g, software. This is performed by converting pixels on the TEM images into nanometers by applying the scale of the image. Each nanoparticle was marked manually. Polydisperse silver

nanoparticles were observed and the diameter was found to range between 4 – 15 nm, with a high yield of size 4 nm.

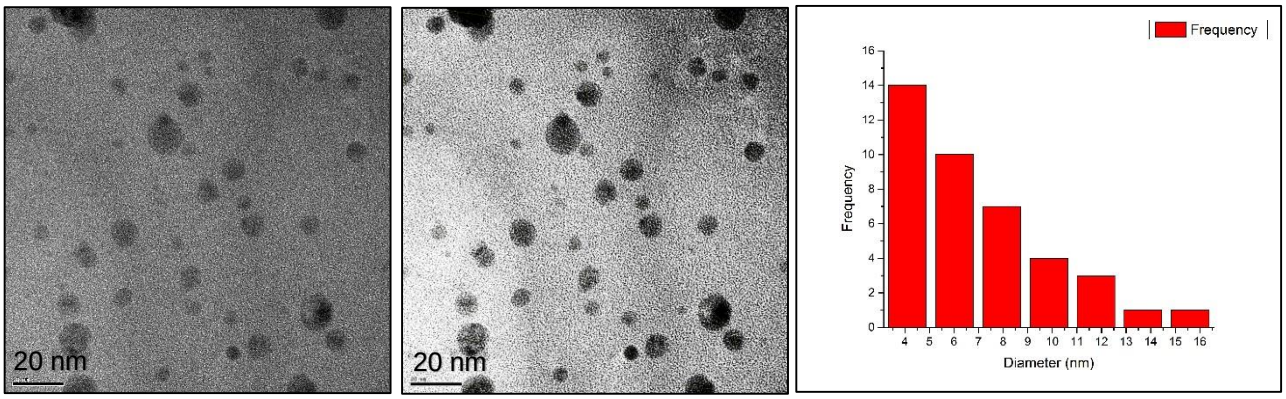

Figure 4.28: TEM image and corresponding size distribution histogram of silver nanoparticles synthesized using 8 mM glucose and gelatin.

Silver nanoparticles (AgNPs) synthesized using $AgNO_3$, glucose and NaOH:

[Fig. 4.30] shows the absorption spectrum of the silver nanoparticles that were synthesized using glucose (1, 2, 4, 7, 9, 10, 20 mM) as a reducing agent [section 4.1.1]. The formation of nanoparticles was confirmed by the presence of a surface plasmon resonance band centered in the range of 404 - 428 nm depending on the concentration of glucose. [Fig. 4.29] demonstrates a linear inverse proportional relation between the peak position (blue shift) of silver nanoparticles surface plasmon resonance (SPR) band and the glucose concentration, this indicates that as the concentration of glucose increases, the size of the nanoparticles decreases [refer to section 4.1]. Thus, the peak position (shift) of silver nanoparticles surface plasmon resonance (SPR) band can be used for the determination of glucose concentrations.

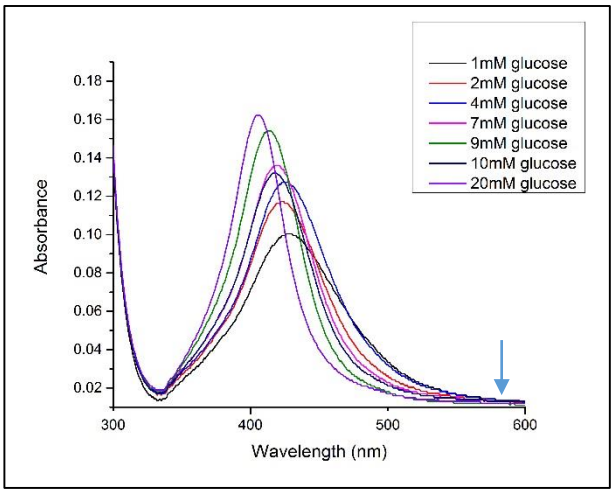

Figure 4.29: UV-Vis absorption spectra of silver nanoparticles synthesized using different glucose concentrations, NaOH and $AgNO_3$. The arrow indicates the reference point for the determination of the height of the absorbance.

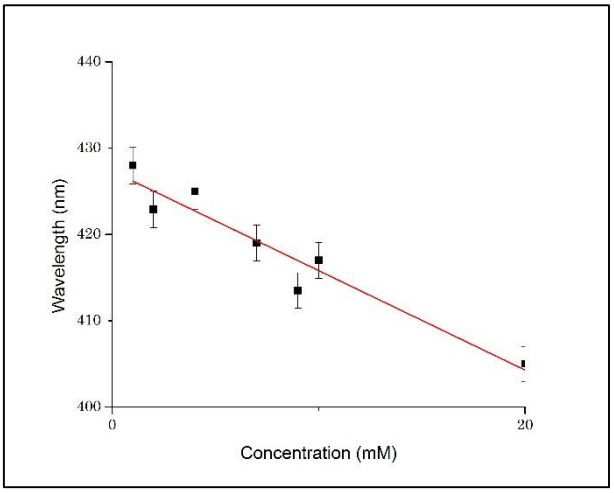

Figure 4.30: UV-Vis absorption spectra of silver nanoparticles synthesized using different glucose concentrations, NaOH and $AgNO_3$ changes in peak wavelength.

Mie plot software was used to estimate the diameter of silver nanoparticles synthesized using 1 mM of glucose. The procedure was performed as described in (83). The position of the surface plasmon resonance peak depends on the diameter of nanoparticles. A number of calculations were performed at different diameters of nanoparticles and the calculated data (theoretical) was compared and fitted to the experimental absorption data using Origin9 software. From the fit, the size of silver nanoparticles was measured and found to be 65 nm [Fig. 4.31]. This may not be the real value due to the existence of nanoparticles with different sizes in the synthesized sample. In Fig 4.31, the first sharp peak at 377 nm corresponds to the quadrupole plasmon resonance (small particles), while the second peak at 428 nm corresponds to the dipole plasmon resonance (83).

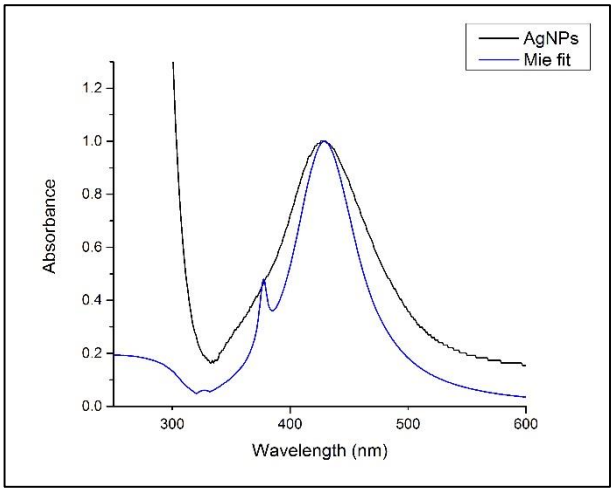

Figure 4.31: Comparison of theoretical and experimental absorption spectrums of silver nanoparticles synthesized using 1mM glucose, NaOH and $AgNO_3$.

4.2.2 Gold Nanoparticles

Gold nanoparticles (AuNPs) synthesized using trisodium citrate:

[Fig. 4.33] shows the absorption spectrum of the gold nanoparticles that were synthesized using trisodium citrate as a reducing agent and mixed with different concentrations of glucose (1, 3, 6, 8 and 10 mM) [section 4.1.2]. The formation of nanoparticles was confirmed by the presence of a surface plasmon resonance band centered at 517 nm (black line). No peak broadening was observed for three days which indicates gold nanoparticles stability [Fig. 4.32]. [Fig. 4.34] demonstrates a linear inverse proportional relation between the absorbance of gold nanoparticles surface plasmon resonance band and the glucose concentration, this indicates that as the concentration of glucose increases, the size of the nanoparticles decreases [refer to section 4.1]. Therefore, the absorbance of gold nanoparticles surface plasmon resonance band can be used for the determination of glucose concentrations.

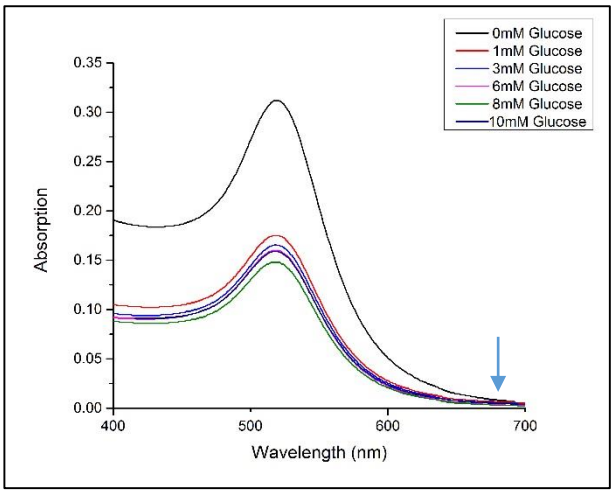

Figure 4.32: UV-Vis absorption spectra of gold nanoparticles synthesized with trisodium citrate and mixed with glucose. The arrow indicates the reference point for the determination of the height of the absorbance.

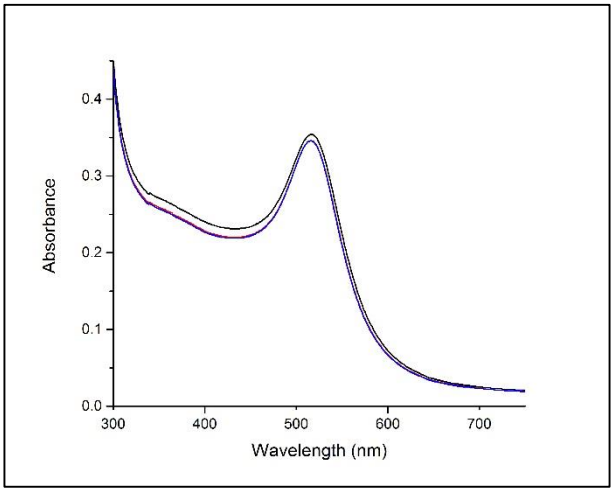

Figure 4.33: UV-Vis absorption spectrums of gold nanoparticles synthesized using trisodium citrate for three days.

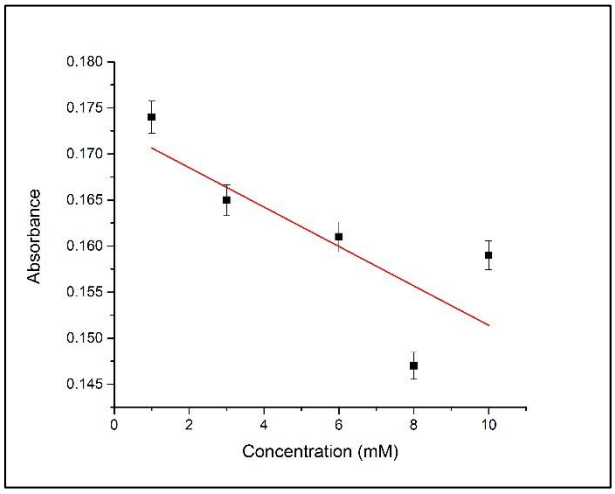

Figure 4.34: UV-Vis absorption spectra of gold nanoparticles synthesized using trisodium citrate changes in absorbance at different glucose concentrations.

[Fig. 4.35] is the TEM images of gold nanoparticles. The size distribution of nanoparticles was analyzed using ImageJ 1.5g, software. This is performed by converting pixels on the TEM images into nanometers by applying the scale of the image. Each nanoparticle was marked manually. Spherical monodisperse

gold nanoparticles were observed and the diameter was found to range between 9 – 23 nm, with a high yield of size 12.5 nm.

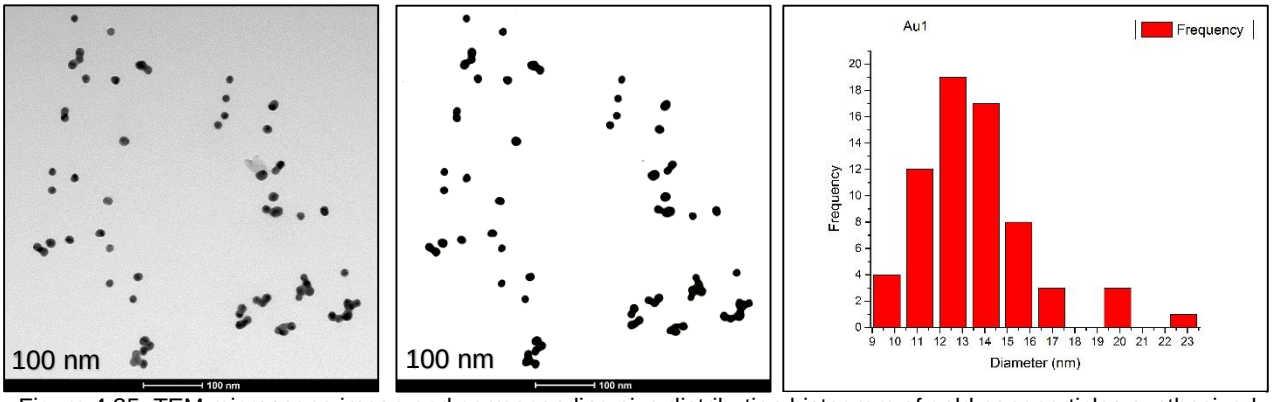

Figure 4.35: TEM microscope image and corresponding size distribution histogram of gold nanoparticles synthesized using trisodium citrate.

Mie plot software was used to determine the diameter of gold nanoparticles by comparing theoretical and experimental absorption spectra. From the fit the diameter of gold nanoparticles was measured and found to be 10 nm [Fig. 4.36]. The diameter measured using Mie plot software (10 nm) is close to the real diameter (12.5 nm) found In TEM images.

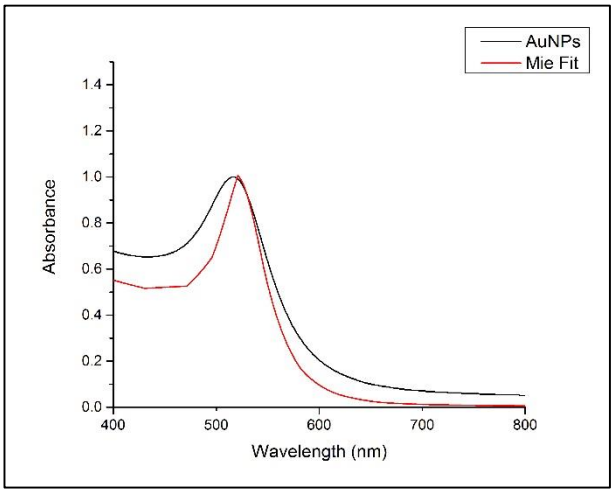

Figure 4.36: Comparison of theoretical and experimental absorption spectrums of gold nanoparticles synthesized using trisodium citrate.

X-ray diffraction (XRD) was used to investigate the presence and the formation of gold nanoparticles. XRD was operated at 10 kV. As shown in Fig. 4.37, the

XRD pattern verifies the presence of gold (Au) and other elements such as carbon (C), nitrogen (N), sodium (Na), oxygen (O) and chlorine (Cl). XRD was direct evidence for the formation of gold nanoparticles. XRD was done only for this sample because of unavailability of the equipment in RCSI-Bahrain and difficulties to get an access to the instrument in other institutes in region.

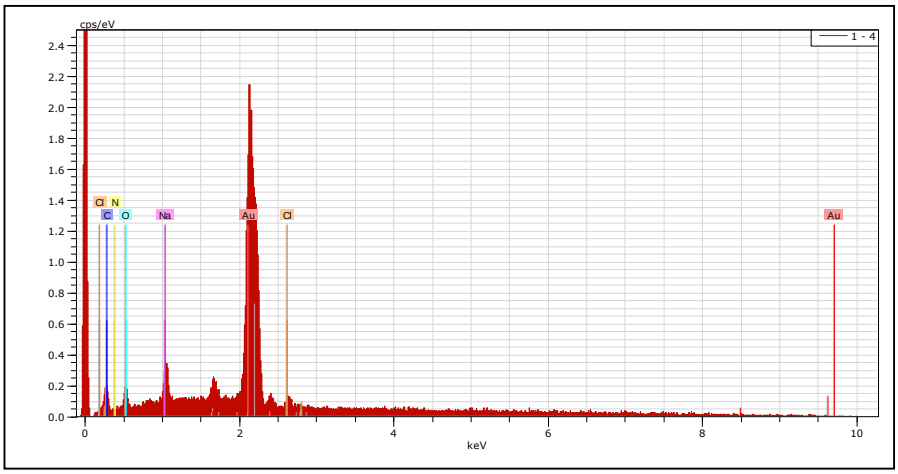

Figure 4.37: XRD pattern of gold nanoparticles synthesized using trisodium citrate.

Gold nanoparticles (AuNPs) synthesized using curcumin:

[Fig. 4.38] shows the absorption spectrum of the gold nanoparticles that were synthesized using curcumin as a reducing agent [section 4.1.2]. The formation of nanoparticles was confirmed by the presence of a surface plasmon resonance band centered at 530 nm. For glucose detection refer to z-scan [section 5.3.2].

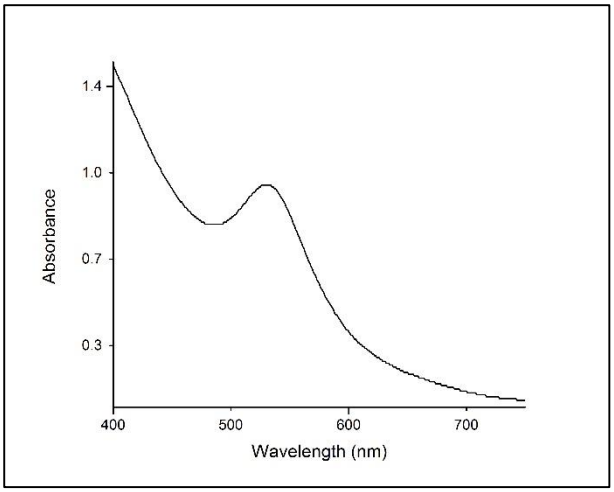

Figure 4.38: UV-Vis absorption spectra of gold nanoparticles synthesized using curcumin.

[Fig. 4.39] is the TEM images of gold nanoparticles. The size distribution of nanoparticles was analyzed using ImageJ 1.5g, software. This is performed by converting pixels on the TEM images into nanometers by applying the scale of the image. Each nanoparticle was marked manually. Polydisperse gold nanoparticles with different shapes were observed such as spherical, rod, diamond and triangular. The diameter was found to range between 13 – 33 nm, with a high yield of size 20 nm (by considering the particles to be spherical).

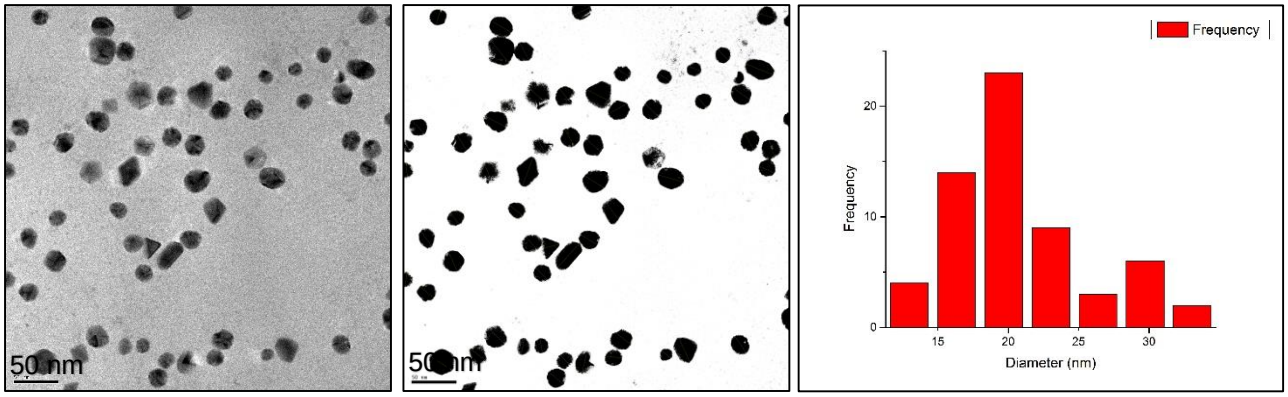

Figure 4.39: TEM image and corresponding size distribution histogram of gold nanoparticles synthesized using curcumin.

Gold nanoparticles (AuNPs) synthesized using glucose and gelatin:

[Fig. 4.41] shows the absorption spectrum of the gold nanoparticles that were synthesized using glucose (1, 2, 3, 5, 6, 7, 9, 11, 12 and 14 mM) as a reducing agent and gelatin as a capping agent [section 4.1.2]. The formation of nanoparticles was confirmed by the presence of a surface plasmon resonance band centered at 526 nm. [Fig. 4.40] demonstrates a linear proportional relation between the absorbance of gold nanoparticles surface plasmon resonance band and the glucose concentration. This indicates that as the concentration of glucose increases, nanoparticles size increases [refer to section 4.1]. Therefore, the absorbance of gold nanoparticles surface plasmon resonance band can be used for the determination of glucose concentrations.

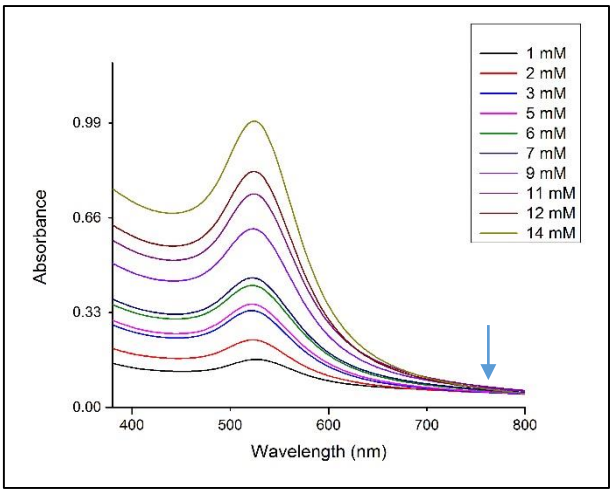

Figure 4.41: UV-Vis absorption spectra of gold nanoparticles synthesized using different glucose concentrations and gelatin. The arrow indicates the reference point for the determination of the height of the absorbance.

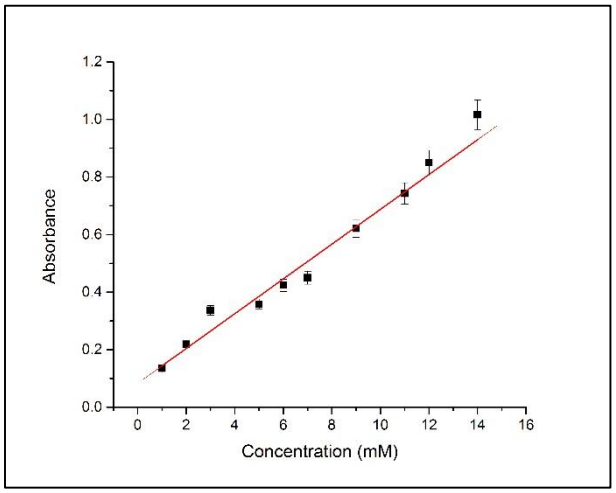

Figure 4.40: UV-Vis absorption spectra of gold nanoparticles synthesized using different glucose concentrations and gelatin changes in absorbance.

[Fig. 4.43] and [Fig. 4.42] are the TEM images of gold nanoparticles synthesized using glucose 8 mM and 14 mM. The size distribution of nanoparticles was analyzed using ImageJ 1.5g software. This is performed by converting pixels on

the TEM images into nanometers by applying the scale of the image. Each nanoparticles was marked manually. Polydisperse gold nanoparticles synthesized using 8 mM of glucose were observed, and the diameter was found to range from 3 – 28 nm with a high yield of size 3.7 nm. Polydisperse gold nanoparticles synthesized using 8 mM of glucose were observed, and the diameter was found to range 8 – 22 nm with a high yield of size 9 nm. Larger nanoparticles are synthesized as the concentration of glucose increases. Shades observed around the gold nanoparticles is that of gelatin.

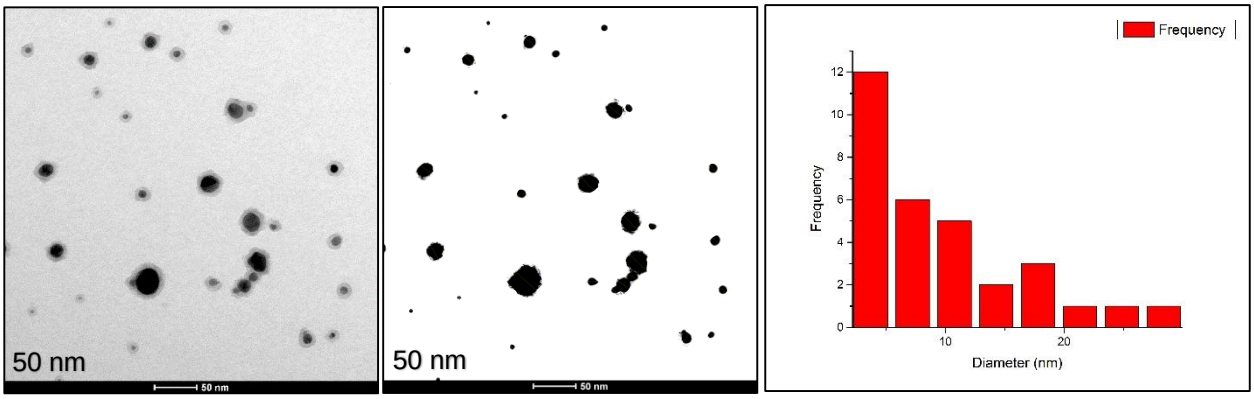

Figure 4.42: TEM image and corresponding size distribution histogram of gold nanoparticles synthesized using 8 mM glucose and gelatin.

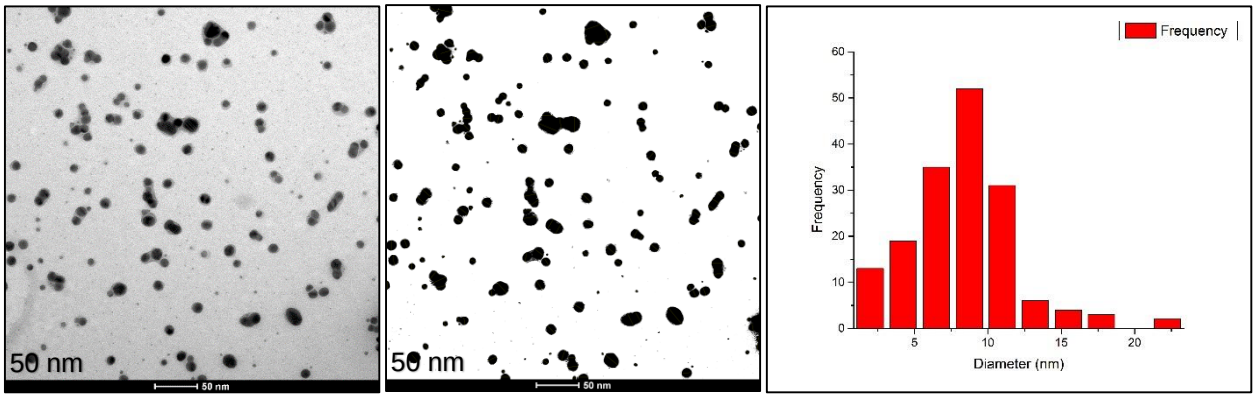

Figure 4.43: TEM image and corresponding size distribution histogram of gold nanoparticles synthesized using 14 mM glucose and gelatin.

Gold nanoparticles (AuNPs) synthesized using glucose, NaOH and $HAuCl_4$:

[Fig. 4.44] shows the absorption spectrum of the gold nanoparticles that were synthesized using glucose (1, 2, 3.5, 4.5 and 5.5 mM) as a reducing agent [section 4.1.2]. The formation of nanoparticles was confirmed by the presence of a surface plasmon resonance band centered in the range of 545 – 565 nm depending on glucose concentration. [Fig. 4.45] demonstrates a linear inverse proportional relation between the peak position of gold nanoparticles surface plasmon resonance (SPR) band and the glucose concentration. Peak position of SPR band shifts towards shorter wavelengths (blue shift) as the concentration of glucose increases. This indicates that as the concentration of glucose increases, the size of nanoparticles decreases [refer to section 4.1]. Thus, the peak position (shift) of SPR band can be used for the determination of glucose concentrations.

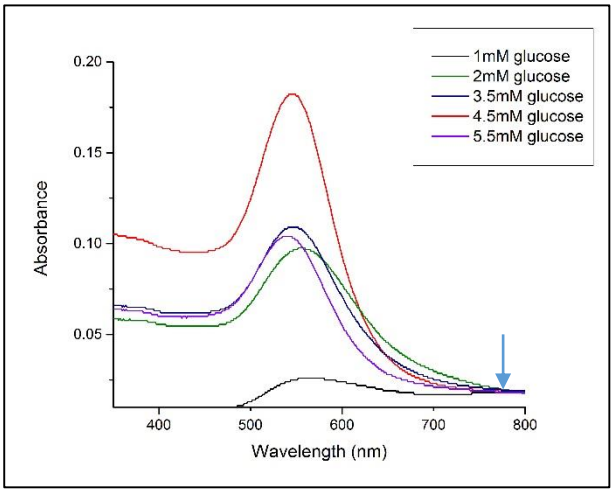

Figure 4.44: UV-Vis absorption spectra of gold nanoparticles synthesized using different concentrations of glucose, NaOH and $HAuCl_4$. The arrow indicates the reference point for the determination of the height of the absorbance.

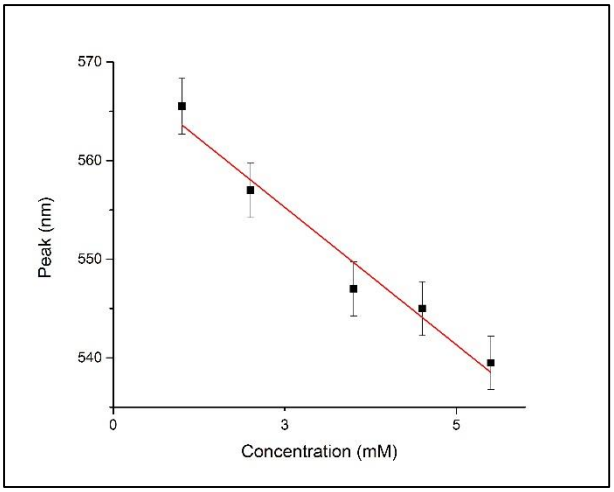

Figure 4.45: UV-Vis absorption spectra of gold nanoparticles synthesized using different concentrations of glucose, NaOH and $HAuCl_4$ changes in peak wavelength.

According to Mie plot software by comparing theoretical and experimental absorption spectra. From the fit the diameter of gold nanoparticles synthesized using 1 mM of glucose was found to be 95 nm [Fig. 4.46]. This may not be the real value due to the existence of nanoparticles with different sizes and shapes in the synthesized sample.

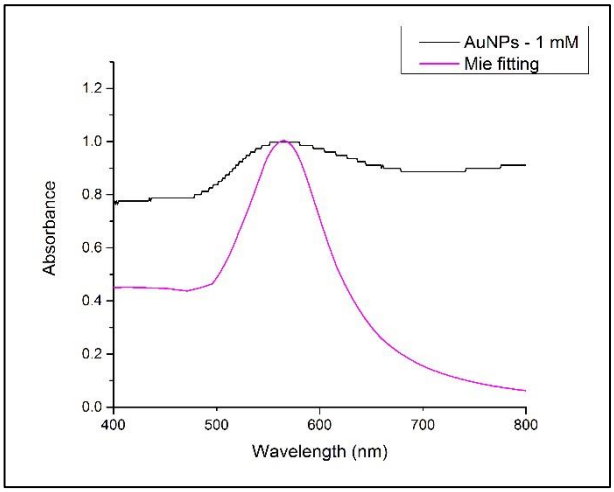

Figure 4.46: Comparison of theoretical and experimental absorption spectrums of gold nanoparticles synthesized using 1mM glucose, NaOH and $HAuCl_4$.

4.2.3 Gold-Silver (Au-Ag/core-shell) Nanoparticles

Gold-silver nanoparticles (Au-Ag/core-shell NPs) synthesized using $HAuCl_4$, $AgNO_3$, NaOH and L-ascorbic acid:

[Fig. 4.47] shows the absorption spectrum of gold-silver nanoparticles that were synthesized using $HAuCl_4$, $AgNO_3$, NaOH and L-ascorbic acid [section 4.1.3]. The formation of nanoparticles was confirmed by the presence of a surface plasmon resonance band centered at 385 & 487 nm (black line). The peak at 385 nm corresponds to silver nanoparticles, while the peak at 487 nm corresponds to silver-coated gold nanoparticles (84). The appearance of both longitudinal and transverse plasmon bands indicates that rod-shaped nanoparticles are synthesized. This corresponds to electron oscillations along the long or the short axis of the rod (85). Peak broadening was observed (red line) after three days which indicates the existence of gold-silver nanoparticles with different size distribution or nanoparticles aggregation. For glucose detection refer to z-scan section [5.3.3].

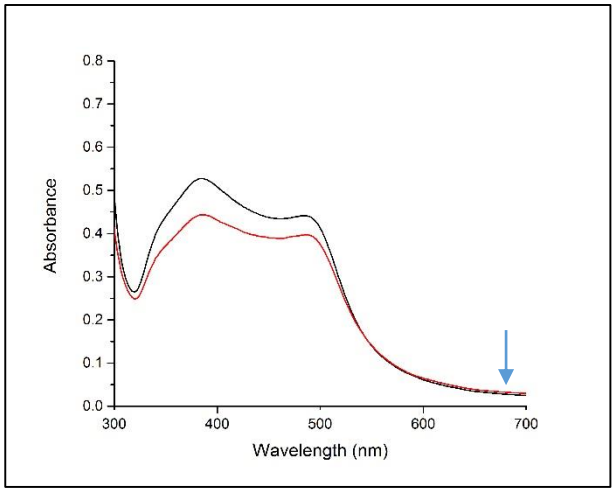

Figure 4.47: UV-Vis absorption spectra of gold-silver nanoparticles synthesized using $HAuCl_4$, $AgNO_3$, NaOH and L-ascorbic acid (black line) and UV-Vis absorption spectra after three days (red line). The arrow indicates the reference point for the determination of the height of the absorbance.

Chapter 5: Nonlinear Optics (NLO)

As Geetha (1998) says, “Nonlinear optics is a field that involves the study of modification of a suitable optical system by the presence of intense electromagnetic radiation”. Optical properties of materials are not affected by low intensities of light, while sufficiently intense light such as laser light, modify the optical properties of materials according to the intensity and other characteristics of light. Light wave’s interaction with each other within a medium may occur, but high intensities are required (86). Nonlinear optics field evolution started after the invention of lasers in 1960. The effect can be utilized in optical devices and important techniques, which have applications in optical information processing, telecommunications and integrated optics (87). Nonlinear optics deal with the interaction of the electromagnetic field of a light wave with the electromagnetic fields of matter. Nonlinear optical material properties will change due to the interaction with light and the next photon that arrives will "see" a different material. Light electric field interacts with other electric fields within the material as light travels through a material. These internal fields are a function of the time-dependent electron density distribution (polarization) in the material and the electric fields of the other light waves. Strong interactions can exist among the various fields. Frequency, phase, polarization, or path of incident light may be changed after these interactions (88).

In order to describe the meaning of optical nonlinearity, we will take into consideration the dependence of polarization P(t) of a material system on the strength of E(t) of an applied optical field. For a linear regime, the dielectric of the medium is characterized by a linear relation between the polarization density and the electric field strength:

$$P=\varepsilon_0 \chi^1 E \qquad (1)$$

where ε_0 is the permittivity of free space and χ^1 is the linear susceptibility.

The optical response in nonlinear optics, is often described by expressing the polarization P as a power series in the electric field strength E as

$$P=\varepsilon_0 [\chi^1 E+\chi^2 E^2+ \chi^3 E^3+\ldots] \quad (2)$$

where χ^2 and χ^3 are the second-order and third-order nonlinear susceptibilities of the medium respectively. The physical processes that occur as a result of the second-order polarization (χ^2) are second harmonic generation, sum and difference of frequency generation and parametric oscillation. The physical processes that occur as a result of the third-order polarization (χ^3) are third harmonic generation, intensity-dependent refractive Index and intensity dependent absorption.

Consider the third-order contribution to the nonlinear polarization

$$P^3(t)=\varepsilon_0 \chi^3 E^3 \quad (3)$$

A simplified form in which the applied field is monochromatic is

$$E(t)= E \cos \omega t \quad (4)$$

where ω is the frequency and t is the time.

By using $\cos^3 \omega t = \frac{1}{4}\cos 3\omega t+ \frac{3}{4}\cos \omega t$, the nonlinear polarization is

$$P^3(t)= \frac{1}{4}\varepsilon_0 \chi^3 E^3 \cos 3\omega t+ \frac{3}{4}\varepsilon_0 \chi^3 E^3 \cos \omega t \quad (5)$$

Third-harmonic generation is processed by the first term in equation (5). In the microscopic description of this process three photons of frequency ω are destroyed and one photon of frequency 3ω is created. A nonlinear contribution to the polarization at the frequency of the incident field is described in the second term of equation (5). This term leads to a nonlinear contribution to the refractive index which is the related real part of χ^3 through

$$n_2 = \frac{3}{2n^2\varepsilon_0 c}\chi^3_R \quad (6)$$

where n_2 is a nonlinear refractive index, c is the speed of light and $I=\frac{1}{2} n_o \varepsilon_0 c E^2$ is the intensity of the incident beam. For incident intensity I, n_2 can be represented as $n = n_0 + n_2 I$, where n is the total refractive index and n_0 is a linear refractive index (89).

Self-action such as self-focusing and self-defocusing is a process that can occur as a result of the intensity dependent refractive index change and a spatial profile

of the laser beam intensity which is usually Gaussian. For positive nonlinear refractive index (n_2), the material effectively acts as a thin positive lens, which causes the rays to curve toward each other and for negative nonlinear refractive index (n_2), the material effectively acts as a thin negative lens, which causes the rays to curve outward from each other. The self-focusing process is of great practical importance because the intensity at the focal spot of the self-focus beam is usually sufficiently large to lead to optical damage of the material. The self-defocusing process is important for optical limiting.

The various types of self-action effects depend on whether the susceptibility is real or imaginary and on the temporal and spatial distribution of the incident light. The real part of the nonlinear susceptibility gives rise to spatial effects of self-focusing and self-defocusing. The imaginary part of the susceptibility is responsible for nonlinear absorption.

The third order susceptibility χ^3 in general is a complex quantity having both real χ^3_R and imaginary parts χ^3_I,

$$\chi^3 = \chi^3_R + i\chi^3_I \qquad (7)$$

where the imaginary part is related to the nonlinear absorption coefficient (β) through

$$\chi^3_I = \frac{2n\varepsilon_o c^2}{\omega}\beta \qquad (8)$$

For low intensity, the following substitution was made

$$\alpha = \alpha_o + I\beta \qquad (9)$$

where α is the linear absorption coefficient.

From above one conclude that the imaginary part of the refractive index describes the absorption of radiation. Saturation absorption and reverse saturation absorption and two photon absorption are the processes that can occur as a result of the transfer of population from the atomic ground state to an excited state. These processes are intensity dependent (90).

5.1 Z-scan Theory

Z-scan technique is an accurate and simple method introduced by Sheik-Bahae for the measurement of optical nonlinear properties (91). Because of its simplicity, the z-scan technique is being used widely for investigating the nonlinear refractive index (n_2) and the nonlinear absorption coefficient (β). The experimental setup for z-scan technique is shown in Fig. 5.1. Briefly, the technique relies on the fact that intensity varies along the axis of the convex lens and is maximum in the focus. Hence by shifting the sample through the focus, the nonlinear refraction can be measured by observing the spot size variation at the plane of finite aperture/detector combination (92).

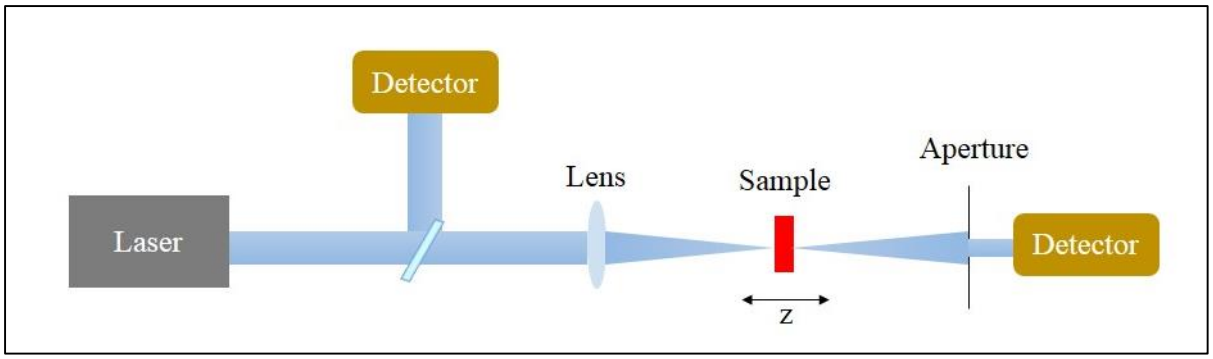

Figure 5.1: Z-scan technique experimental setup.

The nonlinear refraction of the sample causes a spatial beam broadening or narrowing in the far field and thus modifies the fraction of light that passes through the aperture as the sample position is changed. If the sample has a positive nonlinear refractive index (n_2) and as it moves toward the focal plane, the transmission will decrease. This is because as the intensity increases it creates a positive lensing and the beam spread at the detector plane. On the other side of the focus, the lensing effect will tend to reduce the beam spread, resulting in an increase in the measured transmittance. The transmission plotted as function of position shows prefocal transmission minimum followed by post-focal maxima (valley–peak). Similarly, a negative refractive nonlinearity will show a prefocal maximum transmission followed by a postfocal minimum transmission (peak–valley). Therefore, the shape of the curves gives the sign of nonlinearity and the

magnitude of the nonlinearity can be calculated from the transmittance change between peak and valley (ΔT_{p-v}) (15).

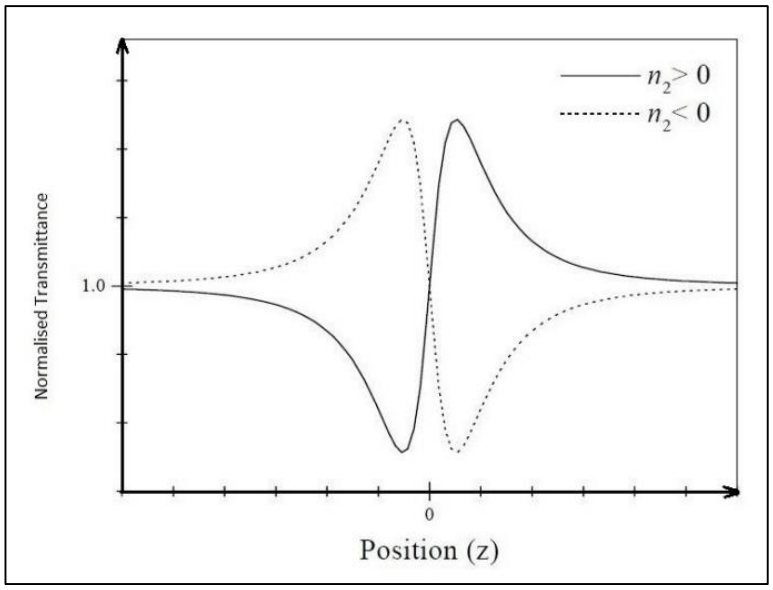

Figure 5.2: Characteristic curves depict both positive and negative nonlinear refraction as measured by Z-scan (126).

In general, for a cubic nonlinearity, the index of refraction n is expressed in terms of nonlinear indexes n_2 (m^2/W) through

$$n = n_0 + \frac{1}{2} n_2 E^2 = n_0 + n_2 I^2 \quad (1)$$

where n_0 is the linear refractive index, E is the peak electric field.

Assuming a TEM_{00} Gaussian beam of waist radius w_0 traveling in the +z direction, the magnitude of the electric field E can be written as

$$E(r,z,t) = E_0(t) \frac{w_o}{w(z)} \exp\left[-\frac{r^2}{w^2} - \frac{ikr^2}{2R(z)}\right] e^{-i\phi(z,t)} \quad (2)$$

where $w^2(z) = w_0^2\left(1+\frac{Z^2}{Z_R^2}\right)$ is the beam radius at z, $z_0 = k^2 w_0 /2$ is the diffraction length of the beam (Rayleigh range) , $k = \frac{2\pi}{\lambda}$ is the wave vector, and λ is the laser wavelength, all in free space. $E_0(t)$ denotes the radiation electric field at the focus and contains the temporal envelope of the laser pulse.

For small sample thickness, the changes in the beam diameter within the sample due to either diffraction or nonlinear refraction can be neglected. For such an assumption, the amplitude I and nonlinear phase change $|\Delta\varphi|$ of the electric field within the sample are given by

$$\frac{d\Delta\varphi}{dz} = \Delta n(I)k \qquad (3)$$

and

$$\frac{dI}{dz} = -\alpha(I)I \qquad (4)$$

where z is the propagation depth in the sample and $\alpha(I)$includes the linear and nonlinear absorption terms. Equations (3) and (4) are solved to give the phase shift $\Delta\varphi$ at the exit surface of the sample, which simply follows the radial variation of the incident irradiance at a given position of the sample *z*:

$$\Delta\varphi(z,r,t) = \frac{\Delta\varphi(t)}{1+z^2/z_o^2}\exp\left[-\frac{2r^2}{w^2(z)}\right] \qquad (5)$$

The on-axis phase shift at the focus is defined as $\Delta\varphi(t) = k\Delta n_0(t)L_{eff}$ and $L_{eff} = (1-e^{-\alpha l})/\alpha$. Here $\Delta n_0 = \gamma I_0(t)$ with $I_0(t)$ being the on-axis irradiance at focus (i.e. z = 0). One can ignore the Fresnel reflection losses such that $I_0(t)$ is the irradiance within the sample (93).

As the sample is being scanned longitudinally through the focus of the laser beam, the changes in transmission at the far field are monitored. The transmittance change between peak and valley (ΔT_{p-v}) is related to nonlinear induced phase shift by:

$$\Delta T_{p-v} = 0.406\,(1-S)^{0.25}\,|\Delta\varphi| \quad (1)$$

where S is the aperture linear transmittance.

$$S = 1 - e^{-2\left(\frac{r_0}{w_0}\right)^2} \quad (2)$$

where w_0 is the Gaussian beam spot radius at the focus (half width at $1/e^2$ of maximum of the irradiance) and $r_0$is radius of curvature.

The nonlinear induced phase shift $\Delta\varphi$ is related to the nonlinear refractive index n_2 by

$$n_2 = \frac{\Delta\phi\,\lambda}{2\,\pi\,I_0 L_{eff}} \qquad (3)$$

where L_{eff} is the effective thickness of the sample ($L_{eff} = \frac{1-e^{-\alpha l}}{\alpha}$), α is the linear absorption coefficient, I_0 is the on-axis irradiance at the focus and n_2 is the nonlinear index of refraction (94).

The nonlinear absorption coefficient is related to sample transmittance T (95) by

$$T = 1 + \frac{\beta\, I\, L_{eff}}{2\sqrt{2}} \quad (4)$$

An incident Gaussian beam leads to an immediate local heating in the medium, as it absorbs the light. Refractive index changes occur as a result of temperature change in the surroundings of the laser beam. The refractive index is assumed to depend linearly on temperature. The non-locality depends on the optical and the thermal properties of the material and it's given by

$$\sigma = \sqrt{\frac{\kappa|n_2|}{\alpha_0\left|\frac{dn}{dT}\right| w_0^2}} \qquad (1)$$

where w_0 is the minimum beam waist, n_2 is the nonlinear refractive index, κ is the heat conductivity, $\frac{dn}{dT}$ is the thermo-optical and α_0 is the linear absorption coefficient of the medium. The more non-local is the medium as the value of σ is larger. While σ=0 means that the medium can only present a local nonlinearity.

When a CW (continuous waves) laser is used, thermal lens effect plays a role in nonlinear optics (NLO). A local heating occurs immediately as the Gaussian beam propagates across the medium. The change in the temperature around the beam laser results in a change in the nonlinear refractive index of the medium. The time dependent far-field on-axis transmittance is expressed by

$$T_N = \frac{I(z, t)}{I(z, 0)} \qquad (2)$$

$$= \frac{1}{1+\left(\frac{\theta}{1+t_c/2t)}\right)\left(\frac{2x}{1+x^2}\right)+\left(\frac{\theta}{1+t_c/2t)}\right)^2\left(\frac{1}{1+x^2}\right)}$$

where $x = \frac{z}{z_0}$, $z_0 = \frac{\pi w^2}{\lambda}$, $t_c = \frac{w^2}{4k/C_p}$. t_c is the thermal diffusion time, k is the thermal conductivity and C_p is the specific heat per volume at constant pressure.

The on-axis phase shift is given by

$$\theta = \frac{\alpha PL}{\lambda \kappa} \frac{dn}{dT} \qquad (3)$$

where P is the power of the Gaussian beam and T is the temperature.

The second term in the denominator in equation (2) is neglected in low power as the nonlinear phase shift $\theta \ll 1$. When the steady state has been reached, $t \gg t_c$ is considered. Then equation (2) is given

$$T_N = \frac{1}{1+(\theta)(\frac{2x}{1+x^2})} \quad (4)$$

The nonlinear refractive index can be measured through fitting equation (4) to the experimental data (96).

The response of noble metal nanoparticles such as gold and silver to nonlinear optics and thermal effect may be described. Fourier heat conduction theory (97) describes the heat transfer from the excited nanoparticles to the surrounding matrix. The nonlinearity aroused from small nanoparticles (size is much smaller than the heat carrier mean free path) is surely of multiphoton origin. This because around the heated metal nanosphere only few carrier-scattering events occur (98).

If a laser with a wavelength of 532 nm is used to excite gold nanoparticles, the electrons in the filled d band are excited to the unoccupied states in the conduction band due to interband transitions. These excited electrons act as free carriers, processing a whole spectra of kinetics and potential energies. This may lead to transient absorption due to free carrier absorption. Excited state absorption is caused by electrons that were pumped to even higher energy levels. The excitations from plasmon band to free carrier band in gold nanoparticles are the origin of the reverse saturable absorption (99). By applying a laser beam with a wavelength of 535 nm to gold nanoparticles, the surroundings temperature increases due to excess thermal energy and a temperature gradient is generated. Nonlinear refractive index variations are resulted due to the temperature gradient and it’s called thermal lens (100). Population lens which is caused by population

redistribution between the excited and the ground-state conduction bands may play an important part in the variations in the nonlinear refractive index (101,102).

5.2 Medical Applications of Z-scan

Z-scan measurements of optical nonlinearities are applied in different areas. In medicine, z-scan is used as a tool to measure blood glucose, total cholesterol and triglycerides and total protein and albumin in blood.

For glucose detection, GOD/POD (glucose oxidase-peroxidase) kit is used. 10 µL of serum is mixed with 1 mL of GOD/POD reagent. The the mixture is incubated at 37 ℃ for 15 minutes. The color changes to a pinkish red color. Finally, z-scan is used to measure the nonlinear refractive index and a linear proportional relation found between the nonlinear refractive index and the glucose concentration (13).

Determination of cholesterol and triglyceride's levels using GPO/POD (glycerolphosphate oxidase-peroxidase) kit. GPO/POD kit mixed with a serum sample for 5 min at 37 ℃. Then the z-scan technique is used to measure the nonlinear refractive index. As the concentration of cholesterol or triglyceride's increases the value of the nonlinear refractive index increases (103).

Determination of protein level in serum. A sample of serum is mixed with a kit supplied by Transasia and incubated for 10 min at 37 ℃. For albumin the mixture of the serum and the kit is incubated for 1 min at 37 ℃. Z-scan measurement show a linear proportional relation between the nonlinear refractive index and protein/albumin levels (104).

5.3 Results

5.3.1 Silver Nanoparticles

Silver nanoparticles (AgNPs) synthesized using trisodium citrate:

The synthesized silver nanoparticles using trisodium citrate [section 4.1.1] were mixed with different concentrations of glucose and subjected to optical nonlinearity measurements using the z-scan technique. The z-scan experiment was performed using 488 nm CW argon-ion laser beam with a power of 30 mW. The normalized transmittance curve is characterized by a prefocal peak followed by a postfocal valley [Fig. 5.3]. This implies that the nonlinear refractive index of silver nanoparticles mixed with glucose is negative $(n_2 < 0)$. [Fig. 5.4] demonstrates a linear inverse proportional relation between the glucose concentrations and the nonlinear refractive index. This indicates that as the concentration of glucose increases, the size of nanoparticles decreases [see section 7.4]. Thus, the nonlinear refractive index can be used for the determination of glucose concentrations. The values of the nonlinear refractive index are shown in Table 5.1.

Table 5.1: The nonlinear refractive index (n_2) values for silver nanoparticles synthesized using trisodium citrate when mixed with different concentrations of glucose.

Concentration (mM)	$\boldsymbol{n_2}$ **(m²/W)**
1	5.73×10^{-13}
6	5.52×10^{-13}
10	4.20×10^{-13}
15	5.23×10^{-13}
20	5.64×10^{-13}
30	4.04×10^{-13}

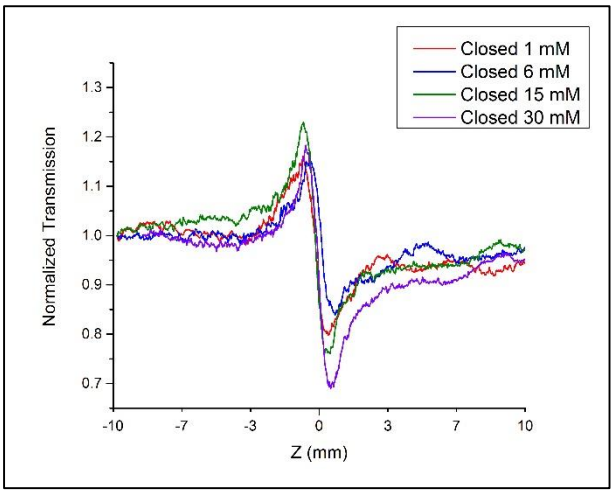

Figure 5.3: Closed aperture z-scan of silver nanoparticles synthesized using trisodium citrate. Using CW argon-ion laser with λ=488 nm, Power=30 mW.

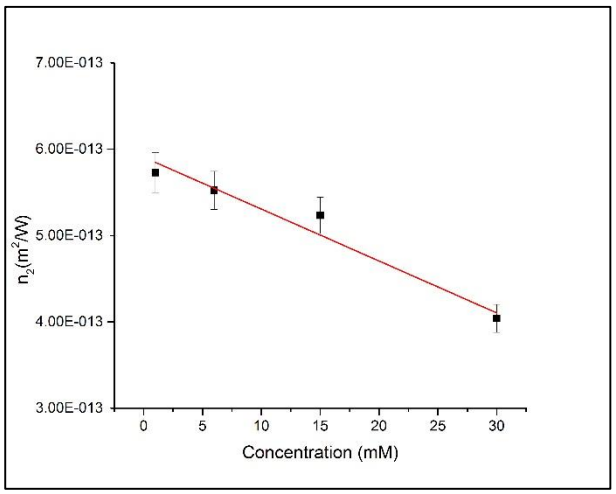

Figure 5.4: Variation in the nonlinear refractive index (n_2) for different glucose concentrations.

Silver nanoparticles (AgNPs) synthesized using glucose and gelatin:

The silver nanoparticles synthesized using different concentrations of glucose [section 4.1.1] were subjected to optical nonlinearity measurements using the z-scan technique. The z-scan experiment was performed using 488 nm CW argon-ion laser beam with a power of 26 mW. The normalized transmittance curve is characterized by a prefocal peak followed by a postfocal valley [Fig. 5.6]. This implies that the nonlinear refractive index of silver nanoparticles synthesized with glucose is negative ($n_2 < 0$). [Fig. 5.5] demonstrates a linear inverse proportional relation between the glucose concentrations and the nonlinear refractive index. This indicates that as the concentration of glucose increases, the size of nanoparticles decreases [see section 7.4]. Therefore, the nonlinear refractive index can be used for the determination of glucose concentrations. The values of the nonlinear refractive index are shown in Table 5.2.

Table 5.2: The nonlinear refractive index (n_2) values for silver nanoparticles synthesized using different concentrations of glucose and gelatin.

Concentration (mM)	n_2 **(m²/W)**
0.1	7.94×10^{-13}
1	7.48×10^{-13}
5	6.28×10^{-13}

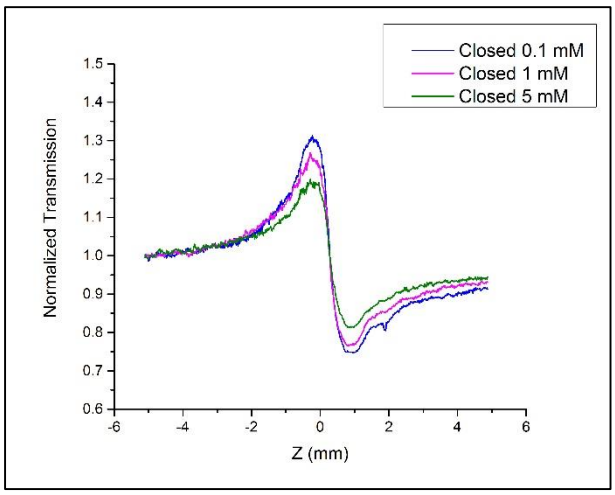

Figure 5.5: Closed aperture z-scan of silver nanoparticles synthesized using glucose and gelatin. Using CW argon-ion laser with λ=488 nm, Power=26 mW.

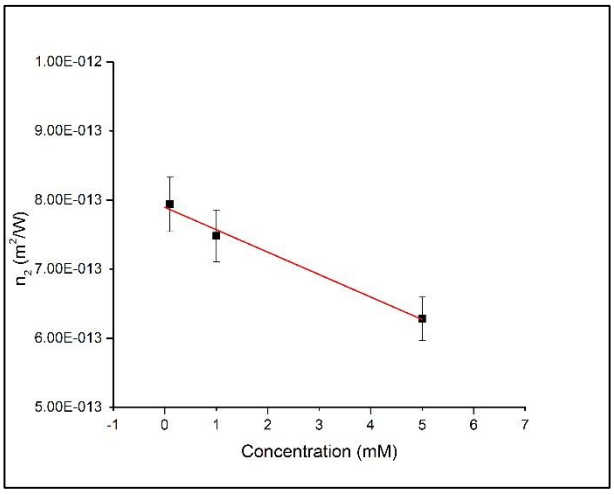

Figure 5.6: Variation in the nonlinear refractive index (n_2) for different glucose concentrations.

5.3.2 Gold Nanoparticles

Gold nanoparticles (AuNPs) synthesized using trisodium citrate:

The synthesized gold nanoparticles [section 4.1.2] were mixed with different concentrations of glucose and subjected to optical nonlinearity measurements using the z-scan technique. The z-scan experiment was performed using 488 nm CW argon-ion laser beam with a power of 15 mW. The normalized transmittance curve is characterized by a prefocal peak followed by a postfocal valley [Fig. 5.7].

This implies that the nonlinear refractive index of gold nanoparticles mixed with glucose is negative ($n_2 < 0$). [Fig. 5.8] demonstrates a linear inverse proportional relation between the glucose concentrations and the nonlinear refractive index. This indicates that as the concentration of glucose increases, the size of nanoparticles decreases [see section 7.4]. Thus, the nonlinear refractive index can be used for the determination of glucose concentrations. The values of the nonlinear refractive index are shown in Table 5.3.

Table 5.3: The nonlinear refractive index (n_2) values for gold nanoparticles synthesized using trisodium citrate when mixed with different concentrations of glucose.

Concentration (mM)	$\boldsymbol{n_2}$ **(m²/W)**
1	1.51×10^{-12}
3	1.62×10^{-12}
6	1.49×10^{-12}
8	1.38×10^{-12}
10	1.47×10^{-12}

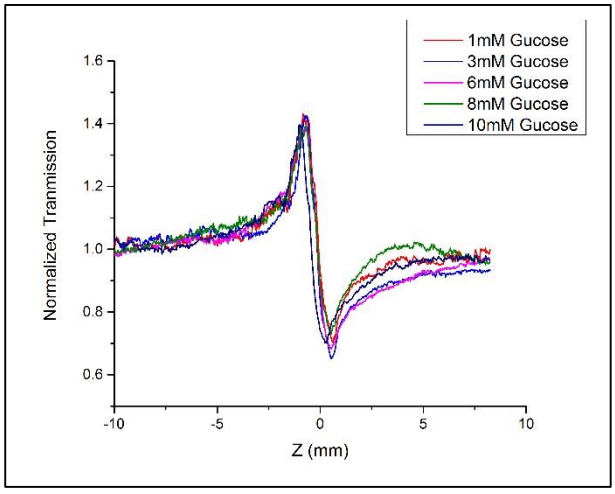

Figure 5.7: Closed aperture z-scan of gold nanoparticles synthesized using trisodium citrate. Using CW argon-ion laser with λ=488 nm, Power=15 mW.

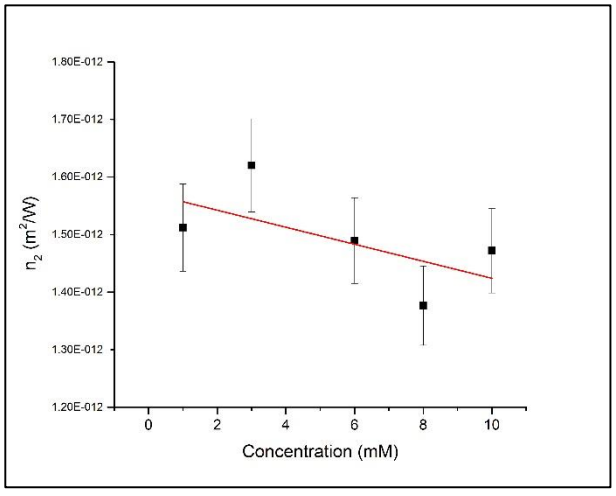

Figure 5.8: Variation in the nonlinear refractive index (n_2) for different glucose concentrations.

Gold nanoparticles (AuNPs) synthesized using curcumin:

The synthesized gold nanoparticles [section 4.1.2] were mixed with different concentrations of glucose and subjected to optical nonlinearity measurements using the z-scan technique. The z-scan experiment was performed using 488 nm CW argon-ion laser beam with a power of 28.1 mW. The normalized transmittance curve is characterized by a prefocal peak followed by a postfocal valley [Fig. 5.9]. This implies that the nonlinear refractive index of gold nanoparticles mixed with glucose is negative ($n_2 < 0$). [Fig. 5.10] demonstrates a linear inverse proportional relation between the glucose concentration and the nonlinear refractive index. This indicates that as the concentration of glucose increases, the size of nanoparticles decreases [see section 7.4]. Therefore, the nonlinear refractive index can be used for the determination of glucose concentrations. The values of the nonlinear refractive index are shown in Table 5.4.

Table 5.4: The nonlinear refractive index (n_2) values for gold nanoparticles synthesized using curcumin when mixed with different concentrations of glucose.

Concentration (mM)	$\boldsymbol{n_2}$ **(m²/W)**
0.01	2.53×10^{-13}
0.1	2.51×10^{-13}
1	2.45×10^{-13}
5	2.41×10^{-13}
10	2.31×10^{-13}

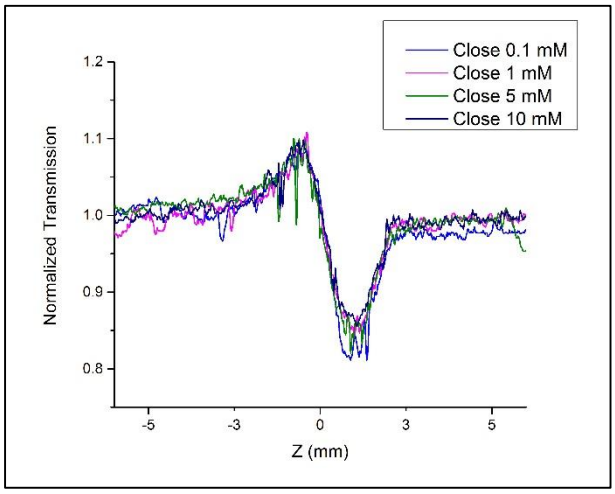

Figure 5.9: Closed aperture z-scan of gold nanoparticles synthesized using curcumin. Using CW argon-ion laser with λ=488 nm, Power=28.1 mW.

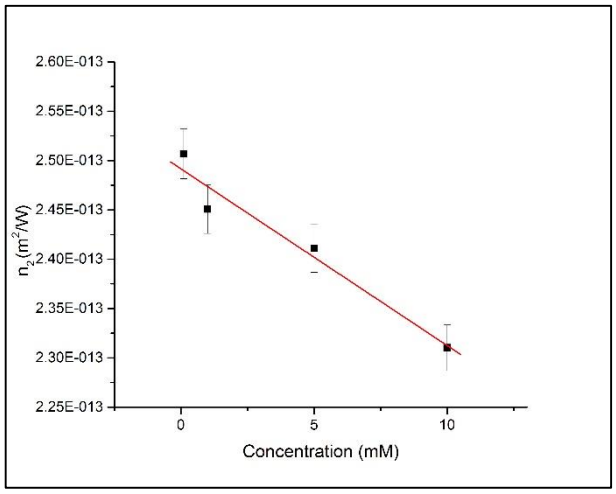

Figure 5.10: Variation in the nonlinear refractive index (n_2) for different glucose concentrations.

Gold nanoparticles (AuNPs) synthesized using glucose and gelatin:

Gold nanoparticles were synthesized using different concentrations of glucose [section 4.1.2] and were subjected to optical nonlinearity measurements using the z-scan technique. The z-scan experiment was performed using 488 nm CW argon-ion laser beam with a power of 29.2 mW. The normalized transmittance curve is characterized by a prefocal peak followed by a postfocal valley [Fig. 5.11]. This implies that the nonlinear refractive index of gold nanoparticles synthesized with glucose is negative ($n_2 < 0$). [Fig. 5.13] demonstrates a linear proportional relation between the glucose concentration and the nonlinear refractive index. This indicates that as the concentration of glucose increases, the size of nanoparticles increases [see section 7.4]. Hence, the nonlinear refractive index can be used for the determination of glucose concentrations. The values of the nonlinear refractive index are shown in Table 5.5.

Table 5.5: The nonlinear refractive index (n_2) values for gold nanoparticles synthesized using different concentrations of glucose and gelatin.

Concentration (mM)	n_2 **(m²/W)**
2	1.26×10^{-12}
3	1.64×10^{-12}
5	1.99×10^{-12}
6	2.32×10^{-12}
7	2.78×10^{-12}
9	3.60×10^{-12}
11	4.55×10^{-12}
12	5.28×10^{-12}
14	6.56×10^{-12}

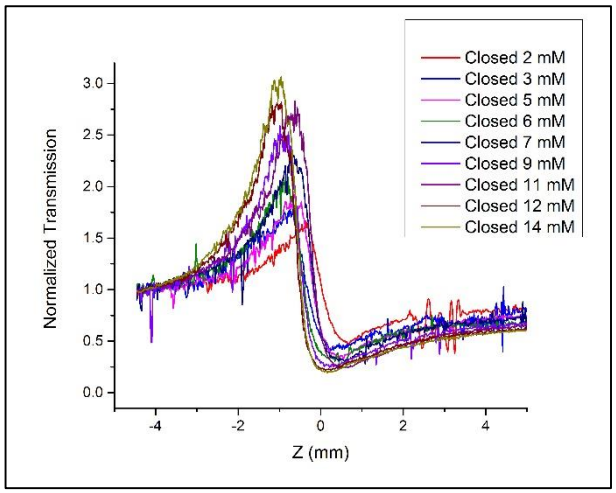

Figure 5.11: Closed aperture z-scan of gold nanoparticles synthesized using glucose and gelatin. Using CW argon-ion laser with λ=488 nm, Power=29.2

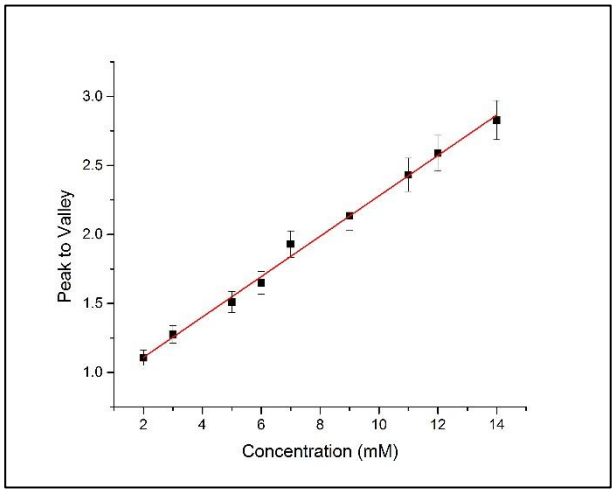

Figure 5.12: Variation in peak to valley (ΔT_{p-v}) for different glucose concentrations.

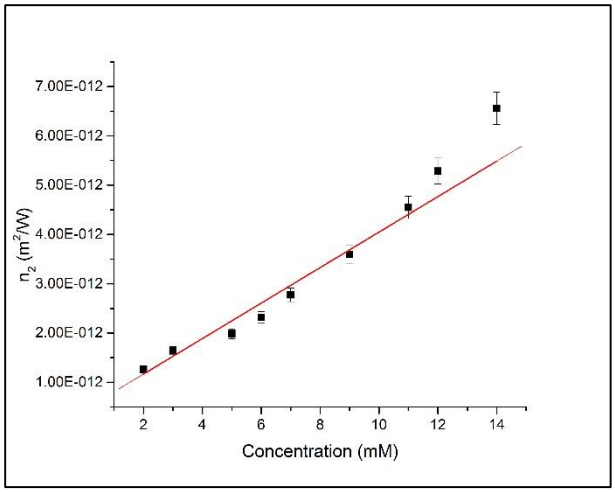

Figure 5.13: Variation in the nonlinear refractive index (n_2) for different glucose concentrations.

Unknown Concentrations

Gold nanoparticles were synthesized using unknown glucose concentrations and gelatin [section 4.1.2] and subjected to optical nonlinearity measurements using the z-scan technique to find the concentration of glucose in the sample. The z-scan experiment was performed using 488 nm CW argon-ion laser beam with a power of 29.2 mW. The experiment was repeated twice. The normalized transmittance curve is characterized by a prefocal peak followed by a postfocal valley, which implies that the nonlinear refractive index of gold nanoparticles synthesized with glucose and gelatin is negative ($n_2 < 0$). As shown in Table 5.6, the samples error doesn't exceed 11% in the first experiment, while for the samples promoted after five days, error exceeds 40%. This can be due to laser power and wavelength insatiability.

Table 5.6: Shows the values of peak to valley and % Error for the unknown glucose concentrations used in synthesizing gold nanoparticles.

Unknown No.	Actual Concentration (mM)	Peak to Valley	Measured Concentration (mM)	% Error
21.1.16				
1	4.5	1.402	4.00	11.06
2	7.5	2.032	8.31	10.80
3	12.5	2.611	12.27	1.85
26.1.16				
4	5	1.255	3.00	40.05
5	10	1.742	6.33	36.73
6	13	2.283	10.03	22.87

5.3.3 Gold-Silver (Au-Ag/core-shell) Nanoparticles

Gold-silver nanoparticles (Au-Ag/core-shell NPs) synthesized using $HAuCl_4$, $AgNO_3$, NaOH and L-ascorbic acid:

The synthesized gold-silver nanoparticles [section 4.1.3] were mixed with different concentrations of glucose and subjected to optical nonlinearity measurements using the z-scan technique. The z-scan experiment was performed using 488 nm CW argon-ion laser beam with a power of 30 mW. The normalized transmittance curve is characterized by a prefocal peak followed by a postfocal valley [Fig. 5.14]. This implies that the nonlinear refractive index of gold-silver nanoparticles mixed with glucose is negative ($n_2 < 0$). [Fig. 5.15] demonstrates a linear inverse proportional relation between the glucose concentration and the peak to valley values ($\Delta T_{p\text{-}v}$). This indicates that as the concentration of glucose increases, the size of nanoparticles decreases [see section 7.4]. It's not necessary to calculate the nonlinear refractive index every time, because peak to valley values are directly proportional to the nonlinear refractive index. Therefore, peak to valley values ($\Delta T_{p\text{-}v}$) can be used for the determination of glucose concentrations.

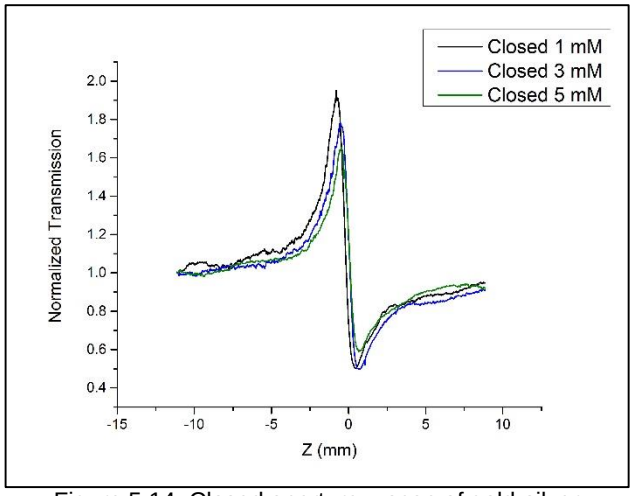

Figure 5.14: Closed aperture z-scan of gold-silver nanoparticles synthesized using $HAuCl_4$, $AgNO_3$, NaOH and L-ascorbic acid. Using CW argon-ion laser with λ=488 nm, Power=30 mW.

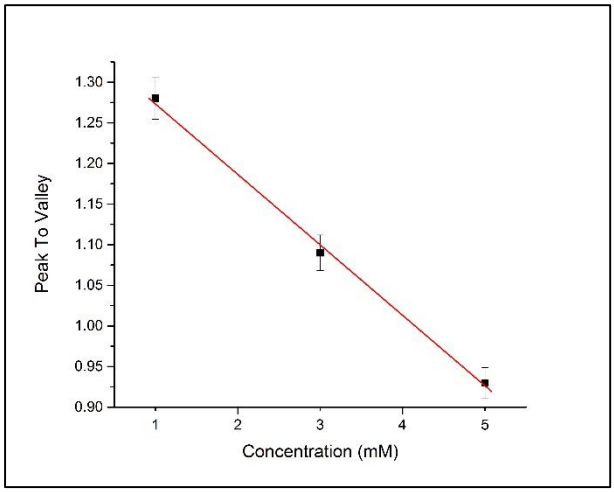

Figure 5.15: Variation in peak to valley (ΔT_{p-v}) for different glucose concentrations.

Chapter 6: Blood

The gold nanoparticles synthesized using glucose and gelatin gave the best results for glucose detection and quantifying. Therefore this method was used to detect glucose in diabetic blood. In this case glucose in blood was used instead of commercial glucose for the synthesis of gold nanoparticles. Both diabetic whole blood and plasma were used, but both methods failed. As human diabetic blood was not available, rats and rabbits diabetic blood was used. Gold nanoparticles affects the viscosity of whole blood and plasma, as it associates strongly with the essential blood proteins. This interaction leads to nanoparticles aggregation (105). Nanoparticles aggregation may be used as an explanation for the failure of below experiments.

Experiment 1]

Synthesis of gold nanoparticles using diabetic whole blood

In this attempt, whole blood was used. In a test tube 68.4 µL of 1% wt. gelatin, 22.8 µL of 1 M NaOH, 454.6 µL of diabetic whole blood and 454.6 µL of 10 mM $HAuCl_4$ were added in sequence. The test tube placed in the center of the microwave [Samsung – Model: ME6124ST] and heated for 30 seconds at low power (power 2) and allowed to cool to room temperature. The mixture coagulated [Fig. 6.1] and the surface plasmon resonance band centered at 393 nm [Fig. 6.2], indicating that there were no gold nanoparticles present.

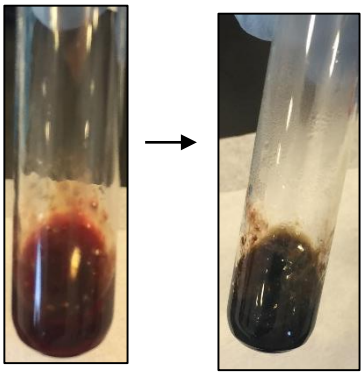

Figure 6.1: Gold nanoparticles synthesized using diabetic whole blood and gelatin before and after heating using microwave.

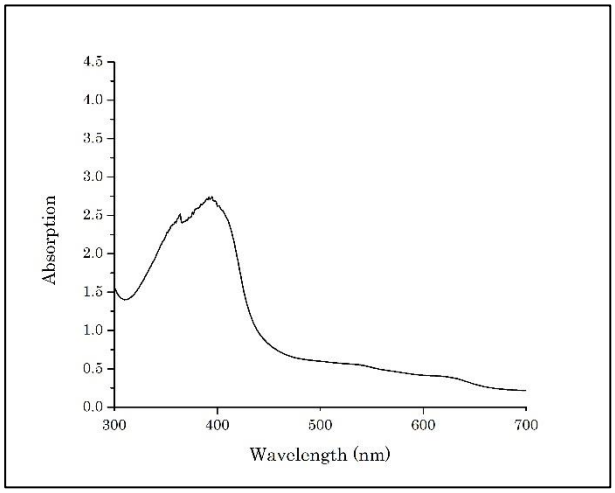

Figure 6.2: UV-Vis absorption spectra of gold nanoparticles synthesized using diabetic whole blood and gelatin).

Experiment 2]

Synthesis of AuNPs using diabetic blood plasma

Blood plasma separation according to the procedure outlined in Ref (106) was performed. The blood sample was centrifuged at 2000 rpm and a temperature of 4℃ for 20 minutes. A clear supernatant (plasma) solution was separated. To a test tube 68.4 µL of 1% wt. gelatin, 22.8 µL of 1 M NaOH, 454.6 µL of blood plasma and 454.6 µL of 10 mM $HAuCl_4$ were added in sequence, and the test tube subsequently placed in the center of the microwave and heated for 30 seconds at low power (power 2). The solution was allowed to cool to room temperature. No color change was observed [Fig. 6.3]. In Fig. 6.4 surface plasmon resonance band centered at 285 nm was observed, thus no gold nanoparticles were synthesized.

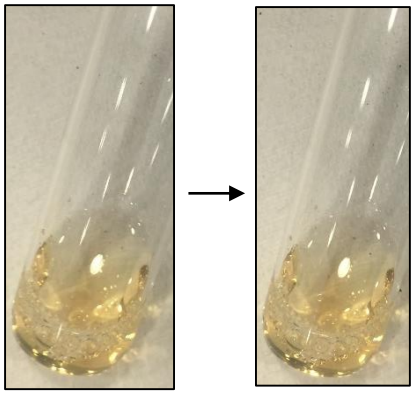

Figure 6.3: Gold nanoparticles synthesized using blood plasma and gelatin.

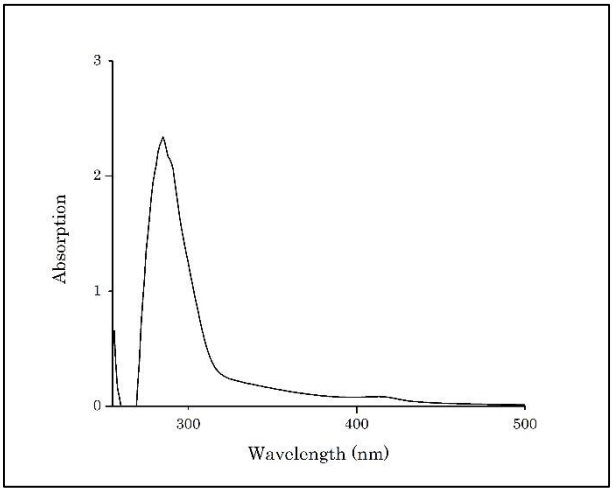

Figure 6.4: UV-Vis absorption spectra of gold nanoparticles synthesized using blood plasma and gelatin.

Chapter 7: Discussion

According to (107) it is possible to detect and quantify glucose in biological samples such as serum by an enzymatic colorimetric method using the z-scan technique, while in our research, the main goal is to detect and quantify glucose combined with nanoparticles using the z-scan technique.

7.1 Synthesis of Nanoparticles

Different methods were used to synthesize gold, silver and gold-silver nanoparticles, in order to find the cheapest and the easiest method, and to find the most suitable and accurate method for detecting and quantifying glucose levels.

Gold, silver and gold-silver nanoparticles were synthesized using wet chemistry and green synthetic methods. Almost all nanoparticles were synthesized using a reduction method. A reducing agent is used to reduce the metal ions to metal atoms. These atoms nucleate and form clusters and finally form nanoparticles.

$$Ag^{+} + \text{reducing agent} \rightarrow Ag^{0}$$

$$Au^{+3} + \text{reducing agent} \rightarrow Au^{0}$$

In wet chemistry, inorganic reducing agent was used such as trisodium citrate. In green synthesis, organic reducing agents were used such as glucose, curcumin, hibiscus, coffee, tea and gripe water. Some reducing agents such as curcumin and glucose act as a capping agent who stabilizes the nanoparticles and prevents further growth. Hot plate heating, oven heating, microwave heating and room temperature stirring were used to synthesize the nanoparticles.

7.2 Nanoparticles Characterization

Spectroscopy, Mie plot software, TEM microscope and XRD were used to confirm the formation of nanoparticles and for nanoparticles characterization.

UV-Vis spectrometer Shimadzu UV-1800 was used to record absorption spectra of the samples. Silver nanoparticles surface plasmon resonance band ranged from 400 – 433 nm. Where surface plasmon resonance band centered at 433, 420, and 400 for silver nanoparticles synthesized using curcumin, trisodium citrate and glucose & gelatin respectively. Silver nanoparticles synthesized using $AgNO_3$, glucose and NaOH surface plasmon resonance band ranged from 404 – 428 nm, whereas the concentration of glucose increases, surface plasmon resonance band shifts towards shorter wavelength (blue shift).

Gold nanoparticles surface plasmon resonance band ranged from 517 – 565 nm. The surface plasmon resonance band was centered at 517, 530, 535 and 526 for gold nanoparticles synthesized using trisodium citrate, curcumin, starch & glucose and glucose & gelatin respectively. For gold nanoparticles synthesized using glucose, NaOH and $HAuCl_4$, the surface plasmon resonance band ranged from 545 – 565 nm, and as the concentration of glucose increased, the surface plasmon resonance band shifted towards shorter wavelengths (blue shift).

For gold-silver NPs synthesized using $HAuCl_4$, $AgNO_3$, NaOH and L-ascorbic acid the surface plasmon resonance band centered at 385 and 487 nm.

Mie plot v4.5 was used to determine the diameter of silver and gold nanoparticles. The procedure was performed according to (83). Since the diameter of nanoparticles affect the absorption spectrum peak, using Mie plot software different diameters were used to get theoretical data. In OriginPro 9.0, the best fit of both theoretical and experimental absorption spectra indicate the diameter of nanoparticles. For silver nanoparticles synthesized using $AgNO_3$, glucose and NaOH the diameter is 65 nm. For gold nanoparticles synthesized using trisodium citrate the diameter is 10 nm and gold nanoparticles synthesized using glucose, NaOH and $HAuCl_4$ the diameter is 95 nm. These diameters may not be the real values due to the presence of nanoparticles with different sizes and shapes.

Three samples were sent to Timo Meerloo from University of California (UCSD) for transmission electron microscope (TEM) analysis. Gold nanoparticles that were synthesized using trisodium citrate, nanoparticles had diameters ranging from 9 – 23 nm with a high yield size of 12.5 nm. Gold nanoparticles synthesized using 8 mM glucose and gelatin, their nanoparticle diameters ranged from 3 – 28 nm with a high yield size of 3.7 nm. Gold nanoparticles synthesized using 14 mM glucose and gelatin, had nanoparticle diameters ranging from 8 – 22 nm with a high yield size of 9 nm. Larger nanoparticles were synthesized as the concentration of glucose increases. Other samples were analyzed on TEM microscope at University College Dublin (UCD) Ireland. These included gold and silver nanoparticles. For gold nanoparticles synthesized using curcumin, diameters ranged from 13 – 33 nm with a high yield size of 20 nm. For silver nanoparticles synthesized using curcumin, diameters ranged from 3.5 – 44 nm with a high yield size of 16.8 nm. For silver nanoparticles synthesized using trisodium citrate, diameters ranged from 3.5 – 50 nm with a high yield size of 3.6 nm. For silver nanoparticles synthesized using 8 mM glucose and gelatin, diameters ranged from 4 – 15 nm with a high yield size of 4 nm. All TEM images were analyzed and processed using ImageJ 1.5g software by converting pixels into image scale in nanometers. Then each NP was marked manually, and a size distribution histogram was created.

X-ray diffraction (XRD) carried out in the University of Bahrain (UOB) for gold nanoparticles synthesized using trisodium citrate. The XRD operated at 10 kV and as shown in Fig. 4.37 the XRD pattern verifies the presence of gold (Au) and other elements such as carbon (C), nitrogen (N), sodium (Na), oxygen (O) and chlorine (Cl).

7.3 Glucose Detection using UV-Vis Spectroscopy

Some attempts failed for glucose detection, while other succeeded. The optical properties are dependent on the size of the nanoparticles, where SPR band absorbance and peak position (red shift) increase linearly as the size of nanoparticles increases (60). According to ref.(59), as the concentration of glucose increases, the size of the nanoparticles increases, the surface plasmon resonance band absorbance increases or peak position shifts towards longer wavelengths (red shift). However, in ref.(58), as the concentration of glucose increases, the size of the nanoparticles decreases, the surface plasmon resonance band absorbance decreases or peak position shifts towards shorter wavelengths (blue shift). This can be used to describe the negative relations found between the absorbance and peak shift of the surface plasmon resonance band as a function of the glucose concentration, because in these cases glucose acts as a capping agent. Capping agents are used to stabilize and prevent the growth of the nanoparticles, so as the concentration of the glucose increases, nanoparticles with smaller sizes obtained (61). This relation found in silver nanoparticles synthesized using trisodium citrate, silver nanoparticles synthesized using glucose and gelatin, silver nanoparticles synthesized using $AgNO_3$, glucose and NaOH, gold nanoparticles synthesized using trisodium citrate, gold nanoparticles synthesized using starch and glucose and gold nanoparticles synthesized using glucose, NaOH and $HAuCl_4$.

Absorbance and peak position of silver nanoparticles synthesized using trisodium citrate surface plasmon resonance band is inversely proportional to the glucose concentration. The absorbance of silver nanoparticles synthesized using glucose and gelatin surface plasmon resonance band is inversely proportional to the glucose concentration. Peak position of silver nanoparticles synthesized using $AgNO_3$, glucose and NaOH surface plasmon resonance band is inversely proportional to the glucose concentration.

Absorbance of gold nanoparticles synthesized using trisodium citrate the surface plasmon resonance band is inversely proportional to the glucose concentration. Absorbance of gold nanoparticles synthesized using starch and glucose the surface plasmon resonance band is inversely proportional to the glucose concentration. Absorbance of gold nanoparticles synthesized using glucose and gelatin surface plasmon resonance band is directly proportional to the glucose concentration. In this case gelatin acts as a capping agent and its concentration is fixed. Peak position of gold nanoparticles synthesized using glucose, NaOH and $HAuCl_4$ surface plasmon resonance band is inversely proportional to the glucose concentration.

7.4 Glucose Detection using Z-scan

Some attempts failed for glucose detection, while other succeeded. All nanoparticles were subjected to the optical nonlinearity measurements z-scan technique. Z-scan experiments were performed using 488 nm CW argon-ion laser beam with an adjusting power of 15 - 30 mW. The normalized transmittance curve for all samples were characterized by a prefocal peak followed by a postfocal valley, which implies that the nonlinear refractive index of is negative ($n_2 < 0$). The nonlinear refractive index is dependent on the size of the nanoparticles, where the nonlinear refractive index increases linearly as the size of the nanoparticles increases (108). According to ref.(59), as the concentration of glucose increases, the size of the nanoparticles increases, thus the nonlinear refractive index increases. On the other hand, in ref.(58), as the concentration of glucose increases, the size of the nanoparticles decreases, thus the nonlinear refractive index decreases. This can be used as an explanation for the negative relations found between the nonlinear refractive index and the glucose concentration. Where in these cases, glucose acts as a capping agent, thus it prevents further growth of the nanoparticles size, so as the concentration of the glucose increases, smaller nanoparticles are obtained (61). This relation found in silver nanoparticles synthesized using trisodium citrate, silver nanoparticles

synthesized using glucose and gelatin, gold nanoparticles synthesized using trisodium citrate, gold nanoparticles synthesized using curcumin and gold- silver nanoparticles synthesized using $HAuCl_4$, $AgNO_3$, NaOH and L-ascorbic acid.

A linear inverse proportional relation was observed between the nonlinear refractive index (n_2) and the glucose concentration of silver nanoparticles synthesized using trisodium citrate. They have a nonlinear refractive index (n_2) range of 4.04×10^{-13} to 5.73×10^{-13} m^2/W. A linear inverse proportional relation was observed between the nonlinear refractive index (n_2) and the glucose concentration of silver nanoparticles synthesized using glucose and gelatin. They have a nonlinear refractive index (n_2) range of 6.28×10^{-13} to 8.11×10^{-13} m^2/W.

A linear inverse proportional relation was observed between the nonlinear refractive index (n_2) and the glucose concentration of gold nanoparticles synthesized using trisodium citrate, with a nonlinear refractive index (n_2) varying from 1.38×10^{-12} to 1.62×10^{-12} m^2/W. A linear inverse proportional relation was observed between the nonlinear refractive index (n_2) and the glucose concentration for gold nanoparticles synthesized using curcumin, with a nonlinear refractive index (n_2) varying from 2.31×10^{-13} to 2.53×10^{-13} m^2/W. A linear proportional relation was observed between the nonlinear refractive index (n_2) and the glucose concentration for gold nanoparticles synthesized using glucose and gelatin, with a nonlinear refractive index (n_2) varying from 1.26×10^{-12} to 6.56×10^{-12} m^2/W. Concentrations of glucose found after synthesizing gold nanoparticles with unknown glucose concentrations and gelatin, had an error of 2-11%. Three other unknown concentrations were found after five days with larger error of 22-40%. This may be due to laser intensity and wavelength instability.

A linear inverse proportional relation was observed between the peak to valley values (ΔT_{p-v}) and the glucose concentration of gold- silver nanoparticles synthesized using $HAuCl_4$, $AgNO_3$, NaOH and L-ascorbic acid.

A comparison was made between measured concentrations of artificial glucose using glucometer (digital glucose meter) and z-scan. Three concentrations of artificial glucose were used 5, 10 and 13 mM. Using glucometer, glucose was measured directly by placing a drop of artificial glucose on a test strip and the concentration was read. For z-scan measurements, as described in section 4.2.2 & 5.3.2 [Gold nanoparticles (AuNPs) synthesized using glucose and gelatin] artificial glucose was used in addition to $HAuCl_4$, NaOH and gelatin to synthesize gold nanoparticles. Then z-scan experiment was performed using 488 nm CW argon-ion laser beam with a power of 29.2 mW and the nonlinear refractive index (n_2) was calculated. In Fig 7.1, concentration readings of glucometer and the nonlinear refractive index (n_2) are linearly proportional with the concentration of the artificial glucose. Therefore, z-scan technique can be used detecting and measuring glucose concentrations.

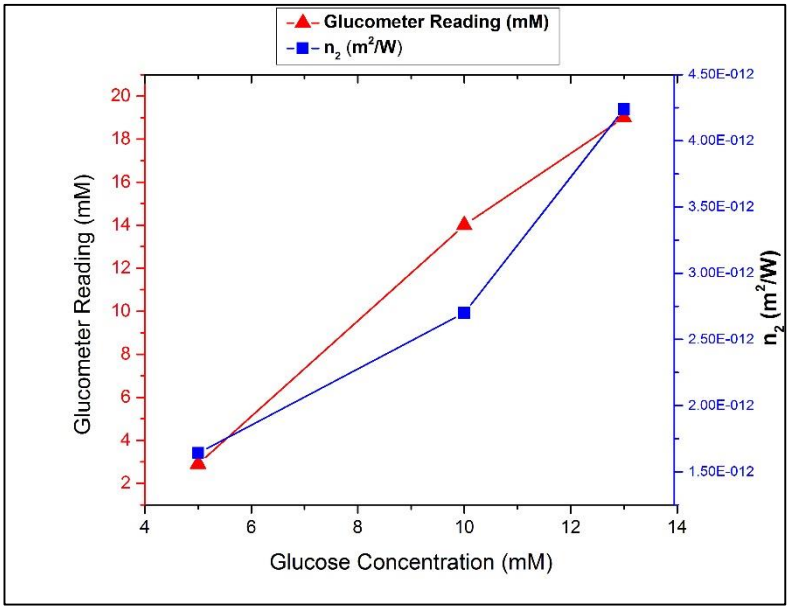

Figure 7.1: Comparison of the measured glucose concentrations using glucometer and z-scan.

Chapter 8: Conclusion

Nanoparticles such as silver, gold and gold-silver were synthesized by reduction methods using wet chemistry and green synthesis methods. In wet chemistry, trisodium citrate was used as a reducing agent, while in a green synthesis glucose and curcumin were used as reducing agents. For glucose detection, some nanoparticles were mixed with glucose after preparation, while others were synthesized using glucose. For gold nanoparticles synthesized using glucose and gelatin, as the concentration of glucose increases, the size of the nanoparticles increases, thus a positive linear correlation was found between the concentration of glucose and the absorbance/peak position shift of the surface plasmon resonance (SPR) band that was recorded using UV-Vis spectrometer. Also, the nonlinear refractive index (n_2) was measured using the z-scan technique, and a positive linear correlation was found between the concentration of glucose and the nonlinear refractive index (n_2) . Similar positive relations were published by Marisol (109) .On the other hand, in other methods as the concentration of glucose increases, the size of the nanoparticles decreases, thus a negative linear correlation was found between the concentration of glucose and the absorbance/peak position shift of surface plasmon resonance (SPR) band that was recorded using UV-Vis spectrometer. The nonlinear refractive index was measured using the z-scan technique and a negative linear correlation was found between the concentration of glucose and the nonlinear refractive index (n_2). In negative relations cases, glucose acts as a capping agent, which stabilize nanoparticles and prevents the nanoparticles size growth. Thus as the concentration of glucose increases, nanoparticles with smaller sizes are obtained. Similar negative relations due to increasing the concentration of the capping agents such as glucose were published by Bansal et al. (110).

In this research, we propose a novel method for synthesizing AuNPs using glucose, gelatin and microwaves. This work demonstrated a new method for the detection and the quantification of glucose using UV-Vis spectroscopy and the z-scan technique using silver, gold and gold-silver nanoparticles.

8.1 Further studies

This study opens up a new area of research into the detection of glucose in diabetic whole blood and plasma using the z-scan technique. First, a proper method for combining whole blood / plasma with nanoparticles should be studied. Then z-scan may be used to measure the optical nonlinearities for the detection and quantifying of glucose. The Improvement of these proposed methods should improve the accuracy. The observed negative relations between the absorbance, the peak shift and the nonlinear refractive index n_2 with the glucose concentration is subjected to further studies.

Chapter 9: References

1. The Global Diabetes Community. How many people have diabetes - Diabetes prevalence numbers [Internet]. [cited 19 November 2015]. Opgehaal van: http://www.diabetes.co.uk/diabetes-prevalence.html
2. Time Out Bahrain. Diabetes in Bahrain [Internet]. 2010 [cited 12 Mei 2016]. Opgehaal van: http://www.timeoutbahrain.com/bodyandmind/features/18066-diabetes-in-bahrain
3. Bahrain News Agency. Bahrain's diabetes rate drops [Internet]. 2011 [cited 12 Mei 2016]. Opgehaal van: http://bna.bh/portal/en/news/484152
4. TradeArabia News. Diabetes "biggest killer in Bahrain" [Internet]. 2014 [cited 29 November 2015]. Opgehaal van: http://www.tradearabia.com/news/HEAL_271291.html
5. Musaiger AO. Diabetes mellitus in Bahrain: an overview. Diabetic medicine [Internet]. Julie 1992 [cited 29 November 2015];9(6):574–8. Opgehaal van: http://www.ncbi.nlm.nih.gov/pubmed/1643809
6. ALNohair S. Obesity in gulf countries. International journal of health sciences [Internet]. Januarie 2014 [cited 29 April 2016];8(1):79–83. Opgehaal van: http://www.pubmedcentral.nih.gov/articlerender.fcgi?artid=4039587&tool=pmcentrez&rendertype=abstract
7. Loghmani E. Chapter 14 Diabetes Mellitis : type 1 and type 2. In Guidelines for Adolescent Nutrition Services Edited by: Stang J, Story M; 2005. 167-182 bl.
8. Diabetes.bh. Type 2 diabetes [Internet]. [cited 12 Mei 2016]. Opgehaal van: http://www.diabetes.bh/diabetes/what-is-diabetes/type-2-diabetes/
9. MacGill M. What is insulin? How does insulin regulate glucose? [Internet].

2016 [cited 12 Mei 2016]. Opgehaal van: http://www.medicalnewstoday.com/info/diabetes/whatisinsulin.php

10. The Euro-Wabb. Diabetes Information | Insulin - What does it do? [Internet]. [cited 12 Mei 2016]. Opgehaal van: http://www.euro-wabb.org/en/diabetes-information-all/insulin-what-does-it-do

11. Pagliuca FW, Millman JR, Gürtler M, Segel M, Van Dervort A, Ryu JH, et al. Generation of functional human pancreatic β cells in vitro. Cell [Internet]. 09 Oktober 2014 [cited 09 Oktober 2014];159(2):428–39. Opgehaal van: http://www.pubmedcentral.nih.gov/articlerender.fcgi?artid=4617632&tool=pmcentrez&rendertype=abstract

12. Ferry Jr. Diabetes Treatment (type 1 and type 2 medications and diet) [Internet]. [cited 29 November 2015]. Opgehaal van: http://www.medicinenet.com/diabetes_treatment/article.htm

13. Dhinaa AN, Nooraldeen AY, Murali K, Palanisamy PK. Z-scan technique as a tool for the measurement of blood glucose. Laser Physics [Internet]. 2008;18(10):1212–6. Opgehaal van: http://link.springer.com/10.1134/S1054660X08100198

14. Lu SZ, Wang HT. Determination of third- and fifth-order nonlinear coefficients by using quasi-one-dimensional slit beam Z-scan technique. Journal of Applied Physics [Internet]. 2009 [cited 11 September 2016];105(3):33104. Opgehaal van: http://scitation.aip.org/content/aip/journal/jap/105/3/10.1063/1.3075831

15. Sheik-Bahae M, Said AA, Wei T-H, Hagan DJ, Van Stryland EW. Sensitive measurement of optical nonlinearities using a single beam. IEEE Journal of Quantum Electronics [Internet]. April 1990 [cited 29 September 2015];26(4):760–9. Opgehaal van: http://ieeexplore.ieee.org/lpdocs/epic03/wrapper.htm?arnumber=53394

16. American Diabetes Association. Diagnosis and classification of diabetes mellitus. Diabetes Care [Internet]. 2012;35(Supplement_1):S64–71.

Opgehaal van: http://care.diabetesjournals.org/cgi/doi/10.2337/dc12-s064

17. Mandal A. History of diabetes [Internet]. 2012 [cited 03 Maart 2016]. Opgehaal van: http://www.news-medical.net/health/History-of-Diabetes.aspx

18. McCoy K. The history of diabetes [Internet]. 2009 [cited 03 Maart 2016]. Opgehaal van: http://www.everydayhealth.com/diabetes/understanding/diabetes-mellitus-through-time.aspx

19. American Diabetes Association. History of diabetes [Internet]. 2014 [cited 03 Maart 2016]. Opgehaal van: http://www.diabetes.org/research-and-practice/student-resources/history-of-diabetes.html?referrer=https://www.google.com.bh/

20. Aronoff SL, Berkowitz K, Shreiner B, Want L. Glucose metabolism and regulation: beyond insulin and glucagon. Diabetes Spectrum [Internet]. 01 Julie 2004 [cited 05 Januarie 2015];17(3):183–90. Opgehaal van: http://spectrum.diabetesjournals.org/content/17/3/183.full

21. Diabetes Research & Wellness Foundation. What is diabetes? Professional nurse (London, England). 1986;1(12):333–4.

22. Thomassian B. Diabetes mellitus : pathophysiology and clinical guidelines. The Academy of Dental Learning & OSHA Training. 2012;12212(800).

23. Canadian Diabetes Association. Types of diabetes [Internet]. [cited 29 November 2015]. Opgehaal van: http://www.diabetes.ca/about-diabetes/types-of-diabetes

24. Hernandez E, RN, BSN, PHN. Diabetes. Clinical Research Center [Internet]. Opgehaal van: https://collab.nlm.nih.gov/webcastsandvideos/drew/diabetes.pdf

25. Diabetes Info. Three types of diabetes : type 1, type 2 and gestational diabetes [Internet]. [cited 29 November 2015]. Opgehaal van:

http://www.diabetes-info.co.uk/what-is-diabetes/types-of-diabetes.html

26. Medline Plus. Long term complications of diabetes [Internet]. 2014 [cited 02 Maart 2016]. Opgehaal van: https://www.nlm.nih.gov/medlineplus/ency/patientinstructions/000327.htm

27. Tonyushkina K, Nichols JH. Glucose meters: a review of technical challenges to obtaining accurate results. Journal of diabetes science and technology [Internet]. Julie 2009 [cited 29 November 2015];3(4):971–80. Opgehaal van: http://www.pubmedcentral.nih.gov/articlerender.fcgi?artid=2769957&tool=pmcentrez&rendertype=abstract

28. Oliver NS, Toumazou C, Cass AEG, Johnston DG. Glucose sensors: a review of current and emerging technology. Diabetic Medicine [Internet]. Maart 2009 [cited 19 April 2015];26(3):197–210. Opgehaal van: http://www.ncbi.nlm.nih.gov/pubmed/19317813

29. The Global Diabetes Community. Continuous glucose monitoring. 2015; Opgehaal van: http://www.diabetes.co.uk/cgm/continuous-glucose-monitoring.html

30. Tura A, Maran A, Pacini G. Non-invasive glucose monitoring: assessment of technologies and devices according to quantitative criteria. Diabetes research and clinical practice [Internet]. Julie 2007 [cited 08 November 2015];77(1):16–40. Opgehaal van: http://www.sciencedirect.com/science/article/pii/S0168822706004931

31. Hubbard CW, Gordon RL. Chemical sensors. 1987; Opgehaal van: http://www.osti.gov/servlets/purl/6804195/

32. Lambrechts M, Sansen W. Biosensors: microelectrochemical devices [Internet]. CRC Press; 1992 [cited 30 November 2015]. 316 bl. Opgehaal van: https://books.google.com/books?id=LDpf_dJotaQC&pgis=1

33. Edmonds TE. Chemical sensors [Internet]. Springer Science & Business

Media; 2013 [cited 30 November 2015]. 326 bl. Opgehaal van: https://books.google.com/books?id=9ZzuCAAAQBAJ&pgis=1

34. National Nanotechnology Initiative. What is nanotechnology? [Internet]. [cited 27 Maart 2016]. Opgehaal van: http://www.nano.gov/nanotech-101/what/definition

35. AZoNano. Nanoparticles defined - what nanoparticles are and what makes them special [Internet]. 2006 [cited 28 Februarie 2016]. Opgehaal van: http://www.azonano.com/article.aspx?ArticleID=1734

36. Heiligtag FJ, Niederberger M. The fascinating world of nanoparticle research. Materials Today [Internet]. Julie 2013 [cited 07 Oktober 2015];16(7–8):262–71. Opgehaal van: http://www.sciencedirect.com/science/article/pii/S1369702113002253

37. Nanotech. Nanotechnology: history [Internet]. [cited 18 Mei 2016]. Opgehaal van: http://nano--tech.blogspot.com/p/history.html

38. Mandal A. What are nanoparticles? [Internet]. [cited 19 November 2015]. Opgehaal van: http://www.news-medical.net/health/What-are-Nanoparticles.aspx

39. Daw R. Nanotechnology is ancient history [Internet]. 2012 [cited 18 Mei 2016]. Opgehaal van: http://www.theguardian.com/nanotechnology-world/nanotechnology-is-ancient-history

40. Gayatri K, Lakshmi G, Preeti K. Nanoparticles: an overview of preparation and characterization. Novel Science International Journal of … [Internet]. 2012;1(8):557–62. Opgehaal van: http://pharmacy.novelscience.info/index.php/nvp/article/viewArticle/13953

41. Mohanraj VJ, Chen Y. Nanoparticles - a review. Tropical Journal of Pharmaceutical Research [Internet]. Faculty of Pharmacy, University of Benin; 31 Julie 2007 [cited 19 November 2015];5(1):561–73. Opgehaal van: http://www.ajol.info/index.php/tjpr/article/view/14634

42. Thos E, Ogos L, Athos P. Methods of preparation of nanoparticles - a review. International Journal of Advances in Engineering & Technology. 2015;7(4):165–98.

43. Buckley, A.M.; Greenblatt MJ. Sol-Gel preparation of silica gels. J Chem Ed. 1994;71(7):599.

44. Iravani S, Korbekandi H, Mirmohammadi S V, Zolfaghari B. Synthesis of silver nanoparticles: chemical, physical and biological methods. Research in pharmaceutical sciences [Internet]. Januarie [cited 27 Oktober 2015];9(6):385–406. Opgehaal van: http://www.pubmedcentral.nih.gov/articlerender.fcgi?artid=4326978&tool=pmcentrez&rendertype=abstract

45. Kurniawan F. New analytical applications of gold nanoparticles [Internet]. University of Regensburg; 2008. Opgehaal van: http://epub.uni-regensburg.de/12113/1/Fredy_Kurniawan_desertation.pdf

46. Trau D, Renneberg R. Encapsulation of glucose oxidase microparticles within a nanoscale layer-by-layer film: immobilization and biosensor applications. Biosensors & bioelectronics [Internet]. 15 Oktober 2003 [cited 08 September 2016];18(12):1491–9. Opgehaal van: http://www.ncbi.nlm.nih.gov/pubmed/12941565

47. Ariga K, Hill JP, Ji Q. Layer-by-layer assembly as a versatile bottom-up nanofabrication technique for exploratory research and realistic application. Physical chemistry chemical physics : PCCP [Internet]. 21 Mei 2007 [cited 08 September 2016];9(19):2319–40. Opgehaal van: http://www.ncbi.nlm.nih.gov/pubmed/17492095

48. Wang B. Microphysiometer using multiwall carbon nanotubes enable constant realtime monitoring of microliters of insulin [Internet]. 2008. Opgehaal van: http://www.nextbigfuture.com/2008/04/microphysiometer-using-multiwall-carbon.html

49. Frasco MF, Chaniotakis N. Semiconductor quantum dots in chemical

sensors and biosensors. Sensors. 2009;9(9):7266–86.

50. Tang B, Cao L, Xu K, Zhuo L, Ge J, Li Q, et al. A new nanobiosensor for glucose with high sensitivity and selectivity in serum based on fluorescence resonance energy transfer (FRET) between CdTe quantum dots and Au nanoparticles. Chemistry [Internet]. 2008 [cited 08 September 2016];14(12):3637–44. Opgehaal van: http://www.ncbi.nlm.nih.gov/pubmed/18318025

51. Rahiman S. Nanomedicine current trends in diabetes management. Journal of Nanomedicine & Nanotechnology [Internet]. 2012;3(4):3–8. Opgehaal van: http://www.omicsonline.org/2157-7439/2157-7439-3-137.digital/2157-7439-3-137.html

52. Boysen E. Nanoparticles applications and uses [Internet]. [cited 26 November 2015]. Opgehaal van: http://www.understandingnano.com/nanoparticles.html

53. D'Almeida C, Roth B. Medical applications of nanoparticles [Internet]. Oakland University; Opgehaal van: https://www.umflint.edu/sites/default/files/groups/Research_and_Sponsored_Programs/MOM/c.dalmeida_b.roth_.pdf

54. Oldenburg SJ. Silver nanoparticles: properties and applications [Internet]. [cited 22 Februarie 2016]. Opgehaal van: http://www.sigmaaldrich.com/materials-science/nanomaterials/silver-nanoparticles.html

55. Bera RK, Anoop A, Raj CR. Enzyme-free colorimetric assay of serum uric acid. Chemical communications (Cambridge, England) [Internet]. The Royal Society of Chemistry; 07 November 2011 [cited 27 Maart 2016];47(41):11498–500. Opgehaal van: http://pubs.rsc.org/en/content/articlehtml/2011/cc/c1cc13349g

56. Sigma-Aldrich. Gold nanoparticles: properties and applications [Internet]. [cited 28 Februarie 2016]. Opgehaal van:

http://www.sigmaaldrich.com/materials-science/nanomaterials/gold-nanoparticles.html

57. What When How. Metal nanostructures synthesized by soft chemical methods and shape control - part 2 (Nanotechnology) [Internet]. [cited 08 Maart 2016]. Opgehaal van: http://what-when-how.com/nanoscience-and-nanotechnology/metal-nanostructures-synthesized-by-soft-chemical-methods-and-shape-control-part-2-nanotechnology/

58. Unser S, Campbell I, Jana D, Sagle L. Direct glucose sensing in the physiological range through plasmonic nanoparticle formation. Analyst [Internet]. The Royal Society of Chemistry; 2015;140(2):590–9. Opgehaal van: http://www.ncbi.nlm.nih.gov/pubmed/25426496

59. Ishihara M, Nguyen VQ, Mori Y, Nakamura S, Hattori H. Adsorption of silver nanoparticles onto different surface structures of chitin/chitosan and correlations with antimicrobial activities. International journal of molecular sciences [Internet]. Multidisciplinary Digital Publishing Institute; 18 Januarie 2015 [cited 06 April 2016];16(6):13973–88. Opgehaal van: http://www.mdpi.com/1422-0067/16/6/13973/htm

60. He YQ, Liu SP, Kong L, Liu ZF. A study on the sizes and concentrations of gold nanoparticles by spectra of absorption, resonance Rayleigh scattering and resonance non-linear scattering. Spectrochimica acta Part A [Internet]. Oktober 2005 [cited 18 Mei 2016];61(13–14):2861–6. Opgehaal van: http://www.sciencedirect.com/science/article/pii/S1386142504005505

61. Arulmozhi KT, Mythili N. Studies on the chemical synthesis and characterization of lead oxide nanoparticles with different organic capping agents. AIP Advances [Internet]. AIP Publishing; 31 Desember 2013 [cited 27 Mei 2016];3(12):122122. Opgehaal van: http://scitation.aip.org/content/aip/journal/adva/3/12/10.1063/1.4858419

62. National Nanotechnology Infrastructure Netwrok. Silver nanoparticles synthesis and spectroscopy [Internet]. 2012 [cited 27 Januarie 2016].

Opgehaal van: http://www.nnin.org/sites/default/files/files/PT1 Silver nanoparticle synthesis_TG.pdf

63. Nadagouda MN, Varma RS. Green synthesis of silver and palladium nanoparticles at room temperature using coffee and tea extract. Green Chemistry. 2008;10(8):859.

64. Bindhu MR, Umadevi M. Synthesis of monodispersed silver nanoparticles using Hibiscus cannabinus leaf extract and its antimicrobial activity. Spectrochimica acta Part A, Molecular and biomolecular spectroscopy [Internet]. 15 Januarie 2013 [cited 27 Januarie 2016];101:184–90. Opgehaal van: http://www.sciencedirect.com/science/article/pii/S1386142512009006

65. Philip D. Green synthesis of gold and silver nanoparticles using hibiscus rosa sinensis. Physica E [Internet]. Maart 2010 [cited 04 November 2015];42(5):1417–24. Opgehaal van: http://www.sciencedirect.com/science/article/pii/S1386947709005177

66. Kirthika P., Dheeba B. SR, Sheik A. Plant mediated synthesis and characterization of silver nanoparticles. International Journal of Pharmacy and Pharmaceutical Sciences [Internet]. 2014 [cited 27 Januarie 2016];6(8). Opgehaal van: http://innovareacademics.in/journals/index.php/ijpps/article/viewFile/2784/pdf_58

67. Bettini S, Pagano R, Valli L, Giancane G. Drastic nickel ion removal from aqueous solution by curcumin-capped Ag nanoparticles. Nanoscale [Internet]. Royal Society of Chemistry; 2014;6(17):10113–7. Opgehaal van: http://www.ncbi.nlm.nih.gov/pubmed/25036541

68. Darroudi M, Ahmad M Bin, Abdullah AH, Ibrahim NA, Shameli K. Effect of accelerator in green synthesis of silver nanoparticles. International Journal of Molecular Sciences. 2010;11(10):3898–905.

69. Palanisamy PK, Kirubha E, Vishista K. Gripe water-mediated green

synthesis of silver nanoparticles and their applications in nonlinear optics and surface-enhanced raman spectroscopy. Applied Nanoscience [Internet]. Springer Berlin Heidelberg; 2014;5:777–86. Opgehaal van: http://dx.doi.org/10.1007/s13204-014-0376-4

70. El-Kheshen AA, El-Rab S. Effect of reducing and protecting agents on size of silver nanoparticles and their anti-bacterial activity. Der Pharma Chemica. 2012;4(1):53–65.

71. Ratyakshi, Chauhan RP. Colloidal synthesis of silver nano particles. Asian Journal of Chemistry. 2009;21(10):113–6.

72. Sreelakshmi C, Goel N, Datta KKR, Addlagatta A, Ummanni R, Reddy BVS. Green synthesis of curcumin capped gold nanoparticles and evaluation of their cytotoxicity. Nanoscience and Nanotechnology Letters [Internet]. 2013;5(12):1258–65. Opgehaal van: http://openurl.ingenta.com/content/xref?genre=article&issn=1941-4900&volume=5&issue=12&spage=1258

73. Sindhu K, Rajaram A, Sreeram KJ, Rajaram R. Curcumin conjugated gold nanoparticle synthesis and its biocompatibility. RSC Advances [Internet]. 2014;4:1. Opgehaal van: http://xlink.rsc.org/?DOI=c3ra45345f

74. Engelbrekt C, Sørensen KH, Zhang J, Welinder AC, Jensen PS, Ulstrup J. Green synthesis of gold nanoparticles with starch–glucose and application in bioelectrochemistry. Journal of Materials Chemistry. 2009;19:7839–47.

75. McFarland AD, Haynes CL, Mirkin CA, Duyne RP Van, Godwin HA. Color My Nanoworld. J Chem Educ [Internet]. 2004 [cited 31 Januarie 2016];81(4):544A. Opgehaal van: http://education.mrsec.wisc.edu/277.htm

76. Dackiw AP. Induction and modulation of monocyte I macrophage tissue factorifibrin deposition and Tnf secretion in the microenvironment of inflammation : the role of tyrosine. University of Toronto; 1998.

77. Kirubha E, Palanisamy PK. Green synthesis, characterization of Au–Ag core–shell nanoparticles using gripe water and their applications in nonlinear optics and surface enhanced Raman studies. Advances in Natural Sciences: Nanoscience and Nanotechnology [Internet]. IOP Publishing; 2014;5(4):45006. Opgehaal van: http://stacks.iop.org/2043-6262/5/i=4/a=045006?key=crossref.eeb98f64f466e9b9ab329b3fdb858127

78. Samal AK, Polavarapu L, Rodal-Cedeira S, Liz-Marzán LM, Pérez-Juste J, Pastoriza-Santos I. Size tunable Au@Ag core-shell nanoparticles: synthesis and surface-enhanced raman scattering properties. Langmuir. 2013;29(48):15076–82.

79. NanoComposix. UV/VIS/IR spectroscopy analysis of nanoparticles. 2012 [cited 10 September 2016]; Opgehaal van: http://50.87.149.212/sites/default/files/nanoComposix Guidelines for UV-vis Analysis.pdf

80. Oldenburg SJ. Silver nanoparticles: properties and applications [Internet]. Opgehaal van: http://www.sigmaaldrich.com/materials-science/nanomaterials/silver-nanoparticles.html

81. Sigma-Aldrich. Gold nanoparticles: properties and applications [Internet]. Opgehaal van: http://www.sigmaaldrich.com/materials-science/nanomaterials/gold-nanoparticles.html

82. Madou MJ. Solid-state physics, fluidics, and analytical techniques in micro- and nanotechnology [Internet]. CRC Press; 2011. Opgehaal van: books.google.com.bh/books?id=sRvSBQAAQBAJ&pg=PA368&lpg=PA368&dq=interaction+of+em+with+rod+nanoparticles&source=bl&ots=M_KUORCZM1&sig=VHY_O-AsZnbguOF3QwyBh8o5rQQ&hl=en&sa=X&ved=0ahUKEwjbgYbSwp3PAhVFLsAKHfu3D74Q6AEIIjAB#v=onepage&q=interaction of em with r

83. Bumm LA. Size determination of gold nanoparticles using Mie theory and

extinction spectra. Nanolab [Internet]. 2007;1–10. Opgehaal van: http://www.nhn.ou.edu/~bumm/NanoLab/pdf/Au_NP_spectrophotometery_activity.pdf

84. Jian Z, Yongchang W, Yimin L. Fluorescence spectra characters of silver-coated gold colloidal nanoshells. Colloids and Surfaces A: Physicochemical and Engineering Aspects. 2004;232(2–3):155–61.

85. Kotov NA. Nanoparticle assemblies and superstructures [Internet]. CRC Press; 2005. Opgehaal van: https://books.google.com.bh/books?id=APDKBQAAQBAJ&printsec=frontcover#v=onepage&q&f=false

86. Varier GK. Investigations on Nonlinear and Radiative Properties of Certain Photonic Materials [Internet]. Cochin University of Science & Technology; 1998. Opgehaal van: https://dyuthi.cusat.ac.in/xmlui/bitstream/handle/purl/2305/Dyuthi-T0596.pdf?sequence=1

87. Suresh S, Ramanand A, Jayaraman D, Mani P. Review on theoretical aspect of nonlinear optics. Reviews on Advanced Materials Science. 2012;30(2):175–83.

88. Stucky GD, Marder SR, Sohn JE. Linear and nonlinear polarizability - A primer. ACS Symp Ser. 1991;455(Mater. Nonlinear Opt.):2–30.

89. Boyd RW. The nonlinear optical susceptibility - Chapter 1. Nonlinear Optics. 1961. 1-67 bl.

90. Prasad PN, Williams DJ. Introduction to nonlinear optical effects in molecules and polymers [Internet]. Wiley. 1991. 320 bl. Opgehaal van: http://www.gbv.de/dms/ilmenau/toc/019503016.PDF

91. Pálfalvi L, Tóth BC, Almási G, Fülöp JA, Hebling J. A general Z-scan theory. Applied Physics B [Internet]. 30 Julie 2009 [cited 19 November 2015];97(3):679–85. Opgehaal van:

http://link.springer.com/10.1007/s00340-009-3656-z

92. Chapple PB, Staromlynska J, Hermann JA, Mckay TJ, Mcduff RG. Single-beam z-Scan: measurement techniques and analysis. Journal of Nonlinear Optical Physics & Materials [Internet]. World Scientific Publishing Company; 25 September 1997 [cited 19 November 2015];6(3):251–93. Opgehaal van: http://www.worldscientific.com/doi/abs/10.1142/S0218863597000204?src=recsys&journalCode=jnopm

93. Sheik-bahae M, Said A a, Wei T, Hagan DJ, Stryland EW Van. Special 30th anniversary feature sensitive measurement of optical nonlinearities using a single beam. IEEE LEOS Newsletter [Internet]. 2007;(February):17–26. Opgehaal van: http://photonicssociety.org/newsletters/feb07/special30th.pdf

94. Arularasan P, Sivakumar B, Raj SG, Kumar GR, Mohan R. Determination of nonlinear absorption (β) and refraction (n 2)by the Z-scan method: third-order nonlinear optical properties of π- conjugated potassium pentaborate crystal. Journal of Applied Physics [Internet]. 2013 [cited 19 November 2015];4(4):48–54. Opgehaal van: http://www.academia.edu/7132060/Determination_of_nonlinear_absorption_%CE%B2_and_refraction_n_2_by_the_Z-scan_method_third-order_nonlinear_optical_properties_of_%CF%80-_conjugated_Potassium_Pentaborate_crystal

95. Stryland EW Van, Sheik-Bahae M. Z-Scan measurements of optical nonlinearities - Characterization techniques and tabulations for organic nonlinear materials. 1998;18(3):655–92.

96. Trejo-Duran M, Cornejo-Monroy D, Alvarado-Mendez E, Olivares-Vargas A, Castano VM. Nonlinear optical properties of Au-nanoparticles conjugated with lipoic acid in water. Journal of the European Optical Society: Rapid Publications [Internet]. 2014;9:14030. Opgehaal van:

http://www.scopus.com/inward/record.url?eid=2-s2.0-84907345503&partnerID=tZOtx3y1

97. Chen G. Particularities of heat conduction in nanostructures. Journal of Nanoparticle Research. Kluwer Academic Publishers; 2000;2(2):199–204.

98. Karthikeyan B, Thomas J, Philip R. Optical nonlinearity in glass-embedded silver nanoclusters under ultrafast laser excitation. Chemical Physics Letters. 2005;414(4):346–50.

99. Philip R, Kumar GR, Sandhyarani N, Pradeep T. Picosecond optical nonlinearity in monolayer-protected gold, silver, and gold-silver alloy nanoclusters. Physical Review B. American Physical Society; 15 November 2000;62(19):13160–6.

100. Gordon JP, Leite RCC, Moore RS, Porto SPS, Whinnery JR. Long-transient effects in lasers with inserted liquid samples. Journal of Applied Physics. 1965;36(1):3–8.

101. Sreeja R, Aneesh PM, Aravind A, Reshmi R, Philip R, Jayaraj MK. Size-dependent optical nonlinearity of Au nanocrystals. Journal of The Electrochemical Society. 2009;156(10):167–72.

102. Jacinto C, Messias DN, Andrade AA, Lima SM, Catunda T. Thermal lens and Z-scan measurements: Thermal and optical properties of laser glasses – A review. Journal of Non-Crystalline Solids. 2006;352(32):3582–97.

103. Dhinaa AN, Palanisamy PK. Z-scan technique for measurment of total cholesterol and triglycerides in blood. Journal of Innovative Optical Health Sciences [Internet]. World Scientific Publishing Company; 21 Julie 2009 [cited 19 November 2015];2(3):295–301. Opgehaal van: http://www.worldscientific.com/doi/abs/10.1142/S1793545809000565

104. Dhinaa AN, Palanisamy PK. Z-Scan technique: To measure the total protein and albumin in blood. Journal of Biomedical Science and Engineering [Internet]. Scientific Research Publishing; 08 April 2010 [cited

19 November 2015];3(3):285–90. Opgehaal van: http://www.scirp.org/journal/PaperInformation.aspx?PaperID=1529&#abstract

105. Abdelhalim M, Mady M. Rheological parameters assessment in serum, plasma and whole blood of rats after administration of gold nanoparticles of different sizes: In vivo. Journal of Nanomedicine & Nanotechnology [Internet]. OMICS International; 2012 [cited 09 September 2016];3(6). Opgehaal van: http://www.omicsonline.org/2157-7439/2157-7439-3-145.digital/2157-7439-3-145.html

106. Cinj. Procedure for separating plasma and serum from whole blood. Opgehaal van: http://www.cinj.org/sites/cinj/files/documents/C4ProcedureForSerumAndPlasmaSepartion.pdf

107. Alves SI, Silva E a. O, Costa SS, Sonego DRN, Hallack ML, Coppini OL, et al. The validation of the Z-Scan technique for the determination of plasma glucose. Proc of SPIE [Internet]. 2013;8785:87851B. Opgehaal van: http://proceedings.spiedigitallibrary.org/proceeding.aspx?doi=10.1117/12.2025994

108. Shahriari E, Yunus WMM, Saion E. Effect of particle size on nonlinear refractive index of Au nanoparticle in PVA solution. Brazilian Journal of Physics [Internet]. Sociedade Brasileira de Física; Junie 2010 [cited 18 Mei 2016];40(2):256–60. Opgehaal van: http://www.scielo.br/scielo.php?script=sci_arttext&pid=S0103-97332010000200021&lng=en&nrm=iso&tlng=en

109. Garcia M. Truly non invasive glucose optical sensor based on metal nanoparticles generation [Internet]. University of Central Florida; 2006 [cited 30 Mei 2016]. Opgehaal van: https://www.researchgate.net/publication/47713435_TRULY_NON_INVA

SIVE_GLUCOSE_OPTICAL_SENSOR_BASED_ON_METAL_NANOPARTICLES_GENERATION

110. Bansal P, Jaggi N, Rohilla S. “ Green ” Synthesis of CdS nanoparticles and effect of capping agent concentration on crystallite size. Research Journal of Chemical Sciences. 2012;2(8):69–71.

111. Horikoshi S, Serpone N. Introduction to nanoparticles - Microwaves in nanoparticle synthesis [Internet]. Weinheim, Germany: Wiley-VCH Verlag GmbH & Co. KGaA; 2013 [cited 16 Julie 2016]. 1-24 bl. Opgehaal van: http://doi.wiley.com/10.1002/9783527648122.ch1

112. Bloemer MJ, Haus JW, Ashley PR. Degenerate four-wave mixing in colloidal gold as a function of particle size. Journal of the Optical Society of America B [Internet]. Optical Society of America; 01 Mei 1990 [cited 20 April 2016];7(5):790. Opgehaal van: http://www.osapublishing.org/viewmedia.cfm?uri=josab-7-5-790&seq=0&html=true

113. Klemm P, Haug T, Bange S, Lupton JM. Time-domain interferometry of surface plasmons at nonlinear continuum hot spots in films of silver nanoparticles. Physical review letters [Internet]. 31 Desember 2014 [cited 20 April 2016];113(26):266805. Opgehaal van: https://utah.pure.elsevier.com/en/publications/time-domain-interferometry-of-surface-plasmons-at-nonlinear-conti

114. Sheik-Bahae M, Said AA, Wei TH, Hagan DJ, Van Stryland EW. Sensitive measurement of optical nonlinearities using a single beam. IEEE Journal of Quantum Electronics [Internet]. IEEE; 01 April 1990 [cited 20 April 2016];26(4):760–9. Opgehaal van: http://ieeexplore.ieee.org/articleDetails.jsp?arnumber=53394

115. Stryland E, Sheik-Bahae M, Said A, Hagan A. Characterization of nonlinear optical absorption and refraction. Progress in Crystal Growth and Characterization of Materials. 1993;27((3-4)):279–311.

116. Henari FZ, Dakhel AA. Linear and nonlinear optical properties of gold nanoparticle-Eu oxide composite thin films. Journal of Applied Physics [Internet]. AIP Publishing; 11 Augustus 2008 [cited 20 April 2016];104(3):33110. Opgehaal van: http://scitation.aip.org/content/aip/journal/jap/104/3/10.1063/1.2967711

117. Rativa D, Araujo RE, Gomes AS. One photon nonresonant high-order nonlinear optical properties of silver nanoparticles in aqueous solution. Optics Express [Internet]. Optical Society of America; 05 November 2008 [cited 20 April 2016];16(23):19244. Opgehaal van: http://www.osapublishing.org/viewmedia.cfm?uri=oe-16-23-19244&seq=0&html=true

118. Shahriari E, Yunus WMM, Naghavi K, Saion E. The optical nonlinearity of Au and Ag nanoparticle prepared by the Γ-radiation method. American Journal of Engineering and Applied Sciences [Internet]. Science Publications; 01 Februarie 2010 [cited 20 April 2016];3(2):260–4. Opgehaal van: http://thescipub.com/abstract/10.3844/ajeassp.2010.260.264

119. Majles MH, Dehghani Z, Sahraei R, Nabiyouni G. Non-linear optical properties of silver nanoparticles prepared by hydrogen reduction method. Optics Communications [Internet]. April 2010 [cited 20 April 2016];283(8):1650–3. Opgehaal van: http://www.sciencedirect.com/science/article/pii/S0030401809008839

120. Xia Y, Halas NJ. Shape-controlled synthesis and surface plasmonic properties of metallic nanostructures. MRS Bulletin [Internet]. Cambridge University Press; 31 Januarie 2005 [cited 15 April 2016];30(5):338–48. Opgehaal van: http://journals.cambridge.org/abstract_S0883769400012732

121. Šileikaitė A, Prosyčevas I, Puišo J, Juraitis A, Guobienė A. Analysis of silver nanoparticles produced by chemical reduction of silver salt solution. Materials Science [Internet]. 01 Januarie 2006 [cited 20 April 2016];12(4).

Opgehaal van: https://www.researchgate.net/publication/228513723_Analysis_of_Silver_Nanoparticles_Produced_by_Chemical_Reduction_of_Silver_Salt_Solution

122. Shahriari E, Moradi M, Varnamkhasti MG. Investigation of nonlinear optical properties of Ag nanoparticles. International Journal of Optics and Photonics. 2015;9(2):107–14.

123. Srinivas NK, Rao SV, Rao DN. Saturable and reverse saturable absorption of Rhodamine B in methanol and water. Journal of the Optical Society of America B [Internet]. Optical Society of America; 01 Desember 2003 [cited 28 April 2016];20(12):2470. Opgehaal van: http://www.osapublishing.org/viewmedia.cfm?uri=josab-20-12-2470&seq=0&html=true

124. Gurudas U, Brooks E, Bubb DM, Heiroth S, Lippert T, Wokaun A. Saturable and reverse saturable absorption in silver nanodots at 532 nm using picosecond laser pulses. Journal of Applied Physics [Internet]. 01 November 2008 [cited 28 April 2016];104(7):73107. Opgehaal van: https://www.researchgate.net/publication/224442950_Saturable_and_reverse_saturable_absorption_in_silver_nanodots_at_532_nm_using_picosecond_laser_pulses

125. Jacinto C, Messias DN, Andrade AA, Lima SM, Baesso ML, Catunda T. Thermal lens and Z-scan measurements: Thermal and optical properties of laser glasses – A review. Journal of Non-Crystalline Solids [Internet]. 01 September 2006 [cited 20 April 2016];352(32–35):3582–97. Opgehaal van: https://www.researchgate.net/publication/222535088_Thermal_lens_and_Z-scan_measurements_Thermal_and_optical_properties_of_laser_glasses_-_A_review

126. Ule AE. Measurement of the nonlinear refractive index by Z-scan technique

[Internet]. University of Ljubljana; 2015. Opgehaal van: http://mafija.fmf.uni-lj.si/seminar/files/2014_2015/seminarZ-scan2.pdf

Chapter 10: Publications

Title	Statue
Nonlinear Optical Studies of Gold and Silver Nanoparticles (Abstract)	Bahrain Medical Bulletin, Vol. 38, No. 2, June 2016. (attached)
Synthesis of Au, Ag, Au-Curcumin, Ag-Curcumin and Au-Ag and their Nonlinear Refractive Index Properties (Paper)	Submitted to Journal of Nanomaterial's. (attached)
Green Synthesis of Gold Nanoparticles using Glucose & Gelatin using Microwave (Paper)	Pending
Optical Limiting of Gold Nanoparticles (Paper)	Pending

PAPER 1: Nonlinear Optical Studies of Gold and Silver Nanoparticles

Nonlinear Optical Studies of Gold and Silver Nanoparticles

Fatema Abdulwahab*, Fryad Henari**

Objective: To measure the nonlinear refractive index and nonlinear absorption coefficient of Ag and Au particles.

Design: Quantitative measurements

Setting: Royal Collage of Surgeons in Ireland (RCSI) – Kingdom of Bahrain

Method: Ag and Au colloidal solutions were prepared by reduction processes. The nonlinear properties of the samples were investigated using CW laser at 488-514 nm using Z-scan technique.

Result: Closed aperture z-scan displayed a prefocal peak followed by a postfocal valley. These materials show a large negative nonlinear refractive index of the order of 5.85 X $10^{-11}\, m^2/W$ and 3.32 X $10^{-12}\ m^2/W$ for silver and gold respectively and negative nonlinear absorption of the order of 3.45 x 10^{-4} m/W and 7.48 x 10^{-5} m/W for silver and gold respectively.

Conclusion

Z-scan showed that Ag and Au nanoparticles exhibit a nonlinear effect of thermal origin.

* RCSI-MUB Medical Student

** RCSI Faculty

Synthesis of Au, Ag, Curcumin, Au, Ag and Au-Ag nanoparticles and their nonlinear refractive index properties

F. Abdulwahab[1], F. Z. Henari[1], S. Cassidy [1]and K. Winser[2]

[1]Department of Medical Sciences, Royal College of Surgeons in Ireland, Medical University of Bahrain, Building 2441, Road 2835, Block 228, Busaiteen, Kingdom of Bahrain

[2]Department of Physiology & Medical Physics, Royal College of Surgeons in Ireland, 123 St. Stephen's Green, Dublin 2, Ireland

Abstract:

In this work, nanoparticles of gold and silver were prepared by a reduction method and by employing green chemistry principles such as using curcumin as a reducing and a stabilizing agent. The formation of nanoparticles was confirmed by UV-Vis absorption spectra and TEM. Mie- theory was used to determine the particle sizes. The nonlinear refraction and absorption properties of the particles were measured using the *Z*-scan technique. A large value of third order nonlinearities was obtained using the nanoparticles produced.

Keywords: colloidal nanoparticles, absorption spectra, nonlinear properties, Z-scan

1-**Introduction**:

Metallic nanoparticles have attracted a huge interest because their physical and chemical properties are different from those of their bulks properties (111). As a result they are ideal candidates for many applications, such including electronics, optoelectronic devices and in medical applications such as diagnosis, drug deliver and therapy. Metallic nanoparticles form district energy levels, which is shown in the linear absorption spectra by a broad band absorption. This manifests as surface plasmon resonance, which does not exist in the case of bulk materials. Nanoparticles have a large number of conduction electrons. There are more atoms at the surface of the nanoparticles than the number of atoms inside, and thus this property gives rise to interesting properties due to the interaction between nanoparticles and surrounding media. The strong interaction of nanoparticles with light waves takes place because the conduction electrons on the metal surface undergo a combined oscillation when excited by light at specific wavelengths. The collective oscillation of excited electrons in the conduction band also known as surface plasmon resonance (SPR) and the surface area to volume ratio leads to a strong interaction with the incoming electromagnetic wave to enhance the local field, thus boosting the nonlinear optical properties of these materials. The optical properties of nanoparticles are strongly dependent on the particle size, shape and dielectric properties of the matrix. These properties have a vital role in developing optical devices and in the biomedical field. It has been suggested that in the vicinity of the SPR absorption region, the nanoparticles exhibit a large value of optical nonlinearities. Different techniques have been used to investigate the optical nonlinearities such as in four wave mixing (112), nonlinear interferometry (113) and z-scan (114,115). Z-scan is the most popular technique due to its simplicity and it allows the determination of the sign and the magnitude of nonlinear optical properties, such as nonlinear refractive index and nonlinear absorption in a single scan. Many reports have described the nonlinear properties and behavior demonstrated by nanoparticles and their dependence on sizes, shapes, and surrounding medium (116–119).

In this paper we report the nonlinear behavior of gold, silver, curcumin-gold, curcumin-silver and silver- gold nanoparticles which were prepared by the chemical reduction method and green synthesis. The nonlinear refractive index and nonlinear absorption of these samples were measured using the z-scan technique with cw argon-ion laser beam at 488nm and 514 nm. The magnitude of the nonlinear properties was measured with different synthesis methods and found to have no relationship between the values of the nonlinearities and the synthesis method.

2- Synthesis of nanoparticles

Starting materials were purchased from Sigma Aldrich and used without any further purifications. Distilled water was used to prepare the solutions of the reacting materials. The Au colloid was prepared by chemical reduction according to the procedure given in ref (75). A 20 ml of 1 mM $HAuCl_4$ solution was stirred and heated to boiling temperature. Then 2 ml of 1% trisodium citrate was added to the solution. The solution was left boiling until color changed to deep red. In this reaction gold is reduced from $Au^{+3}\ to\ Au^{0}$ by the trisodium citrate. Chemical equation is given below (76)

$$2HAuCl_4 + 4Na_3C_6H_5O_7 \rightarrow\ H_2 + 2Au^0 + 4CO_2 + 4NaC_5H_5O_5 + 8NaCl$$

The gold nanoparticles were synthesized using a green chemistry method. In this method the gold nanoparticles prepared by using curcumin as a reducing and stabilizing agent (73). A 0.11 g of curcumin was dissolved in 15 ml of DMSO and the pH of the solution was increased to 9.3 using Na_2CO_3 (dissolved 0.24 g in 15 mL of water). 1 mM of $HAuCl_4$ was added dropwise with shaking to 2 mL of curcumin, until the color changes from yellow to colorless, black and burgundy red. According to Sindhu et. al (73), the formation of curcumin conjugated gold nanoparticles includes six steps of deprotonation, reduction, nucleation, growth, cleavage and maturation. First curcumin Cur^{-3} is formed after the dissociation of hydrogen atoms from enolic curcumin hydroxyl groups. Then gold is reduced by the electrons on the O^{-} from Au^{+3} to Au^{0}. The Au^{0} atoms form clusters and those

clusters cleave into smaller fragments due to instability and finally spherical and solid nanoparticles are formed.

Ag nanoparticles was prepared using chemical reduction method (70). 84.9 mg of silver nitrate $(AgNO_3)$was dissolved in 500 ml of distilled water. The solution was stirred and heated to boiling temperature and 5 ml of trisodium citrate (1 g dissolved in 100 mL of water) was added to the solution. The solution was left to boil for 2 hours and color changed to greenish. In this reaction silver nitrate is reduced by trisodium citrate to form silver nanoparticles. Chemical equation is given below (71)

$$4Ag^{+} + C_6H_5O_7Na_3 + 2H_2O \rightarrow 4Ag^{0} + C_6H_5O_7H_3 + 3Na^{+} + H^{+} + O_2 \uparrow$$

Another method was used to prepare Ag nanoparticles using curcumin as reducing agent. In this method, 1 g of curcumin was dissolved in 100 ml of DMSO. A solution of 7 mL of 1 mM $AgNO_3$ was heated to boiling temperature with stirring followed by the addition of 3 mL of the prepared curcumin solution. Heating was continued for 5 minutes. Curcumin acts as reducing agent. It is worth mentioning, that the most significant aspect of the above procedure is that the maintenance pH during the synthesis process is not required.

Ag/ Au (core/shell) nanoparticles were prepared using gripe water according to the procedure given in (77). In a flask 2 mL of 0.3 mM $AgNO_3$ was mixed with 10 mL of gripe water. In another flask 2 mL of 0.3 mM of $HAuCl_4$ was left stirring. Under continuous stirring the mixture of gripe water and $AgNO_3$ was added to $HAuCl_4$ and left stirring for 22 hours. In this method Au and Ag nanoparticles are reduced by hydrolyzed sucrose that is present in the gripe water, while they are stabilized by sodium benzoate, sodium methyl paraben, sodium propylparaben and bronopol.

3- Results and Discussions

3.1- Absorption Spectra:

UV-Vis spectrometer Shimadzu UV-1800 was used to record absorption spectra of all the samples. The UV-Vis absorption spectrum for Au and Ag nanoparticles is shown in Fig.1.a, The spectra for Au and Ag nanoparticles is characterized by a broad band in the visible region with a surface SPR peak at 517 nm and 414 nm respectively. The sharp peaks indicate the formation of spherical nanoparticles. The stability of the nanoparticles was monitored by observing the position of the absorption peak over weeks. No obvious shift in the absorption peak was observed. If the particle increases in size the peak absorption will shift to longer wavelength (red shift) (120), however, no such behavior was observed. The Transmission Electron Microscopy (TEM) image of the Au particles is shown in Fig.1b. It can be seen from the figure that Au nanoparticles are spherical in shape with smooth surface. The particle size was determined using Image J 1.5g software by calculating the diameter (d) in pixels. Pixels were converted to nanometers by applying the scale of the image. The diameter (d) of each nanoparticle was marked manually and found to have a range from 9 to 23 nm with high yield of size 12 nm, Fig 1b. It was shown that the full width at half maximum of the absorption spectrum is related to the particle sizes (121). The relative narrow band of absorption observed in this case may be used as an indication of the formation of small sizes of Au particle. It is worth mentioning that the TEM images was taken two weeks after synthesis and no aggregation was observed.

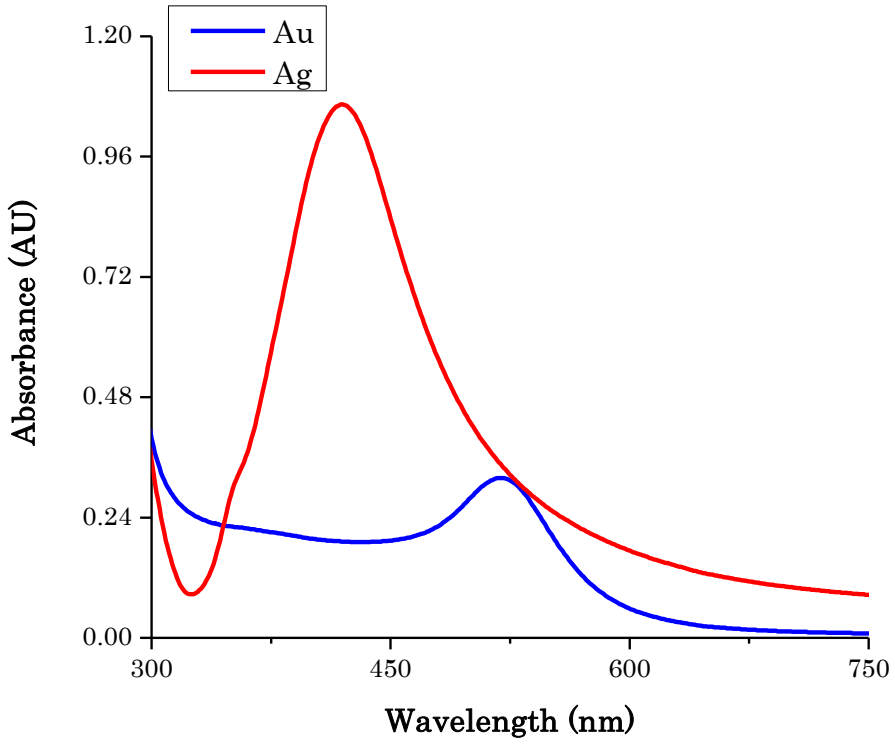

Fig 1(a) UV-Vis absorption spectrum for Au (blue) and for Ag (red) nanoparticles in water

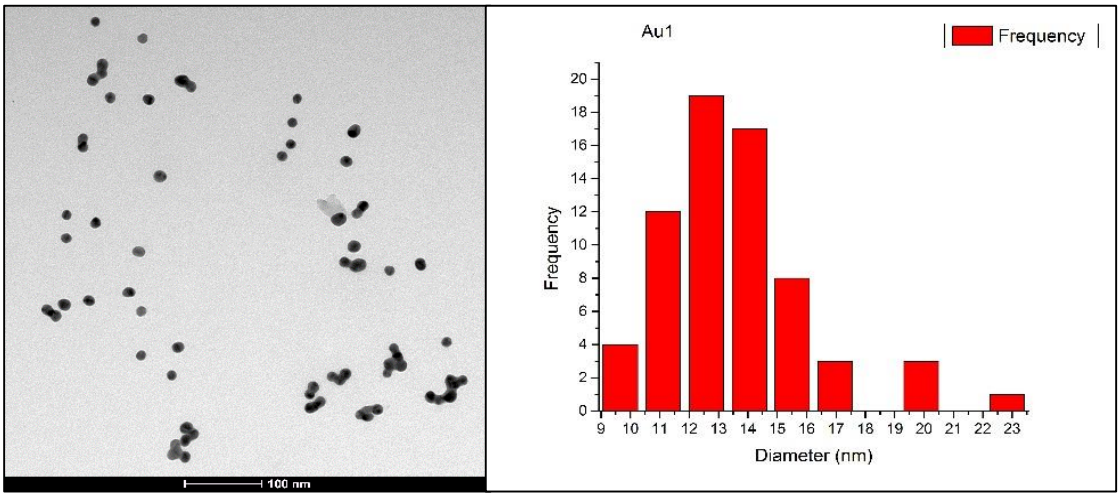

Figure 1(b) TEM Image and size distribution for Au nanoparticles.

Fig.2. shows the UV-Vis absorption spectra of Au, curcumin-Au, Ag, curcumin-Ag, and (core-shell) Au-Ag. The spectra are characterized by a broad band in the visible region with a plasmon resonance peak at 517, 536, 414, 436 and 472 nm respectively. For curcumin-Au and curcumin-Ag, the formation of the nanoparticles are characterized by the disappearance of the absorbance maximum peak (430 nm) of curcumin and the shift of SPR absorbance peak from 517 nm for Au particles, to 536 nm for curcumin-Au, and the shift SPR peak from 430 for Ag particles nm to 436 for Ag- curcumin. This shifting indicates coupling between curcumin –Au and curcumin –Ag. The SPR shift also observed for Ag -Au (472 nm) in comparison to SPR peak for Ag (430nm).

Because facilities for measuring the nanoparticle sizes were not available to the investigators, we used the Mie theory to determine the particles size of colloidal nanoparticles. For this we used a computer simulation program (Mie plot v4.5). The procedure for calculation was performed as described in (83) because the position of the SPR peak depends on the diameter of nanoparticles (121). A number of calculations were performed at different diameters of nanoparticles and the calculated data was fitted to the experimental absorption data, using Origin9 software, see figure (2). The best fit between calculated data and the experimental absorption spectra were found for each particle and estimated values of diameters are given in Table 1. It should be noted that the size of the shell/core particle is larger than the metal particle, which indicates the reaction of curcumin with metals.

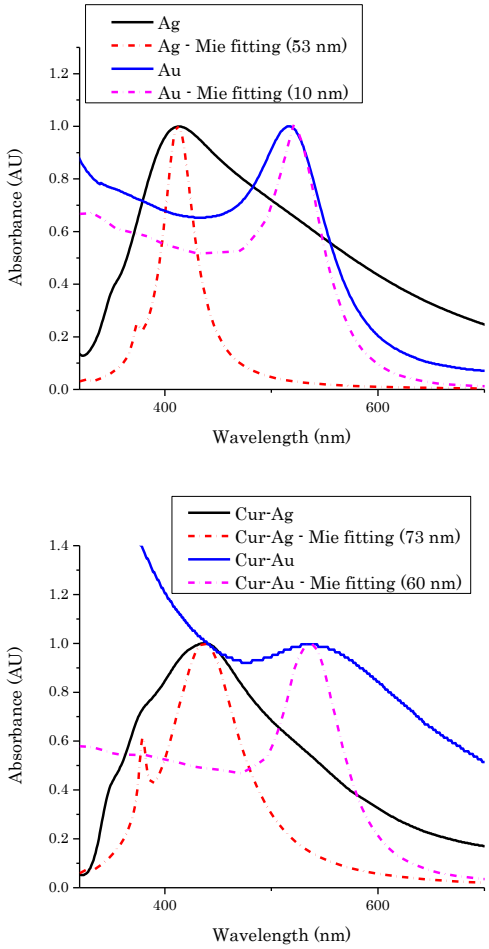

Fig.2: Compression between calculated spectra using the Mie theory and experimental spectra for Au and Curcumin Au and Ag and Curcumin Ag.

Table1: synthesized nanoparticles sizes measured with Mie plot

Type of NPs	Size (nm)
Au	10
Ag	55
Curcumin – Au	60
Curcumin – Ag	73

3.2- Z scan techniques

The nonlinear refractive index n_2 is given by $n = n_o+n_2I$ where n_o is the linear refractive index and I is the intensity of incident light. The nonlinear absorption

coefficient α is given by $\alpha = \alpha_0 + \beta I$, where α_o is the linear absorption coefficient, β is a nonlinear absorption coefficient and I is the intensity of incident light. Z-scan technique (15) was used to measure the nonlinear refractive index and the nonlinear absorption coefficient of nanoparticles. This technique relies on the fact that the intensity varies along the axis of the convex lens and is maximum at the focus. Hence, by shifting the sample through the focus, the intensity dependence can be measured as a change in transmission. In the Z-scan procedure, the transmission for the sample was measured with and without an aperture in the far field of the lens as the sample moved through the focal point. This enables the nonlinear refractive index (closed aperture) to be separated from that of the nonlinear absorption (open aperture).

The experiment was performed with an air-cooled Argon-ion laser beam operating at 488 nm and 514 nm with adjusting power between 15 - 30 mW. The beam was focused to a beam waist of 20 □m with a lens of 10 cm focal length, giving a typical power density range of 2.38×10^7- 4.78×10^7 W/m^2. The transmission for the samples was measured with and without aperture in the far-field of the lens as the samples moved through the focal point.

Fig. 3. Shows a typical normalized transmission at wavelengths 488 nm (closed Z-scan) for sample Ag and cur- Au as a function of the sample position: The normalized transmittance curve for the samples were characterized by a preface peak followed by a post focal valley. This peak valley configuration implies that the nonlinear refractive index of solution is negative ($n_2<0$) (self-defocusing). Similar characteristics were shown by other samples studied. The asymmetry in the closed z-scan curve, is the signature of thermal contribution to nonlinear refractive index and is explained below. The values of the differences between normalized peak-valley transmittance (ΔT_{p-v}) for the samples are shown in Table 2. It is possible from the peak to valley variation of the measured transmittance to calculate the nonlinear refractive index n_2.

The difference between normalized peak–valley transmittance ΔT_{p-v} is given by

$$\Delta T_{p-v} = 0.406(1-S)^{0.25}\left|\Delta\phi\right| \qquad (1)$$

where $\Delta|\phi|$ is the on axis nonlinear phase shift at the focus and S is the linear transmittance of the aperture and is given by

$$S = 1 - \exp(-2r_a^2 / w_a^2) \qquad (2)$$

where r_a is the radius of the aperture and W_a is the radius of the laser at the entrance of the aperture. The nonlinear phase shift is given by

$$\Delta|\phi| = \frac{2PL_{eff}}{\lambda w_o^2} n_2 \qquad (3)$$

where n_2 is the nonlinear refractive index, P is the laser power, λ is the laser wavelength and $L_{eff} = (1 - \exp(-\alpha L))/\alpha$ where α is the linear absorption coefficient at 488 nm, L is the sample thickness and L_{eff} is the effective thickness of the sample.

Equations 1 and 3 were used to calculate the value of nonlinear refractive index n_2. The values of n_2 are shown in Table 2. These values are the average of three close z-scans with estimated an error of 10%.The values reported here are in the same order with values reported in (122).

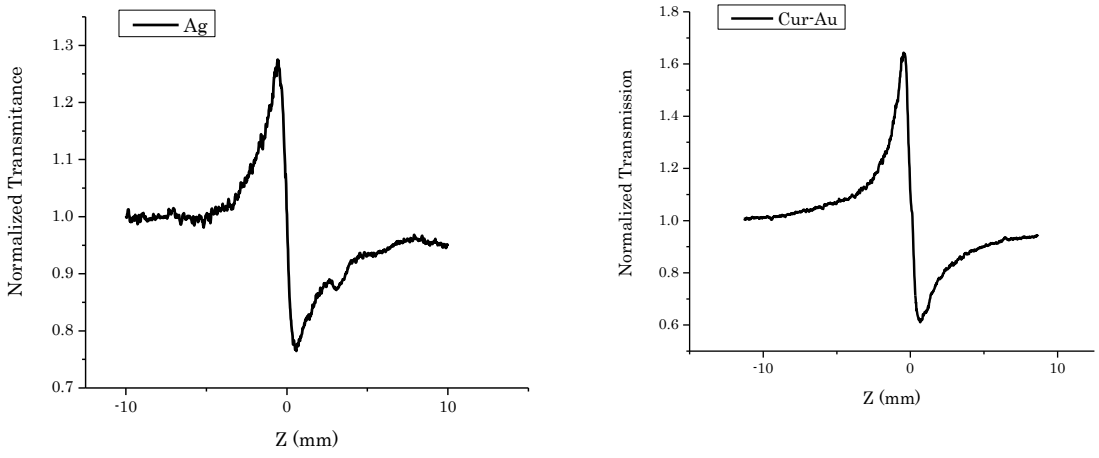

Fig.3. Closed aperture z-scan response (a) for Ag and (b) for Cur-Au

Fig 4 shows a typical normalized transmission at wavelengths 514 nm (open z-scan) for sample Au as a function of the sample position. The normalized transmittance curve for the samples was characterized by a maximum

transmission at focus. This shows that the sample exhibits a saturation absorption (SA). A similar behavior was observed for Ag. Fig. 5 shows the normalized transmission (open z-scan) for cur- Au and cur- Ag samples. The normalized transmission were characterized by a minimum transmission at the focus. Thus the samples exhibit a reverse saturation absorption (RSA). Refractive indices of the matrix around nanoparticles play important roles in tuning the SPR band in turn the nonlinear properties. This may explain the observed RSA for cur- Au and cur- Ag samples. Fig.6 shows an open z-scan for shell/core Ag- Au. The transmission is characterized by saturation absorption (SA).

For open aperture z-scan the nonlinear absorption coefficient (β) is related to sample transmittance T at focus, by (15)

$$T = 1 + \frac{\beta\, I\, L_{eff}}{2\sqrt{2}} \qquad (4)$$

Equation 4 was used to calculate the value of nonlinear absorption coefficient β. The values of β obtained for the samples are shown in Table 2. These values are the average of three open z-scans with an estimated error of 10%. The values reported here are in agreement with previously reported values (122,123).

The process leading to the observed SA and RSA can be explained by considering band gap structures of noble metals (123,124). The optical properties of metals are influenced by the localization of electrons (of) in the d bands and by quasi free electrons in the sp conduction bands. The fermi level lies between 2 to 5 eV above the d- bands. Electron transition between the d bands and the conduction bands can occur for photon energy in the visible region. The processes involved in nonlinear optical properties are surface plasmon absorption, free carrier absorption, and two-photon absorption. The excitation wavelengths used for investigation of the nonlinear absorption were 488 nm and 514 nm, which are almost in the vicinity of the SPR peak of Au and Ag nanoparticles. In this case the main effect involves the excitation of the electrons from the SPR band. The excited electrons interact with the electric

field of the incident beam leading to higher order oscillations, which leads to a difference in frequency between SPR excited electrons and unexcited electrons. The electrons in the original SPR band that cannot further absorb radiation results in SA behavior. The SA behavior for Au particles is shown is in Fig.4. Similar behavior was observed for Ag nanoparticles. For cur- Au and cur- Ag particles RSA were observed. The RSA behavior can be explained by two step resonant two photon absorption (TSA) where in the first step electrons from d bands are excited to fermi level by absorbing a photon of energy (□= 488 nm, E= 2.7 eV, and□□=514 nm, E= 2.4 eV). In the second step electrons are transferred from the fermi level to the conduction band by absorbing a second photon.

The process leading to refractive index change, involves the excitation of the electrons from the SPR band. The excited electrons interact with the electric field of the incident beam leading to higher order oscillations. The excited hot electrons (electrons with higher energy than Fermi energy) are thermalized by dissipating the excess to the surroundings. The excess thermal energy increases the surrounding temperature and generates a temperature gradient. This temperature gradient leads to a variation in refractive index, which is called a thermal lens (125). In addition to the thermal lens, the population redistribution between the excited and ground state conduction bands also plays an important part in the variation in the refractive index called a population lens (125). The plausible explanation for such a high value of nonlinear properties reported in this work arises from the use of cw laser that induces thermal effects that strongly affect the nonlinear properties masking the electronic contribution to the nonlinear properties. The observed asymmetry for close z-scan is an indication of the thermal effect.

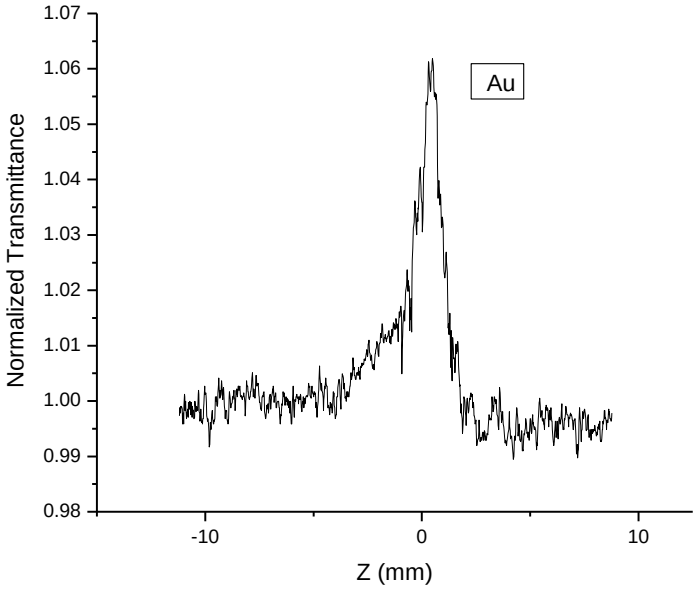

Fig.4 Open aperture z-scan response for Au nanoparticle at 514 nm

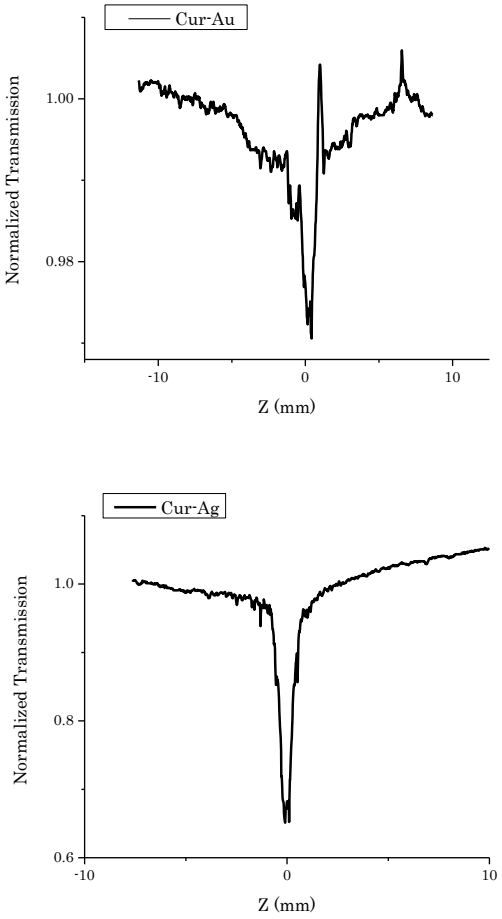

Fig.5. Open aperture z-scan response for cur-Au at 514 nm and cur-Ag at 488 nm

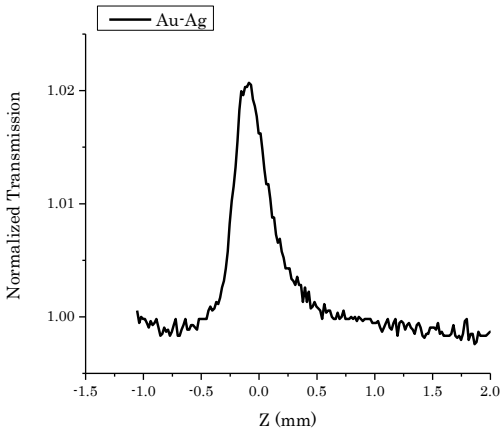

Fig 6. Open aperture z-scan response for Au-Ag at 488 nm

Table 2: Shows the values of ΔT_{p-v}, nonlinear index of refraction and nonlinear absorption coefficient.

Sample	λ **(nm)**	ΔT_{p-v}	$n_2 \times 10^{-12}$ (m^2W^{-1})	$\beta \times 10^{-5}$ $(m\,W^{-1})$
Au	514	1.09	-3.22	-7.87
Cur – Au	514	1.02	-3.26	$+8.58$
Ag	488	0.50	-1.61	$+3.52$
Cur – Ag	488	3.84	-8.82	$+5.45$
Au – Ag	488	0.61	-0.574	-2.7

4 – Conclusions

Nanoparticles such as Au, Ag, (shell- core) Cur-Au, Cur-Ag and Au-Ag were prepared using chemical reduction methods. Both trisodium citrate and curcumin were used as reducing agents. The main significant aspect of the green synthesis procedure, is that the maintenance of pH during the synthesis process is not required. The SPRs in the nanoparticle is confirmed by measuring visible spectra using a UV-Vis spectrometer. For Au nanoparticles, the particle size distribution was determined using TEM. Nanoparticle size distribution was estimated by comparing the calculations from Mie theory and experimental absorption spectra.

Z-scan technique was used to measure the nonlinear properties of nanoparticles. The nonlinear refractive index and nonlinear absorption of these samples were measured using the z-scan technique with cw argon-ion laser beam at 488 nm and 514 nm. Both SA absorption and RSA were observed and found to be dependent on the sample property.

Reference:

1. The Global Diabetes Community. How many people have diabetes - Diabetes prevalence numbers [Internet]. [cited 19 November 2015]. Opgehaal van: http://www.diabetes.co.uk/diabetes-prevalence.html
2. Time Out Bahrain. Diabetes in Bahrain [Internet]. 2010 [cited 12 Mei 2016]. Opgehaal van: http://www.timeoutbahrain.com/bodyandmind/features/18066-diabetes-in-bahrain
3. Bahrain News Agency. Bahrain's diabetes rate drops [Internet]. 2011 [cited 12 Mei 2016]. Opgehaal van: http://bna.bh/portal/en/news/484152
4. TradeArabia News. Diabetes "biggest killer in Bahrain" [Internet]. 2014 [cited 29 November 2015]. Opgehaal van: http://www.tradearabia.com/news/HEAL_271291.html
5. Musaiger AO. Diabetes mellitus in Bahrain: an overview. Diabetic medicine [Internet]. Julie 1992 [cited 29 November 2015];9(6):574–8. Opgehaal van: http://www.ncbi.nlm.nih.gov/pubmed/1643809
6. ALNohair S. Obesity in gulf countries. International journal of health sciences [Internet]. Januarie 2014 [cited 29 April 2016];8(1):79–83. Opgehaal van: http://www.pubmedcentral.nih.gov/articlerender.fcgi?artid=4039587&tool=pmcentrez&rendertype=abstract
7. Loghmani E. Chapter 14 Diabetes Mellitis : type 1 and type 2. In Guidelines for Adolescent Nutrition Services Edited by: Stang J, Story M; 2005. 167-182 bl.
8. Diabetes.bh. Type 2 diabetes [Internet]. [cited 12 Mei 2016]. Opgehaal van: http://www.diabetes.bh/diabetes/what-is-diabetes/type-2-diabetes/
9. MacGill M. What is insulin? How does insulin regulate glucose? [Internet]. 2016 [cited 12 Mei 2016]. Opgehaal van: http://www.medicalnewstoday.com/info/diabetes/whatisinsulin.php
10. The Euro-Wabb. Diabetes Information | Insulin - What does it do? [Internet]. [cited 12 Mei 2016]. Opgehaal van: http://www.euro-wabb.org/en/diabetes-information-all/insulin-what-does-it-do
11. Pagliuca FW, Millman JR, Gürtler M, Segel M, Van Dervort A, Ryu JH, et al. Generation of functional human pancreatic β cells in vitro. Cell [Internet]. 09 Oktober 2014 [cited 09 Oktober 2014];159(2):428–39. Opgehaal van: http://www.pubmedcentral.nih.gov/articlerender.fcgi?artid=4617632&tool=pmcentrez&rendertype=abstract
12. Ferry Jr. Diabetes Treatment (type 1 and type 2 medications and diet) [Internet]. [cited 29 November 2015]. Opgehaal van: http://www.medicinenet.com/diabetes_treatment/article.htm

13. Dhinaa AN, Nooraldeen AY, Murali K, Palanisamy PK. Z-scan technique as a tool for the measurement of blood glucose. Laser Physics [Internet]. 2008;18(10):1212–6. Opgehaal van: http://link.springer.com/10.1134/S1054660X08100198

14. Lu SZ, Wang HT. Determination of third- and fifth-order nonlinear coefficients by using quasi-one-dimensional slit beam Z-scan technique. Journal of Applied Physics [Internet]. 2009 [cited 11 September 2016];105(3):33104. Opgehaal van: http://scitation.aip.org/content/aip/journal/jap/105/3/10.1063/1.3075831

15. Sheik-Bahae M, Said AA, Wei T-H, Hagan DJ, Van Stryland EW. Sensitive measurement of optical nonlinearities using a single beam. IEEE Journal of Quantum Electronics [Internet]. April 1990 [cited 29 September 2015];26(4):760–9. Opgehaal van: http://ieeexplore.ieee.org/lpdocs/epic03/wrapper.htm?arnumber=53394

16. American Diabetes Association. Diagnosis and classification of diabetes mellitus. Diabetes Care [Internet]. 2012;35(Supplement_1):S64–71. Opgehaal van: http://care.diabetesjournals.org/cgi/doi/10.2337/dc12-s064

17. Mandal A. History of diabetes [Internet]. 2012 [cited 03 Maart 2016]. Opgehaal van: http://www.news-medical.net/health/History-of-Diabetes.aspx

18. McCoy K. The history of diabetes [Internet]. 2009 [cited 03 Maart 2016]. Opgehaal van: http://www.everydayhealth.com/diabetes/understanding/diabetes-mellitus-through-time.aspx

19. American Diabetes Association. History of diabetes [Internet]. 2014 [cited 03 Maart 2016]. Opgehaal van: http://www.diabetes.org/research-and-practice/student-resources/history-of-diabetes.html?referrer=https://www.google.com.bh/

20. Aronoff SL, Berkowitz K, Shreiner B, Want L. Glucose metabolism and regulation: beyond insulin and glucagon. Diabetes Spectrum [Internet]. 01 Julie 2004 [cited 05 Januarie 2015];17(3):183–90. Opgehaal van: http://spectrum.diabetesjournals.org/content/17/3/183.full

21. Diabetes Research & Wellness Foundation. What is diabetes? Professional nurse (London, England). 1986;1(12):333–4.

22. Thomassian B. Diabetes mellitus : pathophysiology and clinical guidelines. The Academy of Dental Learning & OSHA Training. 2012;12212(800).

23. Canadian Diabetes Association. Types of diabetes [Internet]. [cited 29 November 2015]. Opgehaal van: http://www.diabetes.ca/about-diabetes/types-of-diabetes

24. Hernandez E, RN, BSN, PHN. Diabetes. Clinical Research Center [Internet]. Opgehaal van:

https://collab.nlm.nih.gov/webcastsandvideos/drew/diabetes.pdf

25. Diabetes Info. Three types of diabetes : type 1, type 2 and gestational diabetes [Internet]. [cited 29 November 2015]. Opgehaal van: http://www.diabetes-info.co.uk/what-is-diabetes/types-of-diabetes.html
26. Medline Plus. Long term complications of diabetes [Internet]. 2014 [cited 02 Maart 2016]. Opgehaal van: https://www.nlm.nih.gov/medlineplus/ency/patientinstructions/000327.htm
27. Tonyushkina K, Nichols JH. Glucose meters: a review of technical challenges to obtaining accurate results. Journal of diabetes science and technology [Internet]. Julie 2009 [cited 29 November 2015];3(4):971–80. Opgehaal van: http://www.pubmedcentral.nih.gov/articlerender.fcgi?artid=2769957&tool=pmcentrez&rendertype=abstract
28. Oliver NS, Toumazou C, Cass AEG, Johnston DG. Glucose sensors: a review of current and emerging technology. Diabetic Medicine [Internet]. Maart 2009 [cited 19 April 2015];26(3):197–210. Opgehaal van: http://www.ncbi.nlm.nih.gov/pubmed/19317813
29. The Global Diabetes Community. Continuous glucose monitoring. 2015; Opgehaal van: http://www.diabetes.co.uk/cgm/continuous-glucose-monitoring.html
30. Tura A, Maran A, Pacini G. Non-invasive glucose monitoring: assessment of technologies and devices according to quantitative criteria. Diabetes research and clinical practice [Internet]. Julie 2007 [cited 08 November 2015];77(1):16–40. Opgehaal van: http://www.sciencedirect.com/science/article/pii/S0168822706004931
31. Hubbard CW, Gordon RL. Chemical sensors. 1987; Opgehaal van: http://www.osti.gov/servlets/purl/6804195/
32. Lambrechts M, Sansen W. Biosensors: microelectrochemical devices [Internet]. CRC Press; 1992 [cited 30 November 2015]. 316 bl. Opgehaal van: https://books.google.com/books?id=LDpf_dJotaQC&pgis=1
33. Edmonds TE. Chemical sensors [Internet]. Springer Science & Business Media; 2013 [cited 30 November 2015]. 326 bl. Opgehaal van: https://books.google.com/books?id=9ZzuCAAAQBAJ&pgis=1
34. National Nanotechnology Initiative. What is nanotechnology? [Internet]. [cited 27 Maart 2016]. Opgehaal van: http://www.nano.gov/nanotech-101/what/definition
35. AZoNano. Nanoparticles defined - what nanoparticles are and what makes them special [Internet]. 2006 [cited 28 Februarie 2016]. Opgehaal van: http://www.azonano.com/article.aspx?ArticleID=1734
36. Heiligtag FJ, Niederberger M. The fascinating world of nanoparticle research. Materials Today [Internet]. Julie 2013 [cited 07 Oktober 2015];16(7–8):262–71. Opgehaal van:

http://www.sciencedirect.com/science/article/pii/S1369702113002253

37. Nanotech. Nanotechnology: history [Internet]. [cited 18 Mei 2016]. Opgehaal van: http://nano--tech.blogspot.com/p/history.html

38. Mandal A. What are nanoparticles? [Internet]. [cited 19 November 2015]. Opgehaal van: http://www.news-medical.net/health/What-are-Nanoparticles.aspx

39. Daw R. Nanotechnology is ancient history [Internet]. 2012 [cited 18 Mei 2016]. Opgehaal van: http://www.theguardian.com/nanotechnology-world/nanotechnology-is-ancient-history

40. Gayatri K, Lakshmi G, Preeti K. Nanoparticles: an overview of preparation and characterization. Novel Science International Journal of … [Internet]. 2012;1(8):557–62. Opgehaal van: http://pharmacy.novelscience.info/index.php/nvp/article/viewArticle/13953

41. Mohanraj VJ, Chen Y. Nanoparticles - a review. Tropical Journal of Pharmaceutical Research [Internet]. Faculty of Pharmacy, University of Benin; 31 Julie 2007 [cited 19 November 2015];5(1):561–73. Opgehaal van: http://www.ajol.info/index.php/tjpr/article/view/14634

42. Thos E, Ogos L, Athos P. Methods of preparation of nanoparticles - a review. International Journal of Advances in Engineering & Technology. 2015;7(4):165–98.

43. Buckley, A.M.; Greenblatt MJ. Sol-Gel preparation of silica gels. J Chem Ed. 1994;71(7):599.

44. Iravani S, Korbekandi H, Mirmohammadi S V, Zolfaghari B. Synthesis of silver nanoparticles: chemical, physical and biological methods. Research in pharmaceutical sciences [Internet]. Januarie [cited 27 Oktober 2015];9(6):385–406. Opgehaal van: http://www.pubmedcentral.nih.gov/articlerender.fcgi?artid=4326978&tool=pmcentrez&rendertype=abstract

45. Kurniawan F. New analytical applications of gold nanoparticles [Internet]. University of Regensburg; 2008. Opgehaal van: http://epub.uni-regensburg.de/12113/1/Fredy_Kurniawan_desertation.pdf

46. Trau D, Renneberg R. Encapsulation of glucose oxidase microparticles within a nanoscale layer-by-layer film: immobilization and biosensor applications. Biosensors & bioelectronics [Internet]. 15 Oktober 2003 [cited 08 September 2016];18(12):1491–9. Opgehaal van: http://www.ncbi.nlm.nih.gov/pubmed/12941565

47. Ariga K, Hill JP, Ji Q. Layer-by-layer assembly as a versatile bottom-up nanofabrication technique for exploratory research and realistic application. Physical chemistry chemical physics : PCCP [Internet]. 21 Mei 2007 [cited 08 September 2016];9(19):2319–40. Opgehaal van: http://www.ncbi.nlm.nih.gov/pubmed/17492095

48. Wang B. Microphysiometer using multiwall carbon nanotubes enable

constant realtime monitoring of microliters of insulin [Internet]. 2008. Opgehaal van: http://www.nextbigfuture.com/2008/04/microphysiometer-using-multiwall-carbon.html

49. Frasco MF, Chaniotakis N. Semiconductor quantum dots in chemical sensors and biosensors. Sensors. 2009;9(9):7266–86.

50. Tang B, Cao L, Xu K, Zhuo L, Ge J, Li Q, et al. A new nanobiosensor for glucose with high sensitivity and selectivity in serum based on fluorescence resonance energy transfer (FRET) between CdTe quantum dots and Au nanoparticles. Chemistry [Internet]. 2008 [cited 08 September 2016];14(12):3637–44. Opgehaal van: http://www.ncbi.nlm.nih.gov/pubmed/18318025

51. Rahiman S. Nanomedicine current trends in diabetes management. Journal of Nanomedicine & Nanotechnology [Internet]. 2012;3(4):3–8. Opgehaal van: http://www.omicsonline.org/2157-7439/2157-7439-3-137.digital/2157-7439-3-137.html

52. Boysen E. Nanoparticles applications and uses [Internet]. [cited 26 November 2015]. Opgehaal van: http://www.understandingnano.com/nanoparticles.html

53. D'Almeida C, Roth B. Medical applications of nanoparticles [Internet]. Oakland University; Opgehaal van: https://www.umflint.edu/sites/default/files/groups/Research_and_Sponsored_Programs/MOM/c.dalmeida_b.roth_.pdf

54. Oldenburg SJ. Silver nanoparticles: properties and applications [Internet]. [cited 22 Februarie 2016]. Opgehaal van: http://www.sigmaaldrich.com/materials-science/nanomaterials/silver-nanoparticles.html

55. Bera RK, Anoop A, Raj CR. Enzyme-free colorimetric assay of serum uric acid. Chemical communications (Cambridge, England) [Internet]. The Royal Society of Chemistry; 07 November 2011 [cited 27 Maart 2016];47(41):11498–500. Opgehaal van: http://pubs.rsc.org/en/content/articlehtml/2011/cc/c1cc13349g

56. Sigma-Aldrich. Gold nanoparticles: properties and applications [Internet]. [cited 28 Februarie 2016]. Opgehaal van: http://www.sigmaaldrich.com/materials-science/nanomaterials/gold-nanoparticles.html

57. What When How. Metal nanostructures synthesized by soft chemical methods and shape control - part 2 (Nanotechnology) [Internet]. [cited 08 Maart 2016]. Opgehaal van: http://what-when-how.com/nanoscience-and-nanotechnology/metal-nanostructures-synthesized-by-soft-chemical-methods-and-shape-control-part-2-nanotechnology/

58. Unser S, Campbell I, Jana D, Sagle L. Direct glucose sensing in the physiological range through plasmonic nanoparticle formation. Analyst [Internet]. The Royal Society of Chemistry; 2015;140(2):590–9. Opgehaal

van: http://www.ncbi.nlm.nih.gov/pubmed/25426496

59. Ishihara M, Nguyen VQ, Mori Y, Nakamura S, Hattori H. Adsorption of silver nanoparticles onto different surface structures of chitin/chitosan and correlations with antimicrobial activities. International journal of molecular sciences [Internet]. Multidisciplinary Digital Publishing Institute; 18 Januarie 2015 [cited 06 April 2016];16(6):13973–88. Opgehaal van: http://www.mdpi.com/1422-0067/16/6/13973/htm

60. He YQ, Liu SP, Kong L, Liu ZF. A study on the sizes and concentrations of gold nanoparticles by spectra of absorption, resonance Rayleigh scattering and resonance non-linear scattering. Spectrochimica acta Part A [Internet]. Oktober 2005 [cited 18 Mei 2016];61(13–14):2861–6. Opgehaal van: http://www.sciencedirect.com/science/article/pii/S1386142504005505

61. Arulmozhi KT, Mythili N. Studies on the chemical synthesis and characterization of lead oxide nanoparticles with different organic capping agents. AIP Advances [Internet]. AIP Publishing; 31 Desember 2013 [cited 27 Mei 2016];3(12):122122. Opgehaal van: http://scitation.aip.org/content/aip/journal/adva/3/12/10.1063/1.4858419

62. National Nanotechnology Infrastructure Netwrok. Silver nanoparticles synthesis and spectroscopy [Internet]. 2012 [cited 27 Januarie 2016]. Opgehaal van: http://www.nnin.org/sites/default/files/files/PT1 Silver nanoparticle synthesis_TG.pdf

63. Nadagouda MN, Varma RS. Green synthesis of silver and palladium nanoparticles at room temperature using coffee and tea extract. Green Chemistry. 2008;10(8):859.

64. Bindhu MR, Umadevi M. Synthesis of monodispersed silver nanoparticles using Hibiscus cannabinus leaf extract and its antimicrobial activity. Spectrochimica acta Part A, Molecular and biomolecular spectroscopy [Internet]. 15 Januarie 2013 [cited 27 Januarie 2016];101:184–90. Opgehaal van: http://www.sciencedirect.com/science/article/pii/S1386142512009006

65. Philip D. Green synthesis of gold and silver nanoparticles using hibiscus rosa sinensis. Physica E [Internet]. Maart 2010 [cited 04 November 2015];42(5):1417–24. Opgehaal van: http://www.sciencedirect.com/science/article/pii/S1386947709005177

66. Kirthika P., Dheeba B. SR, Sheik A. Plant mediated synthesis and characterization of silver nanoparticles. International Journal of Pharmacy and Pharmaceutical Sciences [Internet]. 2014 [cited 27 Januarie 2016];6(8). Opgehaal van: http://innovareacademics.in/journals/index.php/ijpps/article/viewFile/2784/pdf_58

67. Bettini S, Pagano R, Valli L, Giancane G. Drastic nickel ion removal from aqueous solution by curcumin-capped Ag nanoparticles. Nanoscale

[Internet]. Royal Society of Chemistry; 2014;6(17):10113–7. Opgehaal van: http://www.ncbi.nlm.nih.gov/pubmed/25036541

68. Darroudi M, Ahmad M Bin, Abdullah AH, Ibrahim NA, Shameli K. Effect of accelerator in green synthesis of silver nanoparticles. International Journal of Molecular Sciences. 2010;11(10):3898–905.

69. Palanisamy PK, Kirubha E, Vishista K. Gripe water-mediated green synthesis of silver nanoparticles and their applications in nonlinear optics and surface-enhanced raman spectroscopy. Applied Nanoscience [Internet]. Springer Berlin Heidelberg; 2014;5:777–86. Opgehaal van: http://dx.doi.org/10.1007/s13204-014-0376-4

70. El-Kheshen AA, El-Rab S. Effect of reducing and protecting agents on size of silver nanoparticles and their anti-bacterial activity. Der Pharma Chemica. 2012;4(1):53–65.

71. Ratyakshi, Chauhan RP. Colloidal synthesis of silver nano particles. Asian Journal of Chemistry. 2009;21(10):113–6.

72. Sreelakshmi C, Goel N, Datta KKR, Addlagatta A, Ummanni R, Reddy BVS. Green synthesis of curcumin capped gold nanoparticles and evaluation of their cytotoxicity. Nanoscience and Nanotechnology Letters [Internet]. 2013;5(12):1258–65. Opgehaal van: http://openurl.ingenta.com/content/xref?genre=article&issn=1941-4900&volume=5&issue=12&spage=1258

73. Sindhu K, Rajaram A, Sreeram KJ, Rajaram R. Curcumin conjugated gold nanoparticle synthesis and its biocompatibility. RSC Advances [Internet]. 2014;4:1. Opgehaal van: http://xlink.rsc.org/?DOI=c3ra45345f

74. Engelbrekt C, Sørensen KH, Zhang J, Welinder AC, Jensen PS, Ulstrup J. Green synthesis of gold nanoparticles with starch–glucose and application in bioelectrochemistry. Journal of Materials Chemistry. 2009;19:7839–47.

75. McFarland AD, Haynes CL, Mirkin CA, Duyne RP Van, Godwin HA. Color My Nanoworld. J Chem Educ [Internet]. 2004 [cited 31 Januarie 2016];81(4):544A. Opgehaal van: http://education.mrsec.wisc.edu/277.htm

76. Dackiw AP. Induction and modulation of monocyte I macrophage tissue factorifibrin deposition and Tnf secretion in the microenvironment of inflammation : the role of tyrosine. University of Toronto; 1998.

77. Kirubha E, Palanisamy PK. Green synthesis, characterization of Au–Ag core–shell nanoparticles using gripe water and their applications in nonlinear optics and surface enhanced Raman studies. Advances in Natural Sciences: Nanoscience and Nanotechnology [Internet]. IOP Publishing; 2014;5(4):45006. Opgehaal van: http://stacks.iop.org/2043-6262/5/i=4/a=045006?key=crossref.eeb98f64f466e9b9ab329b3fdb858127

78. Samal AK, Polavarapu L, Rodal-Cedeira S, Liz-Marzán LM, Pérez-Juste J, Pastoriza-Santos I. Size tunable Au@Ag core-shell nanoparticles: synthesis and surface-enhanced raman scattering properties. Langmuir. 2013;29(48):15076–82.

79. NanoComposix. UV/VIS/IR spectroscopy analysis of nanoparticles. 2012 [cited 10 September 2016]; Opgehaal van: http://50.87.149.212/sites/default/files/nanoComposix Guidelines for UV-vis Analysis.pdf

80. Oldenburg SJ. Silver nanoparticles: properties and applications [Internet]. Opgehaal van: http://www.sigmaaldrich.com/materials-science/nanomaterials/silver-nanoparticles.html

81. Sigma-Aldrich. Gold nanoparticles: properties and applications [Internet]. Opgehaal van: http://www.sigmaaldrich.com/materials-science/nanomaterials/gold-nanoparticles.html

82. Madou MJ. Solid-state physics, fluidics, and analytical techniques in micro- and nanotechnology [Internet]. CRC Press; 2011. Opgehaal van: books.google.com.bh/books?id=sRvSBQAAQBAJ&pg=PA368&lpg=PA368&dq=interaction+of+em+with+rod+nanoparticles&source=bl&ots=M_KUORCZM1&sig=VHY_O-AsZnbguOF3QwyBh8o5rQQ&hl=en&sa=X&ved=0ahUKEwjbgYbSwp3PAhVFLsAKHfu3D74Q6AEIIjAB#v=onepage&q=interaction of em with r

83. Bumm LA. Size determination of gold nanoparticles using Mie theory and extinction spectra. Nanolab [Internet]. 2007;1–10. Opgehaal van: http://www.nhn.ou.edu/~bumm/NanoLab/pdf/Au_NP_spectrophotometery_activity.pdf

84. Jian Z, Yongchang W, Yimin L. Fluorescence spectra characters of silver-coated gold colloidal nanoshells. Colloids and Surfaces A: Physicochemical and Engineering Aspects. 2004;232(2–3):155–61.

85. Kotov NA. Nanoparticle assemblies and superstructures [Internet]. CRC Press; 2005. Opgehaal van: https://books.google.com.bh/books?id=APDKBQAAQBAJ&printsec=frontcover#v=onepage&q&f=false

86. Varier GK. Investigations on Nonlinear and Radiative Properties of Certain Photonic Materials [Internet]. Cochin University of Science & Technology; 1998. Opgehaal van: https://dyuthi.cusat.ac.in/xmlui/bitstream/handle/purl/2305/Dyuthi-T0596.pdf?sequence=1

87. Suresh S, Ramanand A, Jayaraman D, Mani P. Review on theoretical aspect of nonlinear optics. Reviews on Advanced Materials Science. 2012;30(2):175–83.

88. Stucky GD, Marder SR, Sohn JE. Linear and nonlinear polarizability - A primer. ACS Symp Ser. 1991;455(Mater. Nonlinear Opt.):2–30.

89. Boyd RW. The nonlinear optical susceptibility - Chapter 1. Nonlinear Optics. 1961. 1-67 bl.

90. Prasad PN, Williams DJ. Introduction to nonlinear optical effects in molecules and polymers [Internet]. Wiley. 1991. 320 bl. Opgehaal van: http://www.gbv.de/dms/ilmenau/toc/019503016.PDF

91. Pálfalvi L, Tóth BC, Almási G, Fülöp JA, Hebling J. A general Z-scan theory. Applied Physics B [Internet]. 30 Julie 2009 [cited 19 November 2015];97(3):679–85. Opgehaal van: http://link.springer.com/10.1007/s00340-009-3656-z

92. Chapple PB, Staromlynska J, Hermann JA, Mckay TJ, Mcduff RG. Single-beam z-Scan: measurement techniques and analysis. Journal of Nonlinear Optical Physics & Materials [Internet]. World Scientific Publishing Company; 25 September 1997 [cited 19 November 2015];6(3):251–93. Opgehaal van: http://www.worldscientific.com/doi/abs/10.1142/S0218863597000204?src=recsys&journalCode=jnopm

93. Sheik-bahae M, Said A a, Wei T, Hagan DJ, Stryland EW Van. Special 30th anniversary feature sensitive measurement of optical nonlinearities using a single beam. IEEE LEOS Newsletter [Internet]. 2007;(February):17–26. Opgehaal van: http://photonicssociety.org/newsletters/feb07/special30th.pdf

94. Arularasan P, Sivakumar B, Raj SG, Kumar GR, Mohan R. Determination of nonlinear absorption (β) and refraction (n 2)by the Z-scan method: third-order nonlinear optical properties of π- conjugated potassium pentaborate crystal. Journal of Applied Physics [Internet]. 2013 [cited 19 November 2015];4(4):48–54. Opgehaal van: http://www.academia.edu/7132060/Determination_of_nonlinear_absorption_%CE%B2_and_refraction_n_2_by_the_Z-scan_method_third-order_nonlinear_optical_properties_of_%CF%80-_conjugated_Potassium_Pentaborate_crystal

95. Stryland EW Van, Sheik-Bahae M. Z-Scan measurements of optical nonlinearities - Characterization techniques and tabulations for organic nonlinear materials. 1998;18(3):655–92.

96. Trejo-Duran M, Cornejo-Monroy D, Alvarado-Mendez E, Olivares-Vargas A, Castano VM. Nonlinear optical properties of Au-nanoparticles conjugated with lipoic acid in water. Journal of the European Optical Society: Rapid Publications [Internet]. 2014;9:14030. Opgehaal van: http://www.scopus.com/inward/record.url?eid=2-s2.0-84907345503&partnerID=tZOtx3y1

97. Chen G. Particularities of heat conduction in nanostructures. Journal of Nanoparticle Research. Kluwer Academic Publishers; 2000;2(2):199–204.

98. Karthikeyan B, Thomas J, Philip R. Optical nonlinearity in glass-embedded silver nanoclusters under ultrafast laser excitation. Chemical

Physics Letters. 2005;414(4):346–50.

99. Philip R, Kumar GR, Sandhyarani N, Pradeep T. Picosecond optical nonlinearity in monolayer-protected gold, silver, and gold-silver alloy nanoclusters. Physical Review B. American Physical Society; 15 November 2000;62(19):13160–6.

100. Gordon JP, Leite RCC, Moore RS, Porto SPS, Whinnery JR. Long-transient effects in lasers with inserted liquid samples. Journal of Applied Physics. 1965;36(1):3–8.

101. Sreeja R, Aneesh PM, Aravind A, Reshmi R, Philip R, Jayaraj MK. Size-dependent optical nonlinearity of Au nanocrystals. Journal of The Electrochemical Society. 2009;156(10):167–72.

102. Jacinto C, Messias DN, Andrade AA, Lima SM, Catunda T. Thermal lens and Z-scan measurements: Thermal and optical properties of laser glasses – A review. Journal of Non-Crystalline Solids. 2006;352(32):3582–97.

103. Dhinaa AN, Palanisamy PK. Z-scan technique for measurment of total cholesterol and triglycerides in blood. Journal of Innovative Optical Health Sciences [Internet]. World Scientific Publishing Company; 21 Julie 2009 [cited 19 November 2015];2(3):295–301. Opgehaal van: http://www.worldscientific.com/doi/abs/10.1142/S1793545809000565

104. Dhinaa AN, Palanisamy PK. Z-Scan technique: To measure the total protein and albumin in blood. Journal of Biomedical Science and Engineering [Internet]. Scientific Research Publishing; 08 April 2010 [cited 19 November 2015];3(3):285–90. Opgehaal van: http://www.scirp.org/journal/PaperInformation.aspx?PaperID=1529&#abstract

105. Abdelhalim M, Mady M. Rheological parameters assessment in serum, plasma and whole blood of rats after administration of gold nanoparticles of different sizes: In vivo. Journal of Nanomedicine & Nanotechnology [Internet]. OMICS International; 2012 [cited 09 September 2016];3(6). Opgehaal van: http://www.omicsonline.org/2157-7439/2157-7439-3-145.digital/2157-7439-3-145.html

106. Cinj. Procedure for separating plasma and serum from whole blood. Opgehaal van: http://www.cinj.org/sites/cinj/files/documents/C4ProcedureForSerumAndPlasmaSepartion.pdf

107. Alves SI, Silva E a. O, Costa SS, Sonego DRN, Hallack ML, Coppini OL, et al. The validation of the Z-Scan technique for the determination of plasma glucose. Proc of SPIE [Internet]. 2013;8785:87851B. Opgehaal van: http://proceedings.spiedigitallibrary.org/proceeding.aspx?doi=10.1117/12.2025994

108. Shahriari E, Yunus WMM, Saion E. Effect of particle size on nonlinear

refractive index of Au nanoparticle in PVA solution. Brazilian Journal of Physics [Internet]. Sociedade Brasileira de Física; Junie 2010 [cited 18 Mei 2016];40(2):256–60. Opgehaal van: http://www.scielo.br/scielo.php?script=sci_arttext&pid=S0103-97332010000200021&lng=en&nrm=iso&tlng=en

109. Garcia M. Truly non invasive glucose optical sensor based on metal nanoparticles generation [Internet]. University of Central Florida; 2006 [cited 30 Mei 2016]. Opgehaal van: https://www.researchgate.net/publication/47713435_TRULY_NON_INVASIVE_GLUCOSE_OPTICAL_SENSOR_BASED_ON_METAL_NANOPARTICLES_GENERATION
110. Bansal P, Jaggi N, Rohilla S. “ Green ” Synthesis of CdS nanoparticles and effect of capping agent concentration on crystallite size. Research Journal of Chemical Sciences. 2012;2(8):69–71.
111. Horikoshi S, Serpone N. Introduction to nanoparticles - Microwaves in nanoparticle synthesis [Internet]. Weinheim, Germany: Wiley-VCH Verlag GmbH & Co. KGaA; 2013 [cited 16 Julie 2016]. 1-24 bl. Opgehaal van: http://doi.wiley.com/10.1002/9783527648122.ch1
112. Bloemer MJ, Haus JW, Ashley PR. Degenerate four-wave mixing in colloidal gold as a function of particle size. Journal of the Optical Society of America B [Internet]. Optical Society of America; 01 Mei 1990 [cited 20 April 2016];7(5):790. Opgehaal van: http://www.osapublishing.org/viewmedia.cfm?uri=josab-7-5-790&seq=0&html=true
113. Klemm P, Haug T, Bange S, Lupton JM. Time-domain interferometry of surface plasmons at nonlinear continuum hot spots in films of silver nanoparticles. Physical review letters [Internet]. 31 Desember 2014 [cited 20 April 2016];113(26):266805. Opgehaal van: https://utah.pure.elsevier.com/en/publications/time-domain-interferometry-of-surface-plasmons-at-nonlinear-conti
114. Sheik-Bahae M, Said AA, Wei TH, Hagan DJ, Van Stryland EW. Sensitive measurement of optical nonlinearities using a single beam. IEEE Journal of Quantum Electronics [Internet]. IEEE; 01 April 1990 [cited 20 April 2016];26(4):760–9. Opgehaal van: http://ieeexplore.ieee.org/articleDetails.jsp?arnumber=53394
115. Stryland E, Sheik-Bahae M, Said A, Hagan A. Characterization of nonlinear optical absorption and refraction. Progress in Crystal Growth and Characterization of Materials. 1993;27((3-4)):279–311.
116. Henari FZ, Dakhel AA. Linear and nonlinear optical properties of gold nanoparticle-Eu oxide composite thin films. Journal of Applied Physics [Internet]. AIP Publishing; 11 Augustus 2008 [cited 20 April 2016];104(3):33110. Opgehaal van: http://scitation.aip.org/content/aip/journal/jap/104/3/10.1063/1.2967711

117. Rativa D, Araujo RE, Gomes AS. One photon nonresonant high-order nonlinear optical properties of silver nanoparticles in aqueous solution. Optics Express [Internet]. Optical Society of America; 05 November 2008 [cited 20 April 2016];16(23):19244. Opgehaal van: http://www.osapublishing.org/viewmedia.cfm?uri=oe-16-23-19244&seq=0&html=true

118. Shahriari E, Yunus WMM, Naghavi K, Saion E. The optical nonlinearity of Au and Ag nanoparticle prepared by the Γ-radiation method. American Journal of Engineering and Applied Sciences [Internet]. Science Publications; 01 Februarie 2010 [cited 20 April 2016];3(2):260–4. Opgehaal van: http://thescipub.com/abstract/10.3844/ajeassp.2010.260.264

119. Majles MH, Dehghani Z, Sahraei R, Nabiyouni G. Non-linear optical properties of silver nanoparticles prepared by hydrogen reduction method. Optics Communications [Internet]. April 2010 [cited 20 April 2016];283(8):1650–3. Opgehaal van: http://www.sciencedirect.com/science/article/pii/S0030401809008839

120. Xia Y, Halas NJ. Shape-controlled synthesis and surface plasmonic properties of metallic nanostructures. MRS Bulletin [Internet]. Cambridge University Press; 31 Januarie 2005 [cited 15 April 2016];30(5):338–48. Opgehaal van: http://journals.cambridge.org/abstract_S0883769400012732

121. Šileikaitė A, Prosyčevas I, Puišo J, Juraitis A, Guobienė A. Analysis of silver nanoparticles produced by chemical reduction of silver salt solution. Materials Science [Internet]. 01 Januarie 2006 [cited 20 April 2016];12(4). Opgehaal van: https://www.researchgate.net/publication/228513723_Analysis_of_Silver_Nanoparticles_Produced_by_Chemical_Reduction_of_Silver_Salt_Solution

122. Shahriari E, Moradi M, Varnamkhasti MG. Investigation of nonlinear optical properties of Ag nanoparticles. International Journal of Optics and Photonics. 2015;9(2):107–14.

123. Srinivas NK, Rao SV, Rao DN. Saturable and reverse saturable absorption of Rhodamine B in methanol and water. Journal of the Optical Society of America B [Internet]. Optical Society of America; 01 Desember 2003 [cited 28 April 2016];20(12):2470. Opgehaal van: http://www.osapublishing.org/viewmedia.cfm?uri=josab-20-12-2470&seq=0&html=true

124. Gurudas U, Brooks E, Bubb DM, Heiroth S, Lippert T, Wokaun A. Saturable and reverse saturable absorption in silver nanodots at 532 nm using picosecond laser pulses. Journal of Applied Physics [Internet]. 01 November 2008 [cited 28 April 2016];104(7):73107. Opgehaal van: https://www.researchgate.net/publication/224442950_Saturable_and_reverse_saturable_absorption_in_silver_nanodots_at_532_nm_using_picose

cond_laser_pulses

125. Jacinto C, Messias DN, Andrade AA, Lima SM, Baesso ML, Catunda T. Thermal lens and Z-scan measurements: Thermal and optical properties of laser glasses – A review. Journal of Non-Crystalline Solids [Internet]. 01 September 2006 [cited 20 April 2016];352(32–35):3582–97. Opgehaal van: https://www.researchgate.net/publication/222535088_Thermal_lens_and_Z-scan_measurements_Thermal_and_optical_properties_of_laser_glasses_-_A_review

126. Ule AE. Measurement of the nonlinear refractive index by Z-scan technique [Internet]. University of Ljubljana; 2015. Opgehaal van: http://mafija.fmf.uni-lj.si/seminar/files/2014_2015/seminarZ-scan2.pdf